

**Studies on Preparation and Catalytic Cracking
Reactivity of Novel Zeolite-Containing
Hierarchical Catalysts**

Shinya Matsuura

Division of Material Science
Graduate School of Engineering
Mie University

March 2022

Abstract

With the recent fluctuations in crude oil prices, the spread of COVID-19, and the growing environmental orientation based on the concept of the sustainable development goals (SDGs), the demand for oil and the situation surrounding oil itself are changing drastically. In this period of social transition, the overall demand for oil is on a downward trend, but it is expected to increase in some regions such as developing countries, and refining technology that can meet the demand more efficiently is important for sustainable use of oil resources. In particular, the catalytic cracking process using catalysts can increase the yield of useful fractions by cracking the residual oil (such as atmospheric residue and vacuum gas oil (VGO)) after extracting useful fractions such as liquefied petroleum gas, gasoline, and kerosene from crude oil. In recent years, this process has also been widely studied as a technology for obtaining fuel oil from waste plastics and other materials. In this process, there is a need for a catalyst that can crack the reactants more efficiently.

First, in order to prepare catalysts with mesopores, the gel skeletal reinforcement (GSR) method using a hexamethyldisiloxane (HS)-acetic anhydride (AA) silylating agent, which has been applied only to silica matrices, was applied to alumina and titania matrices. As a result, in the case of alumina, a high temperature peak in the range of 400-600 °C was observed in NH₃ desorption, confirming the introduction of a new acid point. In the case of titania, no transition of the anatase phase to the rutile phase was observed, confirming the improvement of thermal stability. Therefore, alumina and titania matrices with novel physical properties could be prepared by the GSR method. These were used to prepare the mixed catalysts with β -zeolite. The catalytic cracking of *n*-dodecane was carried out to evaluate the reactivity of the prepared mixed catalysts. The mixed catalyst with alumina matrix showed improved conversion and gasoline selectivity compared to the mixed catalyst with β -zeolite single or with alumina matrix without GSR applied.

Second, in order to prepare zeolite-containing two-layered catalysts (ZC2L) with large mesopores with more uniformly dispersed zeolites, zeolite-containing gels were prepared by the sol-gel method using tetraethyl orthosilicate, and the GSR method of HS-AA system was applied. The zeolites used were ZSM-5, Y and β , which are commonly used in catalytic cracking process. As a result of XRD measurement and nitrogen adsorption / desorption measurement of these catalysts, while maintaining the crystal structure peculiar to zeolite, it has a maximum pore volume of 5 cm³/g and pore diameter of 50 nm or more. Thus, it was confirmed that the micropores of each zeolite and the large mesopores derived from GSR silica were combined. In the catalytic cracking of *n*-dodecane using these catalysts, the ZC2L catalyst with ZSM-5 improved the conversion by more than 30 % compared with zeolite single, even though the zeolite content was 26 wt%, indicating the improvement of cracking activity. In the case of ZC2L catalysts with β and Y, the multi-branch/single-branch hydrocarbon ratio (m/s)

and the olefin/paraffin ratio (O/P) in the gasoline fraction increased by 1.5-2 times. The increase in the mesopore diameter affected the O/P and the conversion, and the micropore size of the zeolite affected the *iso-/n-* ratio (*iso-/n-*) in the gasoline fraction.

Third, catalytic pyrolysis of low-density polyethylene was carried out to evaluate the applicability of ZC2L catalysts to feeds with different geometries. A Curie point pyrolyzer was used as the reaction apparatus to compare the catalyst performance in a simple and rapid manner. The results showed that the ZC2L catalyst using ZSM-5 zeolite showed high selectivity for aromatic compounds such as toluene and *p*-xylene. The product selectivity of the ZC2L catalysts was influenced by the type of zeolite used, i.e., the size of the micropores. All ZC2L catalysts showed high conversion despite the small amount of zeolite used due to their hierarchical structure.

Fourth, the effect of the structure on the catalytic cracking of VGO, a bulky reactant, and the acid properties were evaluated using a catalyst with a three-layered structure developed from the ZC2L catalyst. As a result, three-layered catalysts that maintains the crystal structure of the HY zeolite used as well as the structure of the two-layered catalyst, and also has larger mesopores were able to fabricate. The BET surface area, BJH pore volume, and mesopore diameter of the three-layered catalyst were 716 m²/g, 1.44 cm³/g, and 10.6 nm, respectively. As a result of catalytic cracking of VGO using the fabricated two- and three-layered catalysts, the O/P, *iso-/n-*, m/s and RON value in gasoline were greatly improved compared with those of zeolite single and kaolin mixed catalyst. They also showed high activity, be suggested that the activity was largely related to the mesopore volume and the acidity of the catalyst.

In summary, various zeolite-containing hierarchical catalysts were prepared by sol-gel method and GSR method. The catalytic activity of the prepared zeolite-containing hierarchical catalysts was clarified by characterization of them and catalytic cracking of various hydrocarbons using them. Although those catalysts contained less zeolite as the main active catalyst, the product selectivity of zeolite in the catalytic cracking reaction was enhanced by the formation of new active sites and the enhancement of cracking activity by the hierarchical structure.

Contents

1. Introduction	1
1.1 Catalytic cracking reaction in petroleum refining	1
1.2 Catalytic cracking	2
1.3 Catalysts used in catalytic cracking	5
1.3.1 Zeolite	5
1.3.2 Matrix component	10
1.3.3 Mixed catalyst and zeolite-containing two-layered catalyst and three-layered catalyst	15
1.4 Catalytic cracking catalyst in plastic recycle	16
1.5 Structure of this thesis	17
References	18
2. Preparation of β-zeolite mixed catalysts using alumina and titania matrices modified by silication of gel skeletal reinforcement and their reactivity for catalytic cracking of <i>n</i>-dodecane	21
2.1 Introduction	21
2.2 Preparation of β -zeolite mixed catalysts using alumina and titania matrices modified by silication of gel skeletal reinforcement	22
2.2.1 Preparation of matrices by sol-gel and gel skeletal reinforcement method	23
2.2.2 Preparation of mixed catalyst with β -zeolite	25
2.3 Characterization of catalyst samples	25
2.3.1 N_2 adsorption and desorption measurement	25
2.3.2 X-ray diffraction measurement	26
2.3.3 X-ray fluorescence measurement	26
2.3.4 NH_3 adsorption and desorption	26
2.4 Activity test of catalyst samples	27
2.4.1 Catalytic cracking of <i>n</i> -dodecane	27
2.4.2 Measurement of gas and liquid products by GC-FID	27
2.5 Results and discussion	28
2.5.1 Characterization of matrices and mixed catalysts	28
2.5.2 Catalytic cracking of <i>n</i> -dodecane using the GSR-silica-modified alumina and titania mixed catalysts	39

2.5.3	Relationship between catalytic cracking of <i>n</i> -dodecane and catalyst texture	44
2.6	Conclusions	48
	References	50
3.	Preparation of novel zeolite-containing hierarchical two-layered catalysts with large mesopores by gel skeletal reinforcement and their reactivities in catalytic cracking of <i>n</i>-dodecane	57
3.1	Introduction	57
3.2	Catalyst preparation	59
3.2.1	Preparation of zeolite-containing hierarchical two-layered catalysts by gel skeletal reinforcement method	59
3.2.2	Preparation of kaolin mixed catalyst with zeolite	60
3.3	Characterization of zeolite-containing hierarchical two-layered catalysts	61
3.4	Activity test of zeolite-containing hierarchical catalysts in catalytic cracking of <i>n</i> -dodecane	62
3.5	Results and discussion	62
3.5.1	Characterization of zeolite-containing hierarchical catalysts prepared by gel skeletal reinforcement method	62
3.5.2	Catalytic cracking of <i>n</i> -dodecane using zeolite-containing hierarchical two-layered catalysts	69
3.6	Conclusions	72
	Acknowledgements	72
	References	73
4.	Catalytic cracking of low-density polyethylene over zeolite-containing hierarchical two-layered catalyst with different mesopore size using Curie point pyrolyzer	77
4.1	Introduction	77
4.2	Catalyst preparation and characterization	78
4.3	Catalytic cracking of LDPE using the CPP method	79
4.4	Results and discussion	81
4.4.1	Characterization of catalysts	81
4.4.2	Catalytic cracking of LDPE using various ZC2L catalysts, kaolin mixed catalysts and zeolite singles	82

4.4.3	Comparison of the results of catalytic cracking of LDPE and <i>n</i> -dodecane	91
4.5	Conclusions	91
	Acknowledgements	92
	References	93
5.	Estimation of catalytic cracking of vacuum gas oil by a Y zeolite-containing two-layered catalyst and a novel three-layered hierarchical catalyst using a Curie point pyrolyzer method	97
5.1	Introduction	97
5.2	Catalyst preparation	99
5.2.1	Preparation of the HY zeolite-containing two-layered catalyst	99
5.2.2	Preparation of the three-layered catalyst by co-gelation of GSR silica in the presence of the HY zeolite-containing two-layered catalyst	100
5.3	Characterization of catalysts by NH ₃ temperature-programmed desorption, N ₂ adsorption and desorption, and XRD	101
5.4	Catalytic cracking by the CPP method	102
5.5	Results and discussion	103
5.5.1	Characterization of catalysts by XRD, N ₂ adsorption and desorption, and NH ₃ TPD	103
5.5.2	Catalytic cracking of VGO over HY zeolite, kaolin, 2L, and 3L catalysts using the CPP method	107
5.6	Conclusions	113
	Acknowledgements	114
	References	115
6.	Conclusions	121
	List of Publications	123
	Acknowledgements	125

Chapter 1

Introduction

WTI (West Texas Intermediate) crude oil prices in recent years have fluctuated significantly as the world situation changes. In 2019, it was 50-60 dollars/barrel, but it fell to 20 dollars/barrel due to the spread of COVID-19 from the beginning of 2020, and in April it was recorded minus 37.63 dollars/barrel. Oil demand is fluctuating as well as WTI crude oil prices. According to an IEA report [1], the spread of COVID-19 had a significant impact on the global economy, with oil demand in 2020 down about 8 % year-on-year to 91.0 million barrels/day. However, after that, it started to recover, and it is expected to reach 104.1 million barrels/day by 2026. Oil demand is expected to increase in Asia and Africa, but the situation surrounding oil will change significantly due to the establishment of "New normal", especially in developed countries. At such a turning point, the focus of research and technological development is rapidly shifting to refining and sustainable technologies that meet the demand more efficiently.

This chapter focuses on the cracking reactions required for the treatment of heavy fractions among petroleum refining technologies and the catalysts required for those reactions. Section 1.1 outlines the catalytic cracking reaction. Section 1.2 describes the catalyst used in the cracking reaction in line with the content of this thesis. Section 1.3 describes catalysts for fuel conversion and recycling related to recent growing interest in environmental issues, especially waste plastic issues. The structure of this thesis is shown in Section 1.4.

1.1 Catalytic cracking reaction in petroleum refining

There are some treatment processes which required to convert crude oil into various petroleum products such as liquid petroleum gas (LPG), naphtha (raw material for gasoline), kerosene, olefin (raw material for plastics), and heavy oil. First, crude oil is divided into fractions having a certain boiling point range in the atmospheric distillation process. Light fractions such as LPG and naphtha are in relatively high demand and are used as they are or after undergoing processes such as hydrodesulfurization and catalytic reforming. On the other hand, heavier fractions such as vacuum gas oil and atmospheric residue are in relatively low demand, and their use as they are is limited. In addition, petroleum products are mixtures with similar boiling range, and it is difficult to extract only high-demand fractions, and a certain amount of other fractions

Chapter 1

are also produced together. Therefore, in order to manufacture in line with demand, it is necessary to convert to lighter fractions such as LPG and naphtha. The process required at that time is a process by catalytic cracking reaction. Cracking reactions include thermal cracking by heat, catalytic cracking performed in the presence of a catalyst, and hydrocracking performed using a catalyst under a high-pressure hydrogen flow. Since the reaction using hydrogen is not dealt with in this thesis, only catalytic cracking will be described. In addition, petroleum is a mixture of various hydrocarbons, but in this thesis, since *n*-paraffin are treated as raw materials, they are taken as an example.

1.2 Catalytic cracking

The catalytic cracking was discovered in 1923 by E. J. Houdry in France, who used clay minerals as catalysts to crack heavy oils derived from lignite, and obtained better quality gasoline than the pyrolysis process [2, 3]. In 1936, Houdry et al. succeeded in catalytic cracking for the first time on an industrial scale. In the 1940's the catalyst changed to the more active amorphous synthetic silica-alumina, and in the 1960's the application of the crystalline aluminosilicate zeolite made it much more active than the amorphous silica-alumina. Zeolite-based catalysts with good stability and gasoline selectivity have been developed, and catalytic cracking has made great strides. In catalytic cracking, carbon precipitated on the catalyst surface during the reaction is burnt and removed to regenerate the catalyst, and at the same time, the heat required for the reaction is obtained [2, 4, 5]. Since this device uses a powdered solid catalyst in a fluid bed state, it is called fluid catalytic cracking (FCC). In modern times, FCC is one of the major conversion technologies in the oil refinery industry and produces the majority of the world's gasoline [6]. It is also used in the production of raw materials for petrochemical processes such as propylene [2]. In recent years, research has been actively conducted to use biomass and waste plastics as a part of FCC raw materials from the viewpoint of effective utilization of petroleum resources and existing petroleum refining facilities and SDGs [7-12].

Since catalytic cracking is the cleavage of C-C bonds of hydrocarbon molecules and is an endothermic reaction, it is carried out at a high temperature of 500-550 °C which is thermodynamically advantageous even with a catalyst. At this temperature, a reaction by heat also occurs at the same time, but a chain reaction by a carbenium ion mechanism by a solid acid catalyst occurs as a reaction several orders of magnitude faster than that. The reaction by a solid acid catalyst occurs on the acid site (Brønsted acid site) of the catalyst, and the reaction occurs in the form of an intermediate called a carbenium ion. Many carbonium ion reactions are best explained as following; tertiary > secondary > primary > ethyl > methyl, which might well be termed the carbonium ion rule [13]. It is said that the initiation of the reaction occurs by the

Chapter 1

addition of protons in the unsaturated system and by the extraction of hydride in the saturated system [14]. In addition, cracking occurs at the β -position, so it is called β -cleavage. This is because the carbon electron adjacent to the carbenium ion is attracted to the cation, and the β -position bond becomes relatively weak.

Since long carbon chain molecules are more reactive than short carbon chain molecules, the cracking reaction slows down as the carbon chains become smaller and continues until stable carbenium ions are no longer produced. The initial products of β -cleavage are olefins and new carbenium ions. The newly generated carbenium ion continues the reaction, causing a chain reaction. Small ions with 4 or 5 carbon atoms react with other large molecules to extract hydride ions and make them carbenium ions. Then, the decomposition of large carbenium ions proceeds. From the above stability, most of the carbenium ions are tertiary and secondary ions, and when cleaved at the β -position, C_1 and C_2 products can hardly be produced, and the products in catalytic cracking are mainly C_3 and above.

In addition to cracking, isomerization, hydrogen transfer, cyclization, carbon precipitation, etc. also occur, and the reaction is complicated. However, all of these reactions are explained by surface carbenium ion intermediates on solid acids [13]. The product is a mixture of hydrocarbons of various structures such as paraffin, olefins, naphthenes and aromatics [15, 16].

The isomerization reaction is more likely to occur by catalytic cracking than by thermal cracking. In the thermal cracking and catalytic cracking reaction mechanism, bond cleavage is via β -cleavage of carbon radicals and carbenium ions, but the carbenium ions in catalytic cracking are more likely to rearrange to tertiary ions. These carbenium ions repeat cracking and isomerization to produce many branched molecules. Therefore, the octane number of the gasoline fraction obtained by catalytic cracking becomes high, and gasoline with better quality can be obtained.

Hydrogen transfer is a two-molecule reaction, one of which is an olefin. An example of hydrogen transfer is the reaction of two olefins. One of the olefins becomes paraffins and the other becomes cycloolefins. Cycloolefins transfer hydrogen to other olefins to become cyclodiolefins. The cyclodiolefins are further dehydrogenated and eventually become aromatics. Therefore, the hydrogen transfer of olefins is a reaction that converts olefins to paraffins and aromatics. In addition, naphthenic compounds have a high hydrogen donating ability [13] and become aromatics [15, 16] or coke themselves. The hydrogen transfer reaction has many advantages such as improving the yield of liquids such as gasoline, reducing the yield of coke [17], and increasing the stability of produced gasoline [18]. On the other hand, excessive hydrogen transfer activity reduces the proportion of olefins, leading to a decrease in the octane number of FCC gasoline. In FCC gasoline, olefins are hydrogenated by the subsequent hydrodesulfurization treatment. Therefore, it is necessary to suppress the decrease in the octane number of FCC gasoline by

Chapter 1

increasing the number of branched products having a high octane number by the isomerization reaction. It is known that the cracking reaction and the isomerization reaction are monomolecular reactions, whereas the coke formation reaction is a two-molecule reaction like the hydrogen transfer reaction, and is increased by high acid strength and high acid site density [19]. Since the formation of coke on a catalyst results in rapid deactivation of activity, it is required to develop a catalyst that suppresses the formation of such coke. As described above, the reaction related to catalytic cracking can be outlined.

Figure 1.1 shows the reaction pathways [15, 16] in catalytic cracking of *n*-paraffin, and the details will be explained. *n*-Paraffin produces paraffin and olefin 1: 1 by cracking reaction. The paraffin produced repeats the same process. On the other hand, the produced olefin is further cracked or undergoes a dehydrogenation cyclization reaction to produce an aromatic (cyclic) compound. H^+ or H^- generated in the cyclization reaction is supplied to another olefin and becomes paraffin. This reaction is the hydrogen transfer reaction described above. When the olefin is cracked, two olefins are produced. Therefore, when the hydrogen transfer reaction is suppressed, olefins increase, and when the hydrogen transfer reaction is promoted, paraffin and aromatic (and cyclic) compounds increase. The isomerization reaction can occur during the cracking, hydrogen transfer, dehydrogenation, and cyclization processes, as shown in Figure 1.1. In the isomerization reaction, the steric effect such as the pore structure of the catalyst described in the next section is also important.

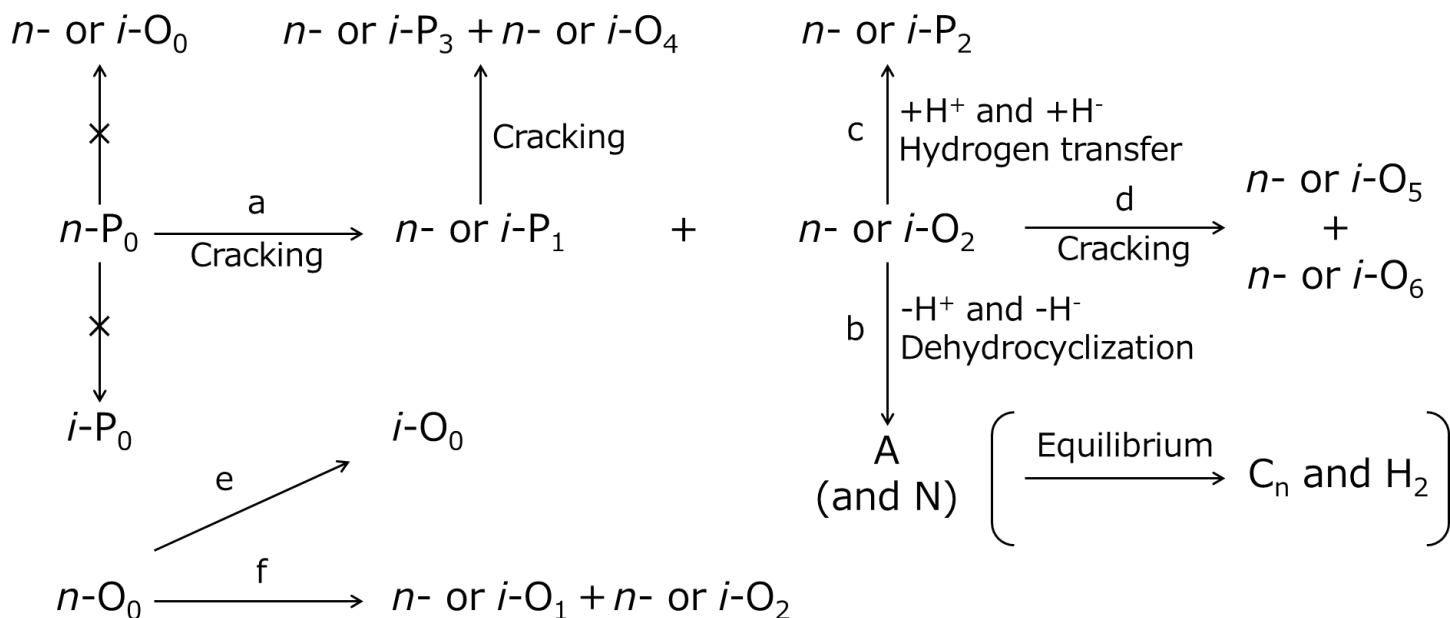


Figure. 1.1 Catalytic cracking reaction of *n*-paraffin [15, 16].

1.3 Catalysts used in catalytic cracking

In recent years, it is required for FCC catalysts to crack heavier oils such as residue oil. However, such heavier oils contain a large amount of hydrocarbons with a large molecular structure that cannot enter the micropores of zeolite, so they are difficult to crack [2, 20]. Therefore, by using a mixed catalyst consisting of a matrix component having mesopores and weak acid sites and zeolite, the heavy fraction can be primary cracked, the introduction of reaction molecules and the internal diffusion are promoted, and then zeolite can crack the primary produced intermediate product [5, 21]. In addition, the diffusion of the reaction product to the outside of the pores can also be promoted. Besides, it is possible to add various functions such as accessibility, hydrothermal stability, abrasion resistance, metal resistance, coke selectivity, improvement of fluidizability, activity by dilution of zeolite, control of selectivity, etc. [2, 4, 5, 22] depending on the matrix component. Currently, a mixed catalyst of zeolite (usually ultra-stabilized Y-zeolite), clay mineral, and amorphous silica-alumina is mainly used, and research and development which improvement of industrial catalytic cracking processes, and matrix design and synthesis according to needs have been advanced [5, 12, 23-25]. The following sections describe the zeolite and matrix components used in this thesis.

1.3.1 Zeolite

Zeolites are generally microporous crystalline aluminosilicates and have a variety of framework structures [26]. As of April 2021, as many as 253 types of framework structures have been discovered and synthesized [27]. There are about 40 types of zeolite that are naturally produced [26]. Zeolites used as industrial catalysts are limited to a few types, all of which are industrially synthesized.

In this section, zeolites mainly used as cracking catalysts will be briefly described with reference [26-29].

All zeolite frameworks can be built by linking in a periodic pattern a basic building unit (BBU), the tetrahedron. In the center of the tetrahedra are atoms with relatively low electronegativities (Si^{IV} , Al^{III} , P^{V} , Zn^{II} , etc.) and in the corners are oxygen anions (O^{2-}). These combinations can be depicted as $[\text{SiO}_4]$, $[\text{AlO}_4]$, $[\text{PO}_4]$, etc. Figure 1.2 depicts a BBU, the tetrahedron. Note that each apical oxygen is shared with the adjacent tetrahedron and as a consequence the framework of zeolite materials always has a metal-to-oxygen ratio of 1: 2. More complex composite building units (CBUs) can be formed linking together groups of BBUs. The simplest examples of CBUs are rings. All zeolite structures can be viewed as if formed of rings of tetrahedra of different sizes. In the aluminosilicate zeolite, a part of the Si framework is repla-

Chapter 1

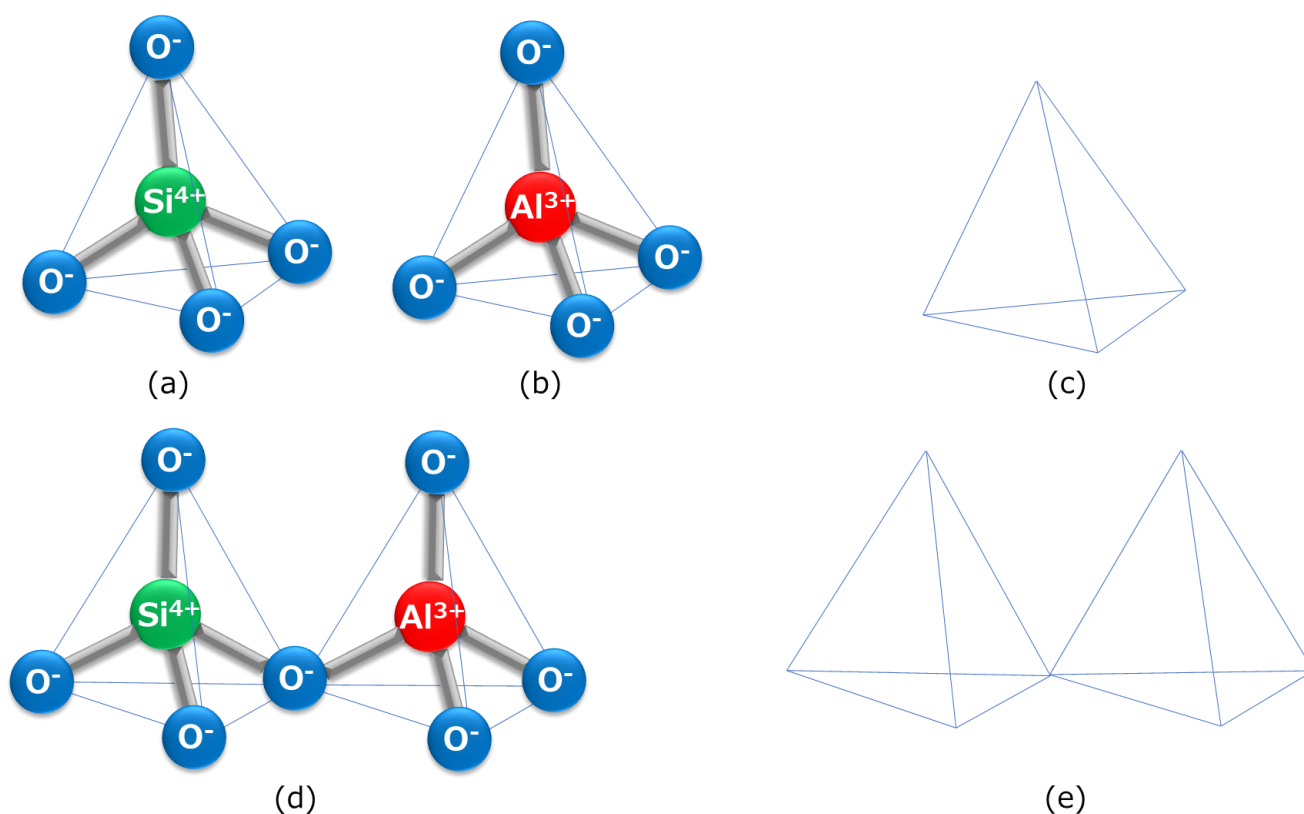


Figure 1.2 Structure of (a) $[\text{SiO}_4]$, (b) $[\text{AlO}_4]$, (d) aluminosilicate and (c, e) those tetrahedron.

ced with an Al atom, so that a negative charge is generated. In order to cancel the negative charge, there are cations in the vicinity of the Al atom. By replacing this cation with a proton, an acidic active site (acid site) such as a Brønsted acid site or a Lewis acid site is formed. Such acid sites are used in processes using zeolite for catalytic reactions, including catalytic cracking. The mechanism of acid site formation is shown in Figure 1.3.

The rigid pore structure leads to steric constraints on molecules within the zeolite resulting in novel reaction pathways in comparison with unconstrained media. This is demonstrated in Figure 1.4 as examples of reactant, product, and transition state selectivities [26, 27]. The increase in size upon methyl substitution is enough to prevent the alkane from entering the zeolite. The higher diffusivity of *p*-xylene by a few orders of magnitude in the channel system of the zeolite in comparison with the *o*- and *m*- isomers facilitates selectivity toward the product. Another example is that of molecular traffic control in ZSM-5, where reactant molecules diffuse through one channel system, while product molecules diffuse through the other channel, minimizing counterdiffusion [26, 28]. In this thesis, Y, ZSM-5, and β -zeolites with the structure shown in Figure 1.5 [29], which are generally used in the FCC process, are used. These zeolites have the

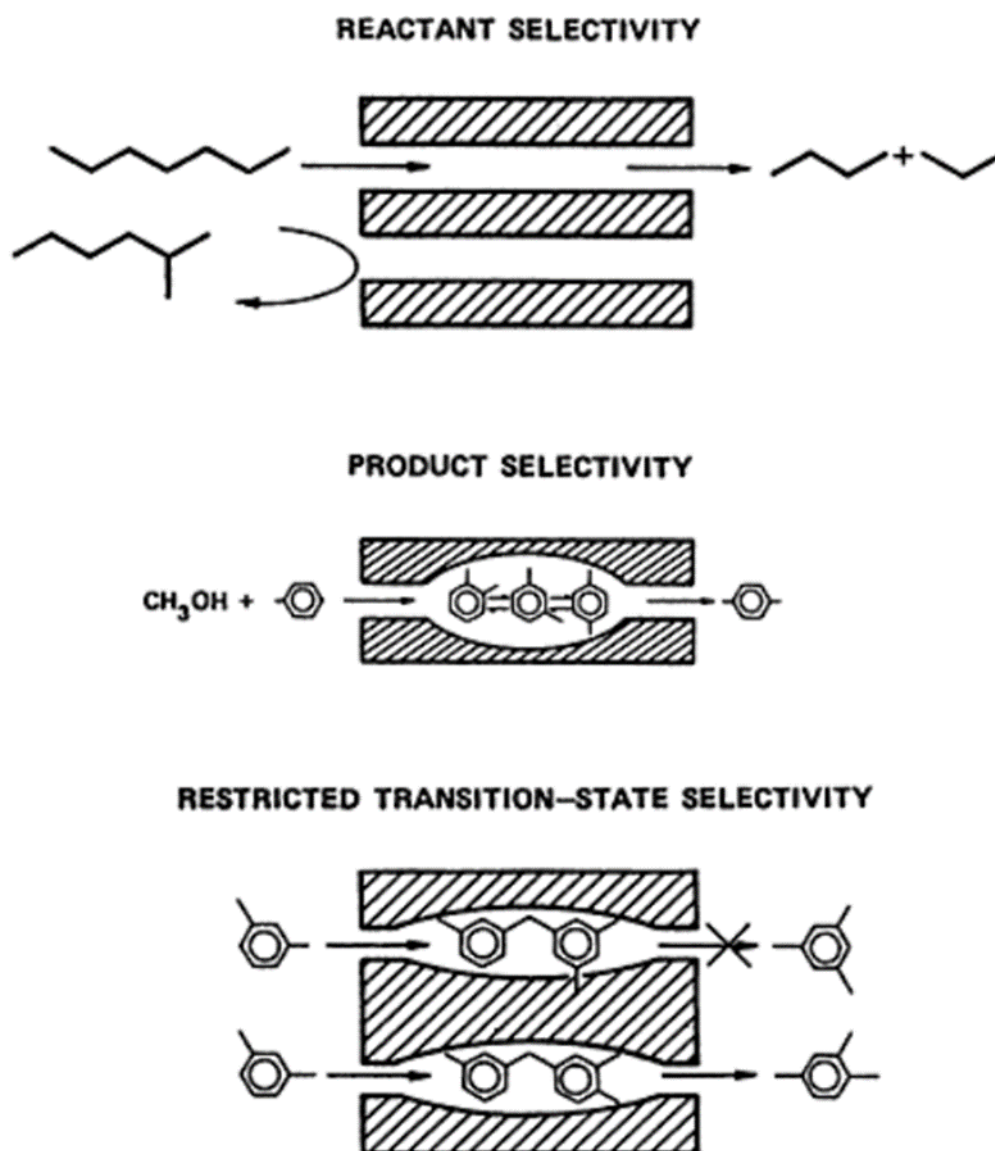


Figure 1.4 Different types of reaction selectivity imposed by the rigid pore structure of the zeolite [26, 27].

Chapter 1

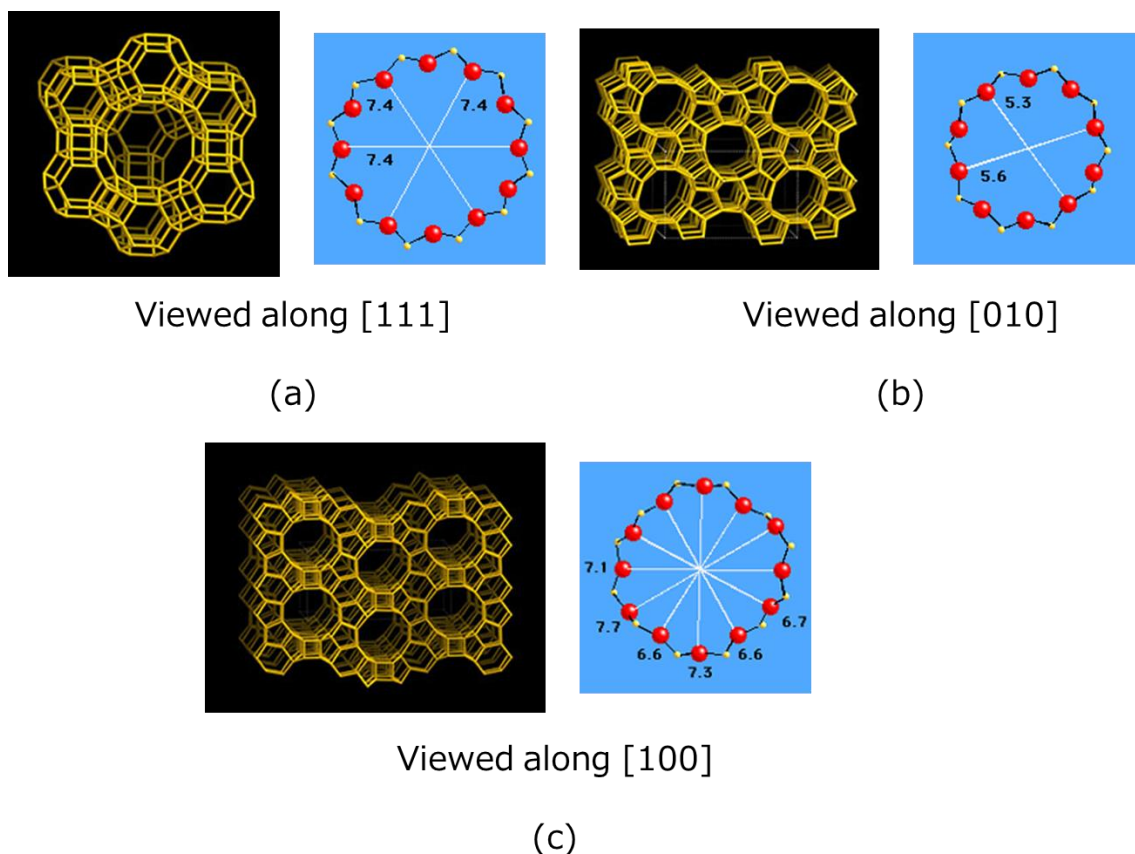


Figure 1.5 Framework and channel of (a) Y-zeolite, (b) ZSM-5-zeolite, (c) β -zeolite [29].

Table 1.1 The application of Y-, ZSM-5- and β -zeolites as catalyst.

Zeolite	Reactant	Application	Product
Y	Crude oil, Residue oil	Fluid catalytic cracking (FCC), Hydrocracking	Gasoline, Diesel, etc.
ZSM-5	Hydrocarbon (ex. <i>m</i> -Xylene)	Isomerization	Hydrocarbon (ex. <i>p</i> -Xylene)
	Hydrocarbon (ex. Benzene, Ethylene)	Alkylation	Hydrocarbon (ex. Ethylbenzene)
	Methanol	Methanol to gasoline (MTG)	Gasoline
β	Hydrocarbon (ex. Benzene, Ethylene)	Alkylation	Hydrocarbon (ex. Ethylbenzene)
	Hydrocarbon	Cracking	Hydrocarbon

1.3.2 Matrix component

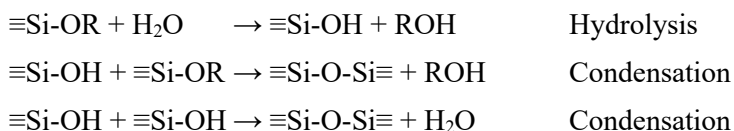
This thesis has been focused on the function of the above-mentioned matrix component in catalytic cracking. Catalysts were prepared by the sol-gel method with the aim of improving the catalytic activity and the product selectivity by the introduction of matrix component having mesopores. This section provides an overview of the formation of mesopores using the sol-gel method [30].

Sol-gel materials are metastable solids that are formed in kinetically controlled reactions from molecular precursors, which constitute the building blocks for the later materials. An immediate consequence is that all reaction parameters, including the precursor properties, have a decisive influence on the structure and thus the properties of sol-gel materials. The sol and the gel are defined as follows:

A sol is a stable suspension of colloidal particles (nanoparticles) in a liquid. The particles can be amorphous or crystalline, and may have dense, porous, or polymeric substructures. The latter can be due to aggregation of subcolloidal chemical units.

A gel consists of a porous, three-dimensionally continuous solid network surrounding and supporting a continuous liquid phase (“wet gel”). In most sol-gel systems for the synthesis of oxide materials, the gelation (i.e., formation of the gels) is due to the formation of covalent bonds between the sol particles. The gel formation can be reversible when other bonds such as van der Waals forces or hydrogen bonds are involved. The structure of the gel network depends to a large extent on the size and shape of the sol particles.

In general, the sol-gel process of oxide materials is the transformation of alkoxide (M-OR) to oxide by condensation reaction. The atom “M” includes "Si", "Al", "Ti", "Zr", "Ce", etc., and a typical example is "Si". Hence, in the following, a Si compound will be described as an example. To obtain a stable gel, the number of siloxane bonds (Si-O-Si) has to be maximized and consequently the number of silanol (Si-OH) and alkoxy (Si-OR) groups has to be minimized. The most common precursors are aqueous solutions of silicates (“water glass”) and silicon alkoxides, Si(OR)₄, mostly tetramethyl orthosilicate (TMOS) or tetraethyl orthosilicate (TEOS). For example, the chemical reaction formulas for the hydrolysis and condensation reactions of Si(OR)₄ are as follows.



From above equations, hydrolysis reactions of Si-OR groups must precede condensation to generate the Si-OH groups, which are necessary for condensation. To promote the condensation reaction (formation of “≡Si-O-Si≡”), it is necessary to remove by-produced alcohol and water to

Chapter 1

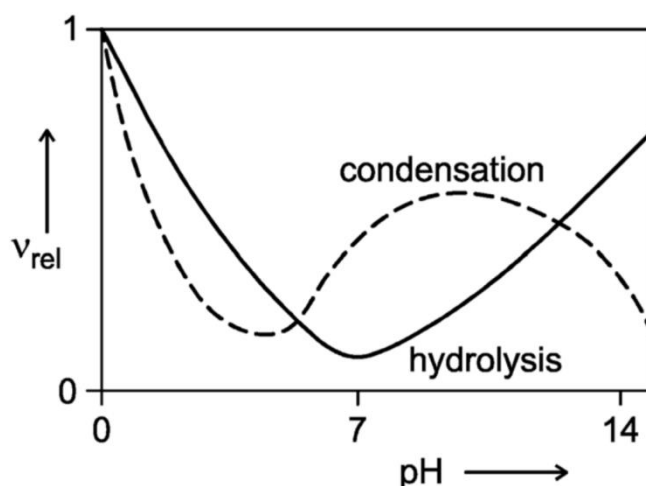


Figure 1.6 Dependence of the relative rates of $\text{Si}(\text{OR})_4$ hydrolysis and of condensation reactions on the pH [30].

the outside of the reaction system. In addition, after one $-\text{OR}$ group of $\text{Si}(\text{OR})_4$ is hydrolyzed, the next reaction has various patterns shown below, (i) Hydrolyze another $-\text{OR}$ group (ii) Attack another $\equiv\text{Si}-\text{OR}$ or $\equiv\text{Si}-\text{OH}$ bond and condense (iii) Attack another $\equiv\text{Si}-\text{OR}$ or $\equiv\text{Si}-\text{OH}$ of the same molecule and cyclize. It turns out that these reactions can occur in any precursor, oligomer and polymer molecule in the solution and are very complex reaction systems. Thus, in the sol-gel process, there are various reaction pathways until the gel is formed from a precursor such as alkoxide.

The most important parameters influencing hydrolysis and condensation (and their relative rate) are

- the kind of precursor

The hydrolysis rates of silicon alkoxide are also influenced by steric factors. Any branching of the alkoxy group or increasing of the chain length lowers the hydrolysis rate of the silicon alkoxides. So, the reaction rate decreases in the order $\text{Si}(\text{OMe})_4 > \text{Si}(\text{OEt})_4 > \text{Si}(\text{O}^i\text{Pr})_4 > \text{Si}(\text{O}^t\text{Pr})_4$.

- the pH (OH^- or H^+ catalysis), or other catalysts

The reaction rates for hydrolysis and condensation of silicon alkoxides have pH dependence (Figure 1.6). The minimal reaction rate for hydrolysis is at pH 7, and for condensation is at around pH 4.5. At $\text{pH} < 5$, hydrolysis is favored, and condensation is the rate-determining step. Many monomers or small oligomers with reactive $\text{Si}-\text{OH}$ groups are simultaneously formed. In contrast, hydrolysis is the rate-determining step at $\text{pH} > 5$, and hydrolyzed species are immediately consumed because of the faster condensation.

- the alkoxy group to water ratio for alkoxide precursors

Increasing the water proportion generally favors the formation of $\text{Si}-\text{OH}$ groups over $\text{Si}-\text{O}-$

Chapter 1

Si groups. The water proportion, together with the kind of catalyst, thus strongly influences the properties of the silica gels.

- the kind of solvent

At the beginning of the sol-gel reaction, homogenization of alkoxide-based precursor mixture solution is necessary. The properties of solvent (ex. polarity and viscosity) are also important to control the structure of the final sol-gel material.

- the presence of electrolytes

The presence of electrolytes (especially included by counter anion of acid and base for catalysis, or brought by contamination) has a strong influence on the gelation behavior. Because of not ionic, ammonia is mostly used as a base catalyst for hydrolysis.

- the temperature, the relative and absolute concentration of the components in the precursor mixtures, and other parameters

Figure 1.7 schematically shows the mechanism of silica gel formation in the sol-gel process [30]. The monomer undergoes hydrolysis and condensation reactions to form three-dimensional oligomeric particles. The primary particles thus formed aggregate at a constant size or grow larger. This changes depending on the experimental conditions, and under the acidic conditions on the left side of the Figure 1.7, the primary particles aggregate to become larger secondary particles, and a wet gel is formed by the formation of a three-dimensional network. On the other hand, under the basic conditions on the right side of the Figure 1.7, the primary particles grow further and become a sol suspended in the solution. As described above, although the silica gel obtained by the experimental system is different, the reactions carried out are all hydrolysis and condensation reactions. As the sol particles aggregate and condense, the viscosity of the sol gradually increases. The sol-gel transition (gel point) is reached when a continuous network is formed. At the gel point, the viscosity increases sharply, and a form-stable, elastic gel body is obtained. The gel time at which the gel point is reached after starting hydrolysis and condensation reactions is determined by turning the reaction vessel upside down. Since all liquid is retained in the gel body, no liquid can flow out of the vessel. For the same reason, the volume of the gel in this stage is the same as that of the original precursor solution.

In the subsequent aging step, the structure and properties of the gel gradually change due to the condensation of monomers and small particles remaining in the three-dimensional structure of the wet gel. Larger particles are also formed by Ostwald ripening, in which smaller particles dissolve and grow into larger particles by condensation of the dissolved species.

For the next drying step, there are the following problems in preparing a matrix component with large pores.

- Cracks caused by a pressure gradient due to the slower shrinkage.
- Shrinkage of pores due to stress caused by the difference in the rate of descent of the liquid meniscus.

Chapter 1

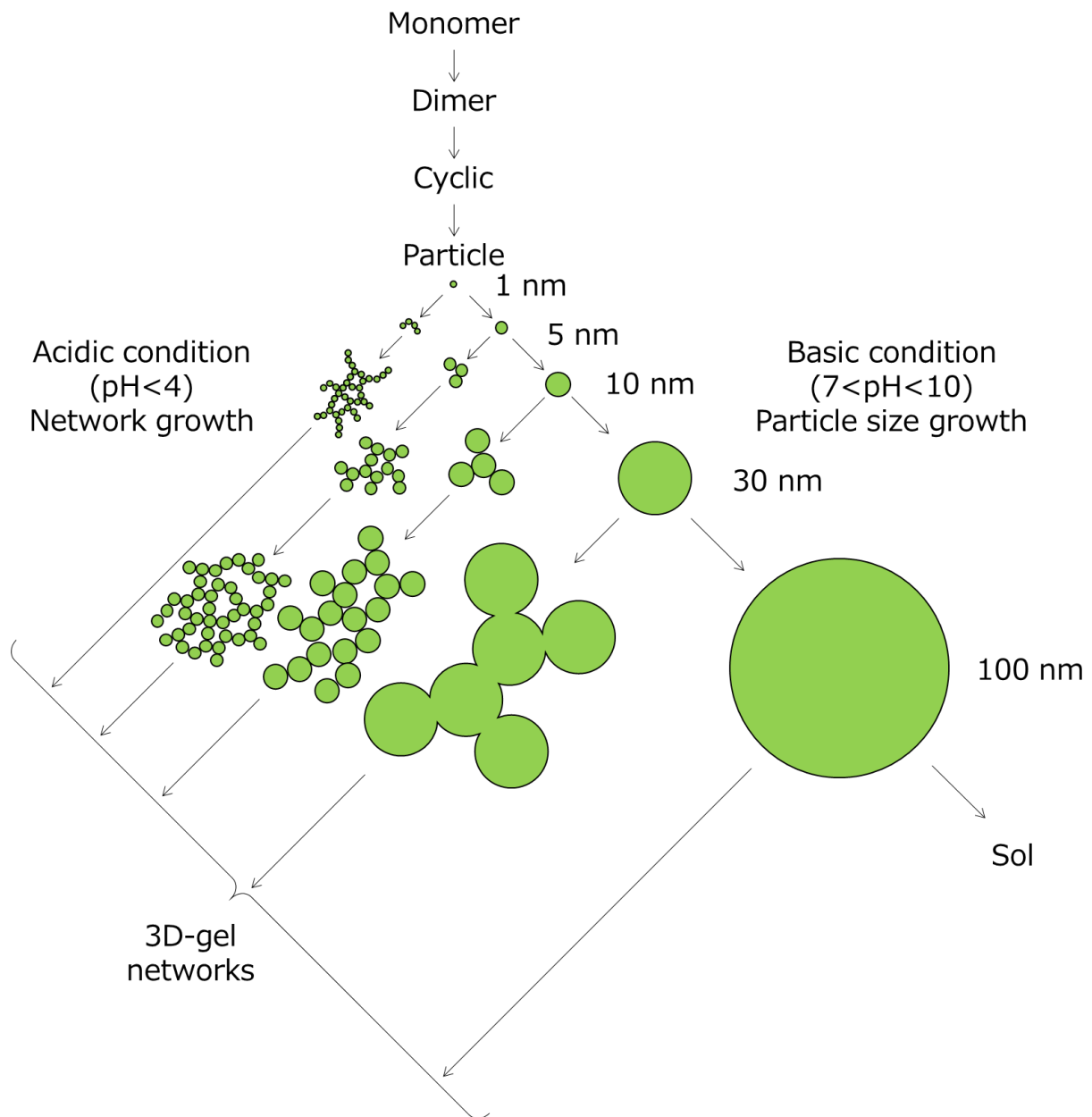


Figure 1.7 Structural development of silica gels [30].

The shrinkage of pores that occurs during drying as described above cannot be avoided. In order to suppress this, techniques such as a drying method using a supercritical fluid and hydrophobization of pore walls have been studied. In this thesis, it was chosen to reduce shrinkage due to hydrophobicity of the pore walls, which can be applied under mild conditions, rather than supercritical fluids that are difficult to handle. Among them, silica modification by the gel skeletal reinforcement (GSR) method using siloxane [31] was incorporated into the existing sol-gel process to try to reduce pore shrinkage. The outline when applied to silica gel is described below

Chapter 1

and, a schematic diagram is illustrated in Figure 1.8.

After gelation of TEOS, it is aged in distilled water to complete the hydration reaction. After that, it is necessary to exchange the solvent with 2-propanol so that the reagent used for modification does not react with water. The type of solvent used at this time is also important, and the shrinkage increases in the order of 2-propanol < methanol < ethanol < propanol < 2-butanol < butanol < hexanol. Then, the gel in which the solvent has been exchanged is put in a mixed solution of hexamethyldisiloxane (HS) and acetic anhydride (AA), and further aging is performed. This process replaces Si-OH on the gel surface with bulky Si-O-Si(CH₃)₃ derived from HS. As a result, further condensation reaction can be prevented and gel shrinkage can be suppressed in the subsequent drying and calcining step.

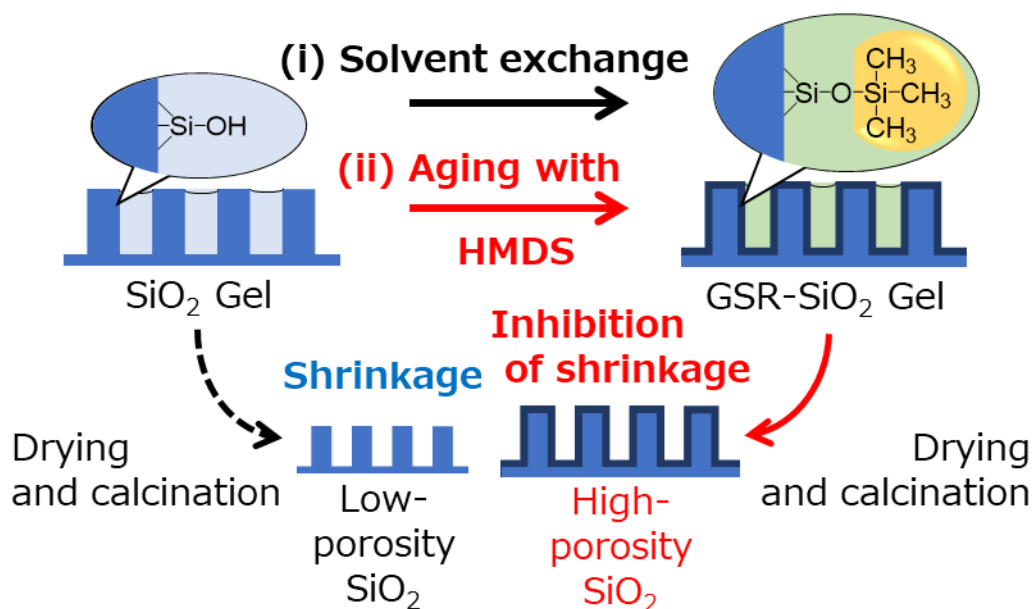


Figure 1.8 Overview of gel skeletal reinforcement.

1.3.3 Mixed catalyst, zeolite-containing two-layered catalyst and three-layered catalyst

The matrix component having mesopores, which is a combination of the sol-gel method and the GSR method described in the previous section, is an important material that greatly affects the reactivity of the catalyst. In this thesis, a mixing catalyst using them and a further developed zeolite-containing two-layered catalyst and three-layered catalyst will be described. Figure 1.9 shows a schematic diagram of the mixed catalyst. Such a mixed catalyst is obtained by mixing a matrix component and zeolite together with a binder, and molding and calcining the mixture. Figure 1.10 shows a schematic diagram of the zeolite-containing two-layered catalyst and three-layered catalyst. The zeolite-containing catalyst is different from the mixed catalyst prepared by physical mixing, and is a catalyst having micropores and mesopores prepared in one pot by adding zeolite in the sol-gel process. Specifically, the zeolite-containing two-layered catalyst is synthesized by dropping TEOS into ethanol in which zeolite is dispersed, forming a gel around the zeolite, and applying the GSR method described in the previous section. Since the two-layered catalyst requires only one calcining step as compared with the mixed catalyst, it is possible to suppress the shrinkage of pores and prepare a binderless catalyst having a micro-meso hierarchical pore structure. The zeolite-containing three-layered catalyst can be prepared as follows. TEOS is dropped into ethanol in which zeolite is dispersed, and an organic acid is added in two roles of an acid catalyst and a template to prepare a material having a micro-meso hierarchical pore structure. It is further dispersed in ethanol to prepare a gel in a two-layered catalyst-like process and the GSR method is applied. In this way, a catalyst having a three-layered pore structure of micro-meso1-meso2 ($1 < 2$) can be prepared.

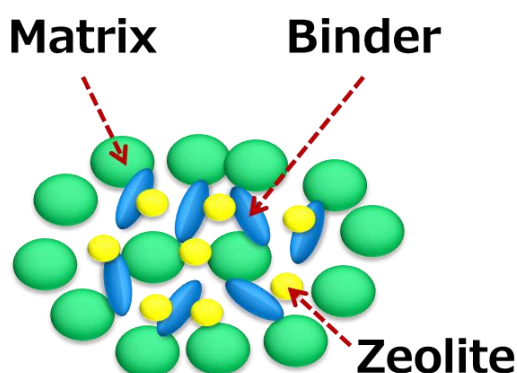


Figure 1.9 Schematic diagram of the mixed catalyst.

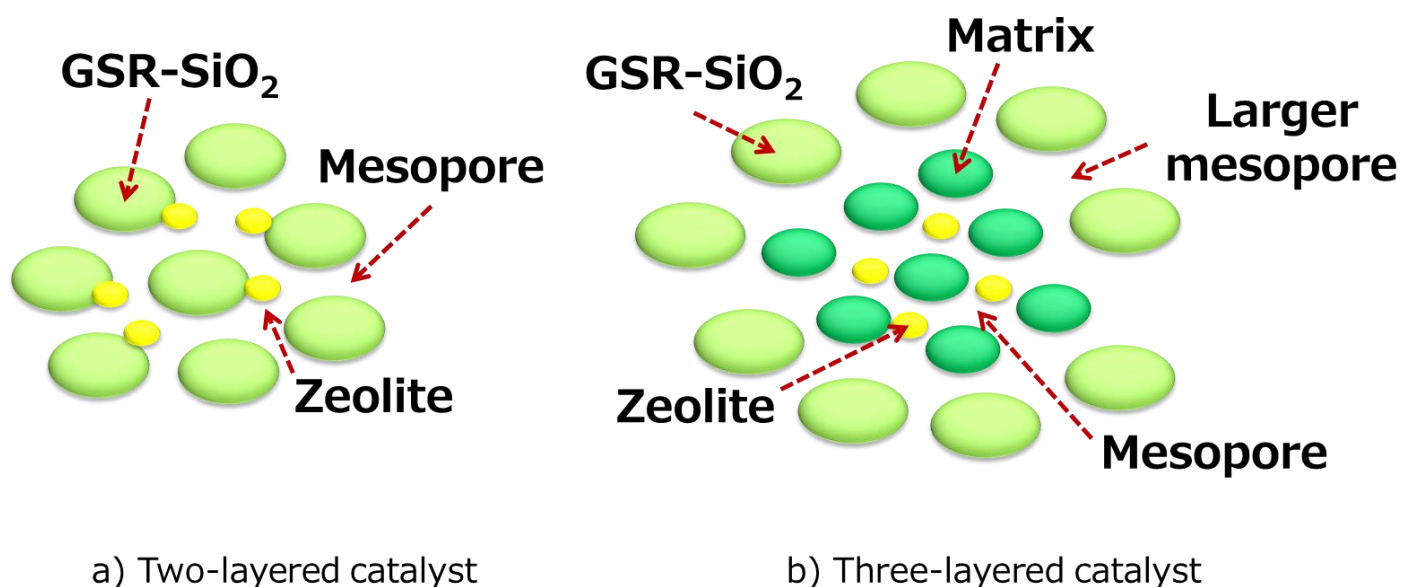


Figure 1.10 Schematic diagram of the zeolite-containing a) two-layered catalyst and b) three-layered catalyst.

1.4 Catalytic cracking catalyst in plastic recycle

Due to the recent growing interest in reducing the use of plastics and recycling, the technology for treating waste plastics using catalytic cracking catalysts has attracted more attention, and its development has started [7-11]. In Chapter 4 of this thesis, a two-layered catalyst is used for catalytic cracking of low-density polyethylene (LDPE). In catalytic cracking of plastics, solid reactants are primarily cracked by heat to produce thermal cracking products with a wide carbon number distribution [32]. Since polyolefins such as polypropylene and polybutylene have many branches in their structures, thermal cracking results in a large amount of branched products. In the case of polystyrene, since it has an aromatic ring in its basic structure, the amount of aromatic compounds increases. Because these hydrocarbons have a wide carbon number distribution of about C_1 - C_{40} , it is considered that the thermal cracking products of plastics could be the same reactants as the catalytic cracking process in petroleum refining. Therefore, catalytic cracking catalysts are often used for recycling plastics by chemical recycling (oilification). Since chemical recycling of plastics is not the reverse reaction of a synthetic reaction in which several types of monomers are polymerized, various products other than the constituent monomers can be obtained. Applying existing oil refining technology to these will greatly contribute to the formation of a sustainable society with defossil fuels.

1.5 Structure of this thesis

This thesis was focused on catalytic cracking catalysts with micropores and mesopores using zeolite as the main catalyst, and evaluated its catalytic properties by catalytic cracking using *n*-dodecane as a model substance. In addition, LDPE and vacuum gas oil (VGO) were used as other reactants for evaluation. The introductory part of each chapter is briefly described below.

In Chapter 2, the HS-AA-based GSR method, which had been applied only to silica, was applied to alumina and titania, and the reactivity as a matrix was evaluated by catalytic cracking of *n*-dodecane. It was found that new physical properties of catalysts appeared by applying the GSR method at the preparation of alumina and titania by the sol-gel method.

In Chapter 3, the HS-AA-based GSR method was applied to the silica-gel prepared by dispersing zeolite, and a zeolite-containing two-layered catalysts were obtained by one-pot synthesis. In addition, catalytic cracking of *n*-dodecane was carried out using them as catalysts. A catalyst with a different pore structure prepared with a different concept from the mixed catalyst in Chapter 2 was used. In addition, the pore characteristics and reaction characteristics according to the type of zeolite were also described.

In Chapter 4, in order to clarify the catalytic activity of the two-layered catalyst for polyethylene, which is a larger molecule than *n*-dodecane, a catalytic cracking reaction was carried out using LDPE as feedstock and the catalyst prepared in Chapter 3. For the evaluation of the reaction characteristics, a Curie point pyrolyzer, which can be evaluated more easily, was used.

In Chapter 5, the catalytic cracking of VGO, which includes a large amount of bulky molecules, was evaluated using a catalyst with a more developed hierarchical structure (three-layered) than the two-layered catalysts described in Chapter 3. The preparation method of a three-layered catalyst and the effect of its structure and acid site on catalytic cracking properties were described.

Finally, Chapter 6 lists the overall summary of this thesis.

References

- [1] IEA (2021), “Oil 2021”, *IEA*, Paris <https://www.iea.org/reports/oil-2021>, accessed May 2021
- [2] E. T. C. Vogt, B. M. Weckhuysen, “Fluid catalytic cracking: recent developments on the grand old lady of zeolite catalysis”, *Chem. Soc. Rev.*, 44 (2015) 7342-737, <https://doi.org/10.1039/C5CS00376H>
- [3] American Chemical Society, The Houdry Process – ANational Historic Landmark, 1996, <http://www.acs.org/content/dam/acsorg/education/whatischemistry/landmarks/houdry/the-houdry-process-catalytic-conversion-commemorative-booklet.pdf>, accessed May 2021
- [4] J. Biswas, I. E. Maxwell, “Recent process- and catalyst-related developments in fluid catalytic cracking”, *Appl. Catal. A Gen.*, 63 (1990) 197-258, [https://doi.org/10.1016/S0166-9834\(00\)81716-9](https://doi.org/10.1016/S0166-9834(00)81716-9)
- [5] M. E. Z. Velthoen, A. L. Paioni, I. E. Teune, M. Baldus, B. M. Weckhuysen, “Matrix Effects in a Fluid Catalytic Cracking Catalyst Particle: Influence on Structure, Acidity, and Accessibility”, *Chem. Eur. J.*, 26 (2020) 11995-12009, <https://doi.org/10.1002/chem.201905867>
- [6] S. Raseev, “Thermal and Catalytic Processes in Petroleum Refining”, *CRC Press* (2003) 1-936, <https://doi.org/10.1201/9780203912300>
- [7] E. Rodríguez, R. Palos, A. Gutiérrez, J. M. Arandes, J. Bilbao, “Production of Non-Conventional Fuels by Catalytic Cracking of Scrap Tires Pyrolysis Oil”, *Ind. Eng. Chem. Res.*, 58 (2019) 5158-5167, <https://doi.org/10.1021/acs.iecr.9b00632>
- [8] H. Yu, F. Li, W. He, C. Song, Y. Zhang, Z. Li, H. Lin, “Synthesis of micro–mesoporous ZSM-5 zeolite with microcrystalline cellulose as co-template and catalytic cracking of polyolefin plastics”, *RSC Adv.*, 10 (2020) 22126-22136, <https://doi.org/10.1039/d0ra03082a>
- [9] K. A. Tarach, K. Pyra, S. Siles, I. Melian-Cabrera, K. Gora-Marek, “Operando Study Reveals the Superior Cracking Activity and Stability of Hierarchical ZSM-5 Catalyst for the Cracking of Low-Density Polyethylene”, *ChemSusChem*, 12 (2019) 633-638, <https://doi.org/10.1002/cssc.201802190>
- [10] Y. Kima, J. Jeong, S. Ryu, H. W. Lee, J. S. Jung, M. Z. Siddiqui, S. Jung, J. Jeon, J. Jae, Y. Park, “Catalytic pyrolysis of wood polymer composites over hierarchical mesoporous zeolites”, *Energy Convers. Manag.*, 195 (2019) 727-737, <https://doi.org/10.1016/j.enconman.2019.05.034>
- [11] D. P. Serrano, J. Aguado, J. M. Escola, “Developing Advanced Catalysts for the Conversion of Polyolefinic Waste Plastics into Fuels and Chemicals”, *ACS Catal.* 2 (2012) 1924-1941, <https://doi.org/10.1021/cs3003403>
- [12] M. Bertero, J. R. Garcia, M. Falco, U. Sedran, “Hydrocarbons from Bio-oils: Performance of the Matrix in FCC Catalysts in the Immediate Catalytic Upgrading of Different Raw Bio-oils”, *Waste Biomass Valor* 8 (2017) 933-948, <https://doi.org/10.1007/s12649-016-9624-z>

Chapter 1

- [13] C.L. Thomas, "CHEMISTRY OF CRACKING CATALYSTS", *Ind. Eng. Chem.*, 41, 11 (1949) 2564-2573, <https://doi.org/10.1021/ie50479a042>
- [14] S. Kotre, H. Knözinger and B. C. Gates, "The Haag–Dessau mechanism of protolytic cracking of alkanes", *Micropor. Mesopor. Mater.*, 35–36 (2000) 11–20, [https://doi.org/10.1016/S1387-1811\(99\)00204-8](https://doi.org/10.1016/S1387-1811(99)00204-8)
- [15] A. Ishihara, H. Negura, T. Hashimoto, H. Nasu, "Catalytic properties of amorphous silica-alumina prepared using malic acid as a matrix in catalytic cracking of n-dodecane", *Appl. Catal. A Gen.* 388 (2010) 68-76, <https://doi.org/10.1016/j.apcata.2010.08.027>
- [16] A. Ishihara, "Preparation of Amorphous Silica-Alumina Using the Sol–Gel Method and its Reactivity for a Matrix in Catalytic Cracking", *Catal. Surv. Asia*, 16 (2012) 36-47, <https://doi.org/10.1007/s10563-012-9132-5>
- [17] T. Prasomsri, R. E. G. Tailleux, W. E. Alvarez, T. Sooknoi, D. E. Resasco, "Conversion of 1-tetralone over HY zeolite: An indicator of the extent of hydrogen transfer", *Appl. Catal. A Gen.* 389 (2010) 140-146, <https://doi.org/10.1016/j.apcata.2010.09.019>
- [18] D. Wallenstein, R.H. Harding, "The dependence of ZSM-5 additive performance on the hydrogen-transfer activity of the REUSY base catalyst in fluid catalytic cracking", *Appl. Catal. A Gen.*, 214 (2001) 11-29, [https://doi.org/10.1016/S0926-860X\(01\)00482-3](https://doi.org/10.1016/S0926-860X(01)00482-3)
- [19] B. C. Gates, J. R. Katzer, G.C. A. Schuit, "CHEMISTRY OF CATALYTIC PROCESSES" *Mcgraw-Hill College* (1979) 1-464, <https://doi.org/10.1002/aic.690250427>
- [20] Q. Yu, H. Sun, H. Sun, L. Li, X. Zhu, S. Ren, Q. Guo, B. Shen, "Highly mesoporous IM-5 zeolite prepared by alkaline treatment and its catalytic cracking performance", *Micropor. Mesopor. Mater.*, 273 (2019) 297-306, <https://doi.org/10.1016/j.micromeso.2018.08.016>
- [21] S. Al-Khattaf, H. de Lasa, "The role of diffusion in alkyl-benzenes catalytic cracking", *Appl. Catal. A Gen.*, 226 (2002) 139-153, [https://doi.org/10.1016/S0926-860X\(01\)00895-X](https://doi.org/10.1016/S0926-860X(01)00895-X)
- [22] O. Bayraktar, E. L. Kugler, "Effect of pretreatment on the performance of metal-contaminated fluid catalytic cracking (FCC) catalysts", *Appl. Catal. A Gen.*, 260 (2004) 119-124, <https://doi.org/10.1016/j.apcata.2003.10.012>
- [23] P. Bai, M. Xie, U. J. Etim, W. Xing, P. Wu, Y. Zhang, B. Liu, Y. Wang, K. Qiao, Z. Yan, "Zeolite Y Mother Liquor Modified γ -Al₂O₃ with Enhanced Brønsted Acidity as Active Matrix to Improve the Performance of Fluid Catalytic Cracking Catalyst", *Ind. Eng. Chem. Res.*, 57, 5 (2018) 1389-1398, <https://doi.org/10.1021/acs.iecr.7b04243>
- [24] M. Xie, Y. Li, U. J. Etim, H. Lou, W. Xing, P. Wu, X. Liu, P. Bai, Z. Yan, "Enhanced Catalytic Performance of the FCC Catalyst with an Alumina Matrix Modified by the Zeolite Y Structure-Directing Agent", *Ind. Eng. Chem. Res.*, 58, 14 (2019) 5455-5463, <https://doi.org/10.1021/acs.iecr.8b04890>
- [25] E. C. Souza, M. M. Pereira, Y. L. Lam, E. Morgado Jr., L. S. Chinelatto Jr., "Aluminum

Chapter 1

- phosphate as active matrix of fluid catalytic cracking catalysts: Y zeolite stabilization”, *Appl. Catal. A Gen.*, 619 (2021) 118156, <https://doi.org/10.1016/j.apcata.2021.118156>
- [26] S. M. Auerbach, K. A. Carrado, P.K. Dutta, “Handbook of Zeolite Science and Technology”, *CRC Press* (2003) 1-1204, <https://doi.org/10.1201/9780203911167>
- [27] S. M. Csicsery, “Shape-selective catalysis in zeolites”, *Zeolites*, 4 (1984) 202-213, [https://doi.org/10.1016/0144-2449\(84\)90024-1](https://doi.org/10.1016/0144-2449(84)90024-1)
- [28] E. G. Derouane, Z. Gabelica, “A novel effect of shape selectivity: Molecular traffic control in zeolite ZSM-5”, *J. Catal.*, 65 (1980) 486-489, [https://doi.org/10.1016/0021-9517\(80\)90328-0](https://doi.org/10.1016/0021-9517(80)90328-0).
- [29] International Zeolite Association, “Database of Zeolite Structures”, <http://www.iza-structure.org/databases/>, accessed May 2021
- [30] David Levy Marcos Zaya, “The Sol-Gel Handbook”, Wiley-VCH (2015) 1-1508, <https://doi.org/10.1002/9783527670819>
- [31] A. Ishihara, H. Oono, T. Hashimoto, H. Nasu, “Preparation of SiO₂ and SiO₂-Al₂O₃ catalysts by gel skeletal reinforcement using hexamethyldisiloxane (HMDS) and acetic anhydride and aluminum tri-sec-butoxide (ASB) systems and elucidation of their catalytic cracking properties as matrices”, *Micropor. Mesopor. Mater.*, 233 (2016) 163-170, <http://dx.doi.org/10.1016/j.micromeso.2016.01.025>
- [32] S. Tsuge, H. Ohtani, W. Chuichi, “Pyrolysis - GC/MS Data Book of Synthetic Polymers: Pyrograms, Thermograms and MS of Pyrolyzates”, Elsevier (2011) 1-390, <https://doi.org/10.1016/B978-0-444-53892-5.10001-X>

Chapter 2

Preparation of β -zeolite mixed catalysts using alumina and titania matrices modified by silication of gel skeletal reinforcement and their reactivity for catalytic cracking of *n*-dodecane

Novel alumina and titania modified by silica in surface were prepared by applying the gel skeletal reinforcement (GSR) method using hexamethyldisiloxane-acetic anhydride system to alumina-gel and titania-gel formed by the sol-gel method. When NH_3 -TPD of silica-modified alumina was measured, it was confirmed that new acid sites were observed in the high temperature range from 400 °C to 600 °C. Regarding silica-modified titania, the thermal stability of the anatase phase was observed in the calcination at 600 °C for 3 h, and the complex oxides with different physical properties were prepared. The mixed catalysts with these silica-modified alumina and titania and β -zeolite were prepared, and their reactivity in catalytic cracking of *n*-dodecane was investigated using a fixed bed reactor at 500 °C. β -zeolite-GSR-silica-modified alumina mixed catalysts was found to have higher conversion and improved gasoline fraction selectivity compared to the cases with the use of β -zeolite single and alumina without GSR modification.

2.1 Introduction

Alumina has various crystalline polymorphs. Among them, γ -alumina is used for catalysts and catalyst supports because it has a high specific surface area [1-4]. Titania is also known to have some polymorphisms, anatase has structural metastability at low temperature, rutile is thermodynamically stable, and brookite is produced only under hydrothermal conditions [5]. Their applications are diverse, and in the field of catalysts, photocatalysts are among the most widely used [6-11].

The sol-gel method is a method for producing an amorphous or polycrystalline body by starting from a solution of a metal organic or inorganic compound [12-15]. Specifically, it is produced by heating a porous gel formed through a sol in which fine particles of a metal oxide or

Chapter 2

a hydroxide by hydrolysis and polymerization is dispersed in a solvent [1,3,12-15]. The inorganic oxides produced by this method often have chemical, physical and thermal properties different from those of oxides obtained by other synthetic methods [12-14]. In addition, they can be synthesized at low temperature, do not contain impurities, and has high homogeneity [13,14]. The skeleton of the gel formed by the sol-gel method causes a decrease in pore diameter and pore volume due to shrinkage by drying stress and condensation of surface hydroxy groups in the subsequent drying and calcining steps [16,17]. In order to reduce these influences, there is a drying method using a subcritical and supercritical fluid [18-21]. However, since this method uses these fluids, there are problems in safety and cost. Thus, our research group has reported that the gel skeletal reinforcement (GSR) method can be used to reinforce the skeleton of the silica-gel produced by the sol-gel method to reduce gel contraction and maintain a large pore size and pore volume [17,22-27]. In the previous studies, GSR method was applied to produce silica having large pore size and pore volume which can be used as a matrix in catalytic cracking [17]. On the other hand, we used alumina and titania prepared by the sol-gel method in order to evaluate their reactivity as matrices in catalytic cracking [28]. However, there are no studies where the GSR method was applied to preparation of silica-modified alumina and titania to discover the new reactivity of catalysts and catalyst supports. Further, it is known that when alumina is doped with silica, it has excellent thermal stability and hydrothermal stability [29], and that when silica or a derivative is added to titania, the phase transition from the anatase phase to the rutile phase can be suppressed [30-32]. Therefore, if the phase transition to the rutile phase can be suppressed by silica covering by the GSR method, it is expected to produce a novel silica-covered titania composite having new physical properties, especially heat resistance.

In this chapter, to the preparation of alumina and titania by the sol-gel applied GSR method with the solution of hexamethyldisiloxane-acetic anhydride as a reinforcing agent system and investigated the change that silica covering by GSR method brings about to the physical properties of alumina and titania. Further, using these oxides as matrices, β -zeolite-containing mixed catalysts were prepared and were used for catalytic cracking of *n*-dodecane.

2.2 Preparation of β -zeolite mixed catalysts using alumina and titania matrices modified by silication of gel skeletal reinforcement

This experiment was begun with preparation of β -zeolite mixed catalysts using alumina and titania matrices modified by silication of GSR. First, alumina and titania were prepared by the

Chapter 2

sol-gel applied GSR method. Second, those matrices were mixed with binder and β -zeolite to fabricate β -zeolite mixed catalysts. Third, the catalytic activity of those catalyst was tested by catalytic cracking of *n*-dodecane.

Reagents used for the preparation of matrices were as follows: For alumina and titania source, aluminum tri-*sec*-butoxide (ASB, $\text{Al}[\text{OCH}(\text{CH}_3)\text{CH}_2\text{CH}_3]_3$, Tokyo Chemical Industry Co., Ltd.) and titanium isopropoxide (TIP, $\text{Ti}[\text{OCH}(\text{CH}_3)_2]_4$, Wako Pure Chemical Corp.) were used, respectively. 2-Butanol (2-BuOH; $\text{CH}_3\text{CH}_2\text{CH}(\text{OH})\text{CH}_3$) and 2-propanol (2-PrOH; $\text{CH}_3\text{CH}(\text{OH})\text{CH}_3$) were used for solvents in alumina and titania preparation, respectively. As a reagent of GSR, hexamethyldisiloxane (HMDS; $\text{O}(\text{Si}(\text{CH}_3)_3)_2$, Nacalai Tesque) and acetic anhydride (AA; $(\text{CH}_3\text{CO})_2\text{O}$, Nacalai Tesque) were mixed. For the preparation of mixed catalysts, β -zeolite (HSZ-940HOA; $\text{SiO}_2/\text{Al}_2\text{O}_3 = 37 \text{ mol/mol}$, Tosoh) and a binder of alumina-sol (Cataloid AP-1; JGC Catalysts and Chemicals) were used.

2.2.1 Preparation of matrices by sol-gel and gel skeletal reinforcement method

The GSR-silica-modified alumina and titania matrices were prepared according to the flow chart shown in Figures 2.1 and 2.2. A typical procedure can be stated as follows [17,28]: Added

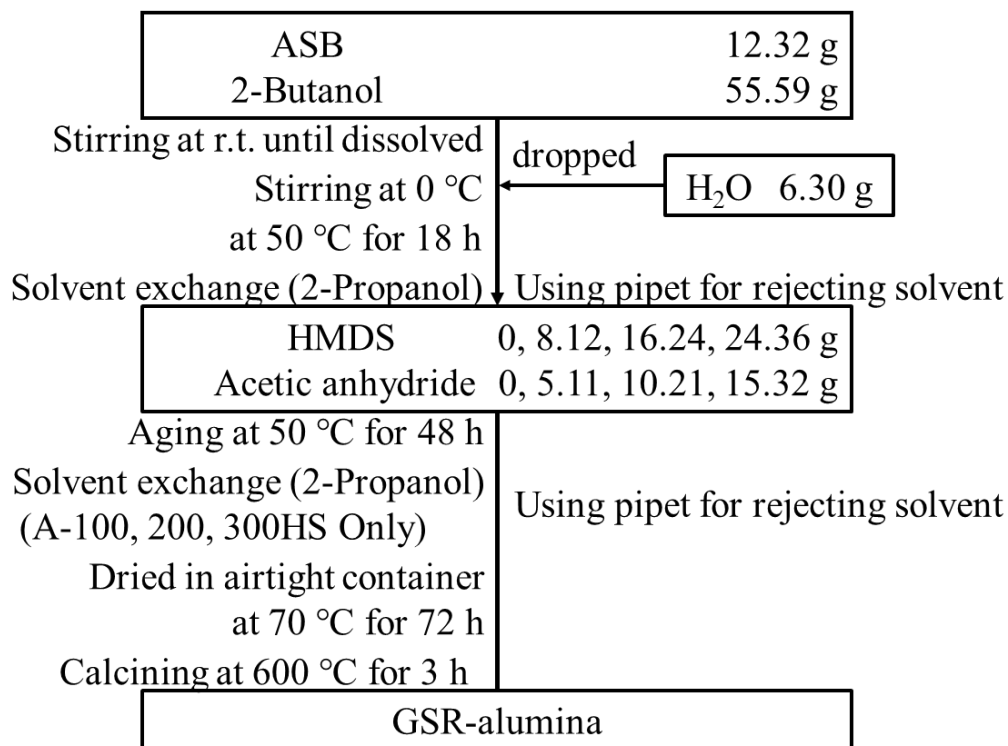


Figure 2.1 Flowchart for preparation of GSR-silica-modified alumina.

Chapter 2

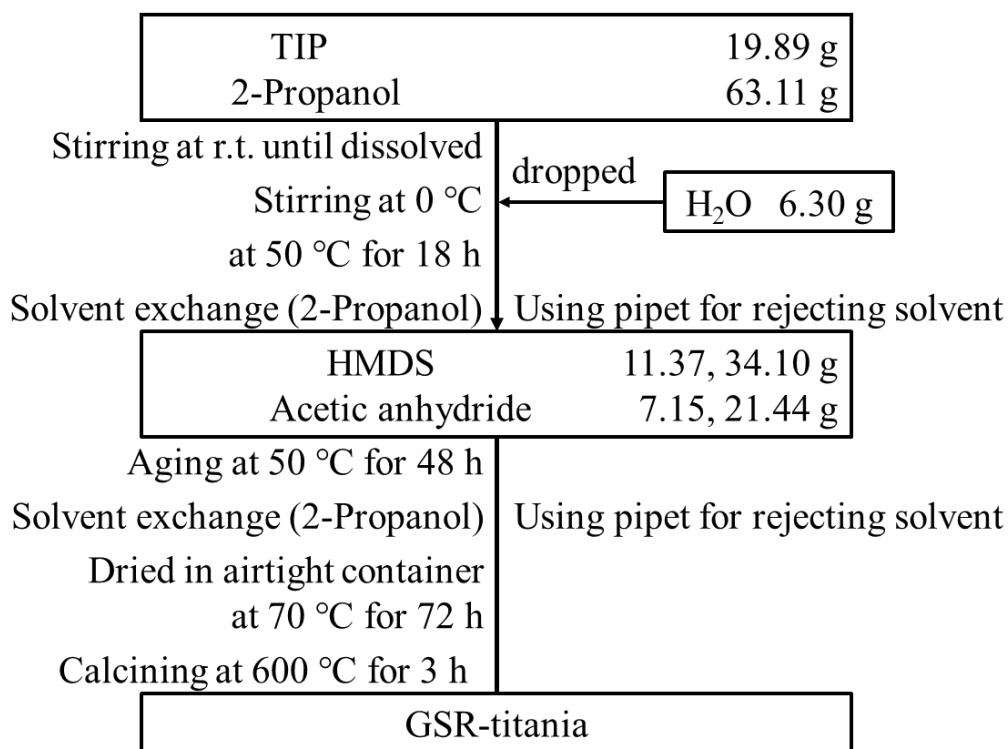


Figure 2.2 Flowchart for preparation of GSR-silica-modified titania.

2-BuOH and ASB (ASB : 2-BuOH = 1:15 (molar ratio)) to a 200 mL beaker containing a stir bar and stirred in an ice bath. Stirring was continued, and after 30 min, ion-exchanged water (ASB: Ion exchanged water = 1:7 (molar ratio)) was added. After the stirrer was stopped, the temperature was raised to 50 °C and the mixture could stand for 18 h. After 18 h, in order to remove water from the pores of the gel, solvent exchange with 2-PrOH was performed according to the procedure shown below. 2-PrOH (30 mL, 50 °C) was added and allowed to stand, and after 5 min, the solvent was removed with a Pasteur pipette. This operation was performed 5 times in total. The gel after the solvent exchange was immersed in the silication agent (Mixed solution of HMDS and AA, ASB: HMDS = 1: 1, 2 or 3, HMDS: AA = 1:1 mol/mol) prepared in a PFA sealed container, and allowed to stand in an oven set at 50 °C for 48 h. The solvent was exchanged again, and the sealed container with reinforced-alumina gel was kept in an oven at 70 °C for 72 h. After that, the gel was calcined at 600 °C for 3 h (2.5 °C/min, dried air 600 mL/min). The calcined material was used as a matrix for catalyst preparation. Table 2.1 shows the molar ratios of the reagents used to prepare each matrix. Alumina without using the GSR reagent was also prepared by the same method except for using the GSR reagent. As for the sample naming, for example, the name of matrix is shown as A-100HS, A is alumina derived from ASB, 100 means HMDS/TEOS molar ratio×100 and HS shows HMDS used as a silication of GSR.

Table 2.1 Sample name and composition of solution for preparation of GSR-alumina and titania.

Sample name	Molar ratio			Molar ratio HMDS for aging/ ASB or TIP of gel source
	ASB or TIP	2-BuOH	H ₂ O	
A-0HS	1	15	7	0
A-100HS	1	15	7	1.0
A-200HS	1	15	7	2.0
A-300HS	1	15	7	3.0
T-100HS	1	15	7	1.0
T-300HS	1	15	7	3.0

GSR-silica-modified titania was prepared using same procedure except for using TIP and 2-propanol. When TIP was used, T is shown in a name of a sample. Titania matrix was also prepared by the sol-gel method using TIP and malic acid as a template and an acid catalyst. Calcination temperature was 550 °C or 600 °C. A sample name of the sol-gel prepared titania includes "T", "600" and "+MA", which mean titania, calcined temp. and malic acid, respectively.

2.2.2 Preparation of mixed catalyst with β -zeolite

Mixed catalysts were prepared using matrix (58 wt.%) denoted in 2.2.1., zeolite (26 wt.%) and alumina-sol (16 wt%) as binder. The mixture was kneaded in a mortar while dropping about 30 drops of 2-PrOH with a Pasteur pipette little by little. A clay-like lump was pelletized into a cylindrical shape having a diameter of 0.5 mm by a sodium press (Natrium press, NP-1; Sanki Seisakusho Co., Ltd.) and calcined under the same conditions as the matrices. The mixture after calcination was crushed in a mortar and sieved, and the catalyst having a particle size of 125–355 μm was used for reaction experiments and characterization. The name of a mixed catalyst was expressed as MAT(matrix name)- β (37).

2.3 Characterization of catalyst samples

2.3.1 N₂ adsorption and desorption measurement

Nitrogen adsorption/desorption measurements were performed to investigate the surface area, pore volume and pore distribution of the matrix and mixed catalyst. The sample was put in

Chapter 2

a sample tube so that the amount was about 40 mg, and the pretreatment was performed using a BELPREP-vac II (MicrotracBEL Corp.) at 350 °C for 3 h under vacuum. Then, the adsorption and desorption isotherms of nitrogen at 77 K were obtained by BELSORP-mini II (Microtrac BEL Corp.). The total surface area (SA) was estimated by the Brunauer-Emmett-Teller (BET) method. Total pore volume (TPV) was estimated by the adsorption in the range from 0 to 0.99 of p/p_0 , and average pore diameter (APD) was calculated by values of BET-SA and TPV. The surface area, pore volume, pore diameter and pore distribution of mesopores with more than 3.3 nm of pore size were calculated by the Barrett-Joyner-Hallenda (BJH) method.

2.3.2 X-ray diffraction measurement

X-ray diffraction (XRD) measurement was performed using Ultima IV (Rigaku Corp.) in order to investigate the crystalline state of the matrix and the catalyst powder. The measurement sample (about 0.1 g) was pressed into a glass sample holder using a slide glass to smooth the measurement surface and set on the device. CuK α ray ($\lambda = 1.5405$ nm) monochromated with Ni filter was used as the X-ray source, and the measurement was performed under the following conditions; the tube voltage-tube current set to 40 kV-20 mA, sampling width: 0.02, scattering slit: $2/3^\circ$, divergence slit: $2/3^\circ$, receiving slit: 0.45 nm, scan speed: $4^\circ/\text{min}$, scan range: $2\theta = 3-70^\circ$.

2.3.3 X-ray fluorescence measurement

An energy dispersive X-ray fluorescence analyzer (EDX-720, Shimadzu Corp.) was used to examine the ratio of elements contained in the prepared matrix. The powdery sample was filled in a sample container in which a sample holding film was set. The measurement was performed in helium atmosphere, and semi-quantitative analysis was performed to evaluate the amounts of SiO₂ and Al₂O₃ or TiO₂.

2.3.4 NH₃ adsorption and desorption

In order to investigate the acidity of the mixed catalyst, ammonia adsorption/desorption measurement was performed by the ammonia pulse method. The mixed catalyst (40 mg) was packed in the center of a stainless tube reactor to be sandwiched between quartz wool (Fine, 2–6 μm , Tosoh Corp.). Then, under a He flow of 30 mL/min, the temperature was raised to 600 °C at a rate of 10 °C/min and held for 3 h. The temperature of the catalyst layer was lowered to 100 °C, and 1.0 mL/pulse of ammonia was introduced into the catalyst layer to adsorb ammonia on the catalyst. The temperature was raised again to 650 °C at a heating rate of 10 °C/min to desorb ammonia from the catalyst. Ammonia was detected using a gas chromatograph thermal conductivity detector (GC-TCD; GC-8A, Shimadzu Corp.). The measurement conditions are shown below. INJ/DET: 170 °C, COL: 140 °C, ATTN: 16, current: 100 mA, carrier gas: He,

column flow rate: 50 mL/ min.

2.4 Activity test of catalyst samples

2.4.1 Catalytic cracking of *n*-dodecane

Reaction apparatus of catalytic cracking of *n*-dodecane is shown in Fig. 1. The mixed catalyst (1.0 g) was sandwiched with quartz wool and quartz sand (Wako Pure Chemical Corp.) and packed in a fixed bed down flow reactor (300 mm length and 8 mm internal diameter). While introducing nitrogen into the reactor at about 30 mL/min, the temperature was raised to 500 °C at 5 °C/min. After stopping the nitrogen flow, *n*-dodecane (CH₃(CH₂)₁₀CH₃, Nacalai Tesque, Inc.) was introduced into the reactor at about 1.3 mL/min for 80 s, and nitrogen was again flowed to the reactor at about 30 mL/min for 30 min. The gas products were collected together with nitrogen in a Tedler bag. The mixed solution of raw material and liquid product was trapped using ethanol at -50 °C for the first 15 min and water at 15 °C for the next 15 min and collected in a test tube. After the reaction was completed, the catalyst packed in the reactor was recovered for the measurement of coke weight by TGA measurement described later.

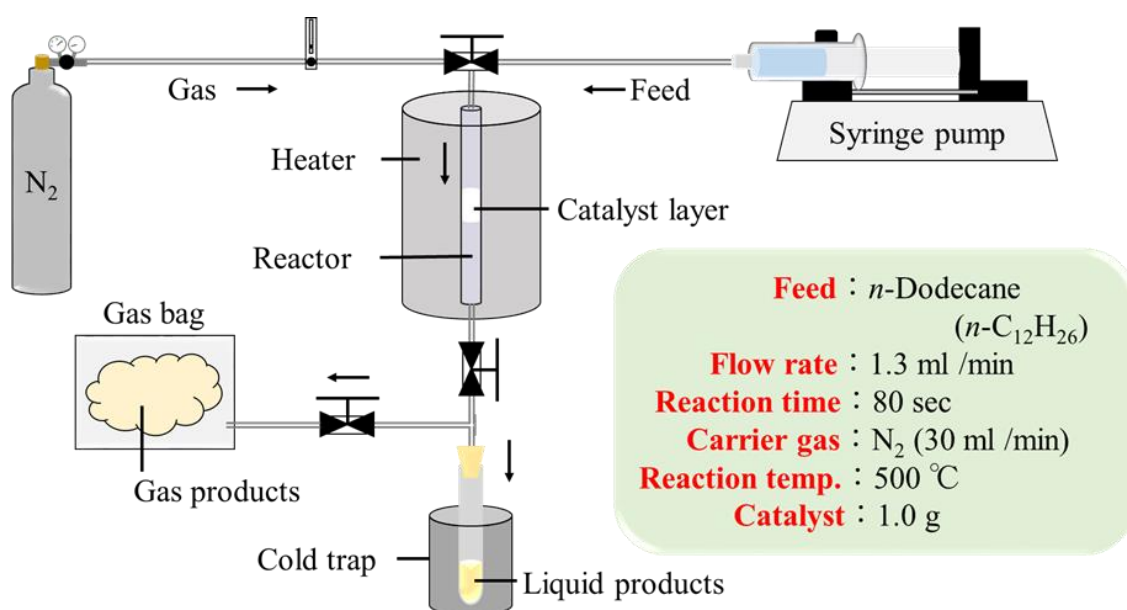


Figure 2.3 Reaction apparatus of catalytic cracking.

2.4.2 Measurement of gas and liquid products by GC-FID

After the catalytic cracking reaction, the gas and liquid products were quantitatively analyzed

Chapter 2

using a GC (GC-2014; Shimadzu Corp.) equipped with a hydrogen flame detector (FID). The measurement conditions are shown below: Injection temp.: 250 °C, injection mode: carrier gas: He, control mode: press., press.: 100.6 kPa, total flow rate: 170.8 mL/ min, column flow rate: 0.86 mL/ min, line speed: 16.8 cm/ sec, purge flow rate: 4.0 mL/ min, split ratio: 200, equilibrium time: 3.0 min, Detector temp.: 320 °C, column: BP-1, column length: 60 m, column inner diameter: 0.25 mm, thickness of liquid phase: 50 µm, initial column temp.: 0 °C (16 min), heating rate: 2 °C/ min (114 min), final temp.: 228 °C. Prior to product analysis, mixed standard gas (contains 1 vol.% each of CH₄, C₂H₆, C₃H₈, *i*-C₄H₁₀, *n*-C₄H₁₀ and CO₂, and the balance is N₂, GL Sciences Inc.) was analyzed, It was used to calibrate the detection intensity of FID. The mixed standard gas (30 µL) and the gas product (30 µL) were injected using a 100 µL gas-tight syringe, and 0.2 µL of the liquid product was injected using an autosampler (AOC-20i; Shimadzu Corp.) and measured. The product peak obtained by the GC measurement was identified from the retention time. For details of the analysis method, refer to the previous report [17]. The coke amount of the catalyst after the reaction was calculated by thermogravimetric analysis (DTG-60AH, Shimadzu Corp.). The measurement conditions are as follows. Sample: 10 mg, cell: Al cell, atmosphere: O₂ (100 mL/ min), initial temp.: 25 °C, heating rate: 10 °C/ min, final temp.: 600 °C, hold time: 0 min (600 °C).

2.5 Results and discussion

In this section, results of matrices and mixed catalysts characterization (N₂ adsorption/desorption measurement, XRD, XRF, NH₃-TPD) are presented. The catalytic activity of each mixed catalyst is also discussed.

2.5.1 Characterization of matrices and mixed catalysts

The XRD measurement results of the GSR-silica-modified alumina matrix are shown in Figure 2.4. In Figure 2.4, no peak indicating a crystalline phase was observed, and it was confirmed that all were amorphous. Figure 2.5 show the results of XRD measurement of the mixed catalysts using these matrices. In Figure 2.5, only the peak of β-zeolite around $2\theta = 23^\circ$ was confirmed, and it was confirmed that the mixed catalyst was prepared by maintaining the amorphous state of the matrix and the crystal structure of β-zeolite. Figure 2.6 shows the XRD measurement results for the titania matrix. In the matrix prepared by the GSR method, only peaks peculiar to the anatase phase were seen. However, rutile phase peak was observed in addition to the anatase phase peak in T-600+MA prepared by using malic acid and calcined at 600 °C. On the other hand, in T-550+MA [28] calcined at 550 °C with the addition of malic acid, the peak of rutile phase was not observed and only the peak of anatase phase was observed. Therefore, it is

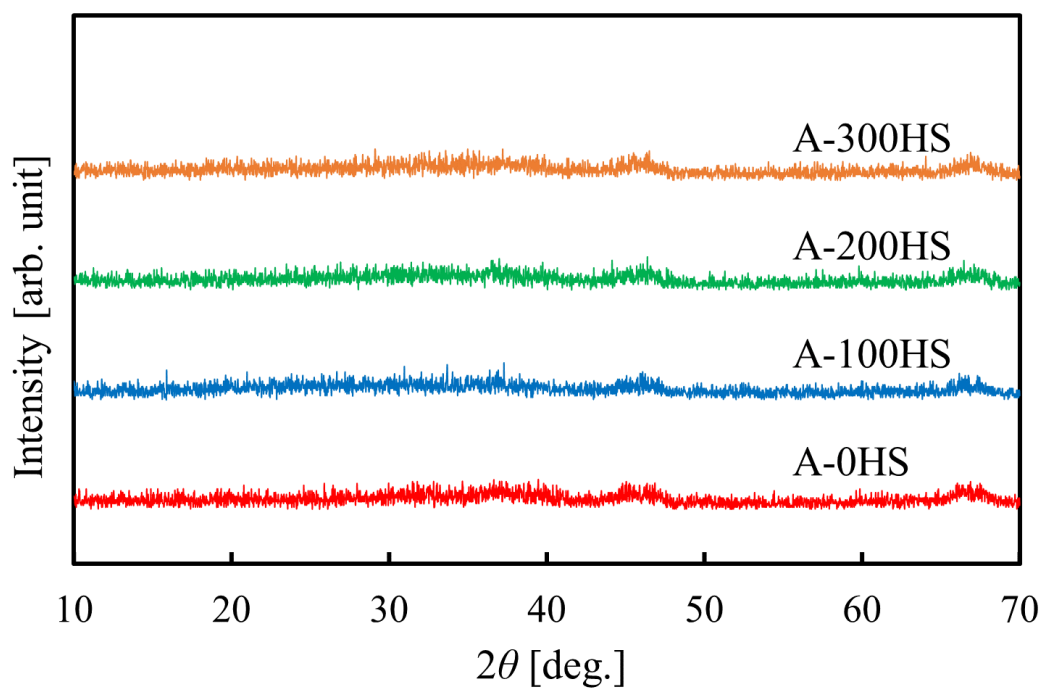


Figure 2.4 XRD patterns of GSR-silica-modified aluminas and alumina without GSR-silica modification.

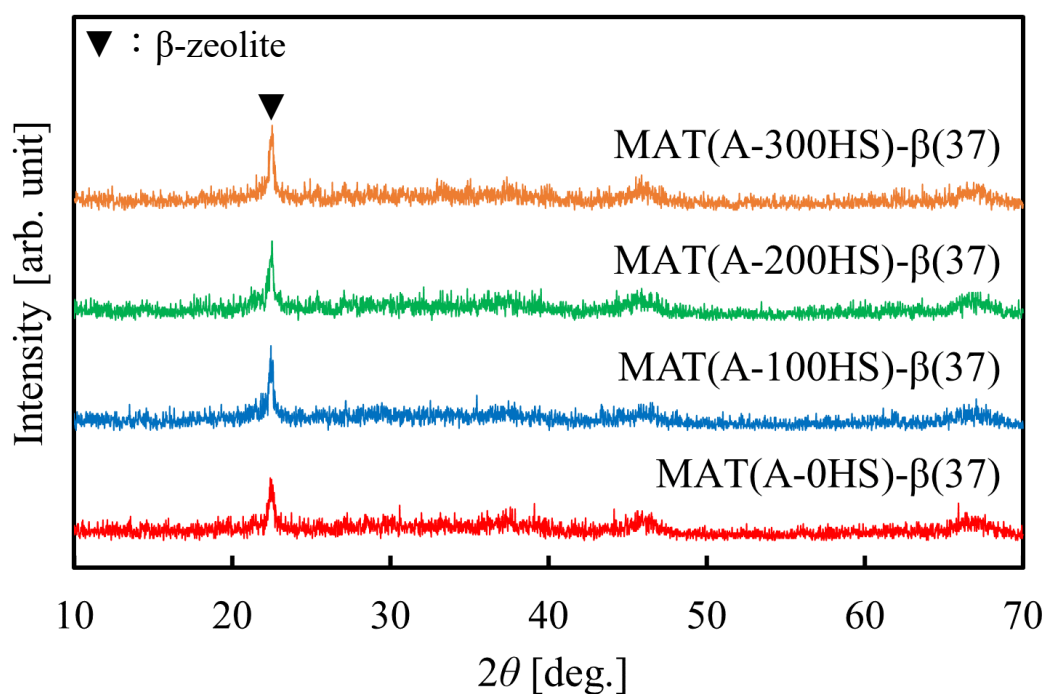


Figure 2.5 XRD patterns of the mixed catalysts using GSR-silica-modified alumina and unmodified alumina.

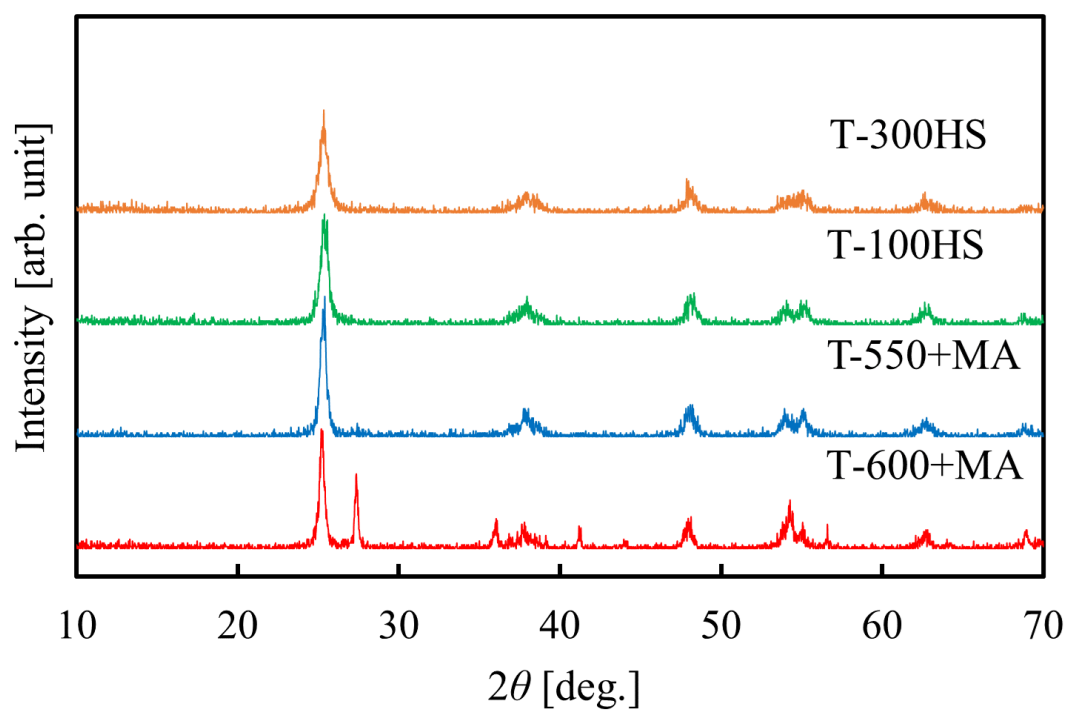


Figure 2.6 XRD patterns of GSR-silica-modified titania and titania prepared using the sol-gel method.

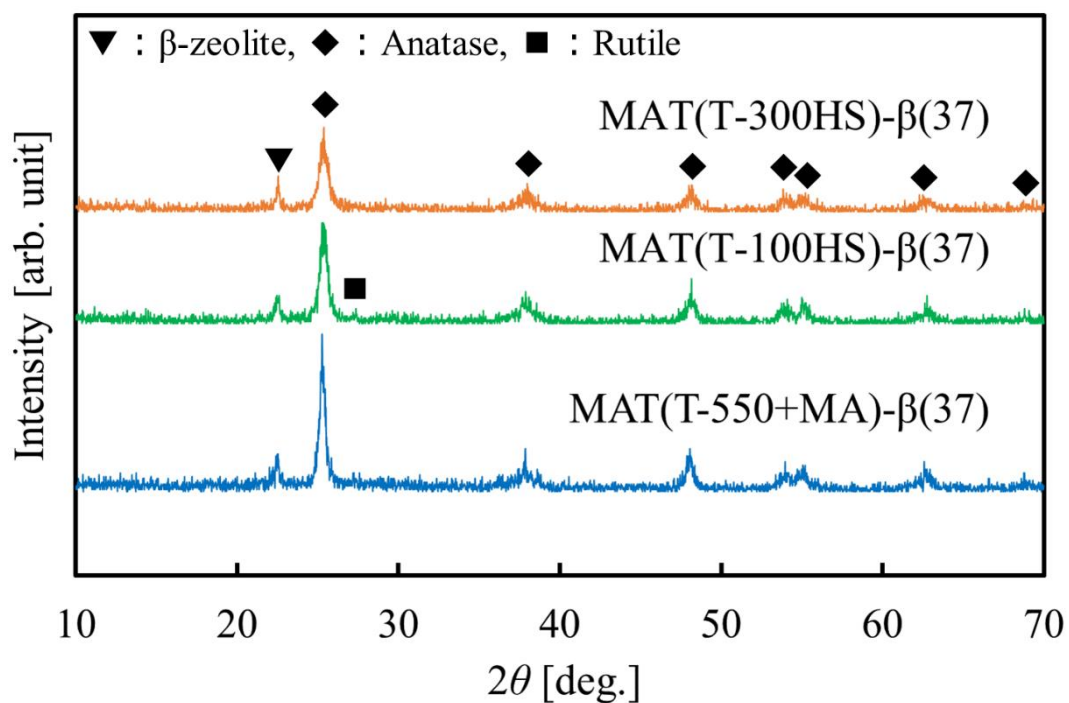


Figure 2.7 XRD patterns of the mixed catalysts using GSR-silica-modified titania and titania prepared using the sol-gel method.

Chapter 2

Table 2.2 Elemental analysis of GSR-silica-modified alumina and titania.

Sample name	Weight ratio (wt.%)		
	SiO ₂	Al ₂ O ₃	TiO ₂
A-100HS	1.94	98.06	-
A-200HS	1.77	98.23	-
A-300HS	1.82	98.18	-
T-100HS	1.35	-	98.65
T-300HS	1.05	-	98.95

considered that the titania matrix produced by GSR method using HMDS-AA system (T-100HS and T-300HS) has improved the thermal stability of titania crystal phase in the catalyst form compared to titania matrix produced without GSR-silica-modification because T-100HS and T-300HS were calcined at 600 °C. Figure 2.7 shows the XRD patterns of the mixed catalyst using each titania matrix. The peak of the anatase phase was observed in all the samples even after the mixed catalyst preparation process accompanied by calcination under the same conditions as the matrix preparation. However, extremely small peak around $2\theta = 27^\circ$ assigned to rutile phase was observed even in MAT(T-550+MA)- β (37) [28] and MAT(T-100HS)- β (37) probably because of twice calcination steps. Even when the titania matrix was used, the peak of β -zeolite was confirmed around $2\theta = 22^\circ$, indicating that the crystal structure of β -zeolite was maintained in the mixed catalysts. Table 2.2 shows the results of elemental analysis of matrix components by the X-ray fluorescence spectrometer. About 1-2 wt% of SiO₂ was detected in the produced alumina and titania matrix regardless of the amount of HMDS used.

Table 2.3, Table 2.4 show the pore characteristics of the matrices and the mixed catalysts by nitrogen adsorption/desorption measurement. The adsorption isotherm is shown in Figures 2.8–2.11, and the mesopore size distributions analyzed by the BJH method is shown in Figures 2.12–2.15. In the case of alumina, the distribution above 20 nm increased as the amount of the GSR reagent increased. There was no significant difference among A-100HS, A-200HS and A-300HS although the amount of HMDS further increased (Figure 2.12). In the case of titania, the distribution of mesopores was similar even when HMDS was increased (Figure 2.13). Table 2.3 summarizes BET-SA, TPV, APD, BJH-SA, BJH-PV and BJH-PD of alumina and titania matrices. The pore volume and pore diameter tended to increase as the amount of GSR reagent increased, but the pore volume reached the maximum in A-200HS. Since BET-SA and TPV are calculated for all pores and the BJH method are calculated only for mesopores, it is considered that, when a

Chapter 2

Table 2.3 Pore properties of matrices obtained by nitrogen adsorption and desorption measurement.

Matrix	BET Surface area (m ² /g)	Total Pore volume (cm ³ /g)	Average Pore diameter (nm)	BJH		
				Surface area (m ² /g)	Pore volume (cm ³ /g)	Pore diameter (nm)
A-0HS	317	2.06	26.0	392	2.10	21.2
A-100HS	234	1.12	19.1	215	1.13	10.5 (15.9)
A-200HS	218	1.66	30.5	196	1.74	38.0 (21.2)
A-300HS	189	1.47	31.1	159	1.48	38.0 (24.4)
T-600+MA	5	0.03	26.1	6	0.03	15.9 (10.5)
T-550+MA	58	0.21	14.5	77	0.22	13.8 (8.08)
T-100HS	64	0.22	13.9	80	0.22	5.46
T-300HS	77	0.21	10.7	89	0.21	4.24

Table 2.4 Pore properties of catalysts obtained by nitrogen adsorption and desorption measurement.

Catalyst	BET Surface area (m ² /g)	Total Pore volume (cm ³ /g)	Average Pore diameter (nm)	BJH		
				Surface area (m ² /g)	Pore volume (cm ³ /g)	Pore diameter (nm)
β(37)	406	0.31	3.14	24	0.07	3.30
MAT(A-0HS)-β(37)	366	1.20	13.1	261	1.15	21.2 (6.20)
MAT(A-100HS)-β(37)	326	0.88	10.8	195	0.83	6.20 (10.5)
MAT(A-200HS)-β(37)	320	0.98	12.2	187	0.94	6.20 (13.8)
MAT(A-300HS)-β(37)	301	0.83	11.0	152	0.77	6.20 (32.4)
MAT(T-550+MA)-β(37)	235	0.29	4.88	92	0.22	5.46 (10.5)
MAT(T-100HS)-β(37)	208	0.31	6.04	89	0.25	5.46
MAT(T-300HS)-β(37)	237	0.27	4.49	102	0.20	4.80

sample has similar values of the BET method and the BJH method, the proportion of mesopores would be higher. On the contrary, as β-zeolite has only a small amount of mesopores, a large difference appears between BET and BJH methods. From these results, it was found that GSR-silica-modified aluminas and titanias contained significant amounts of mesopores. Table 2.4 shows the pore characteristics of the mixed catalysts using alumina and titania matrices. Even after mixing with β-zeolite, the mesopores derived from the matrix were maintained, and there

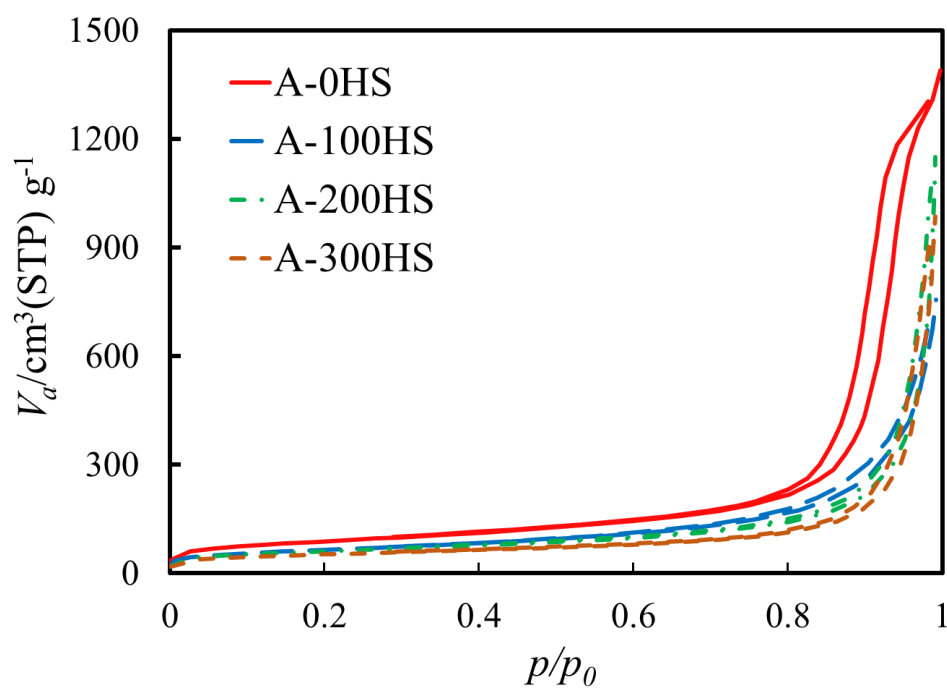


Figure 2.8 Nitrogen adsorption-desorption isotherms of GSR-silica-modified aluminas and alumina without GSR-silica modification.

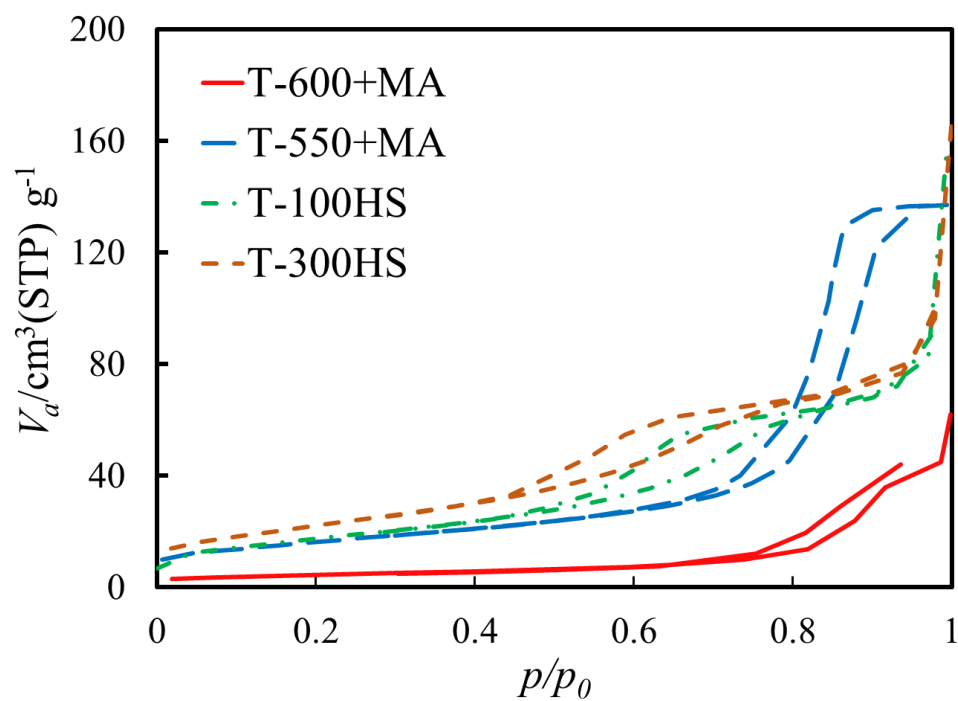


Figure 2.9 Nitrogen adsorption-desorption isotherms of GSR-silica-modified titania and titania prepared by the sol-gel method.

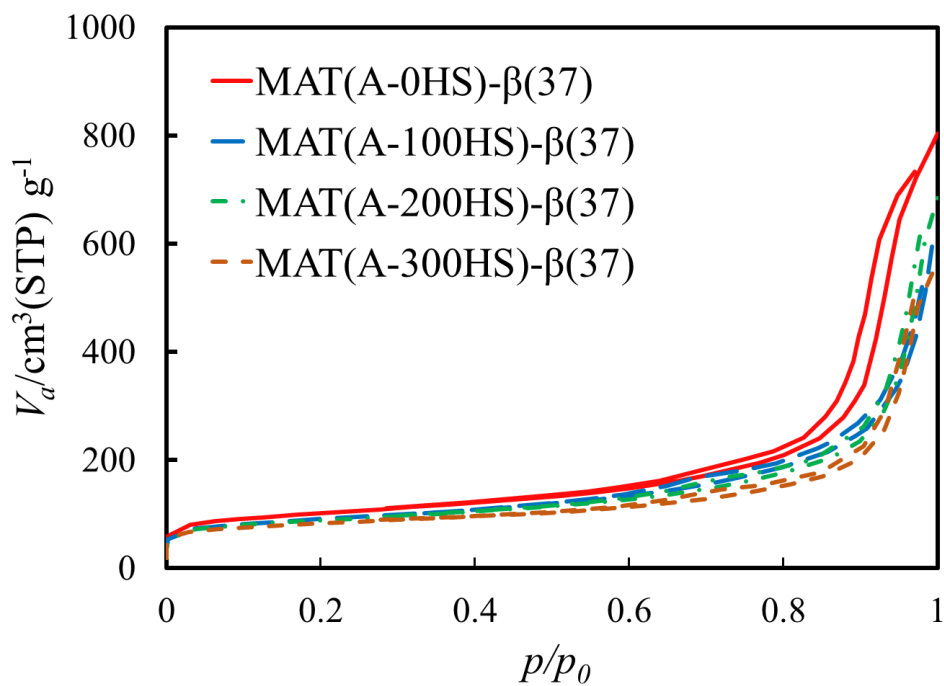


Figure 2.10 Nitrogen adsorption-desorption isotherms of GSR-silica-modified alumina β -zeolite mixed catalysts and an alumina β -zeolite mixed catalyst.

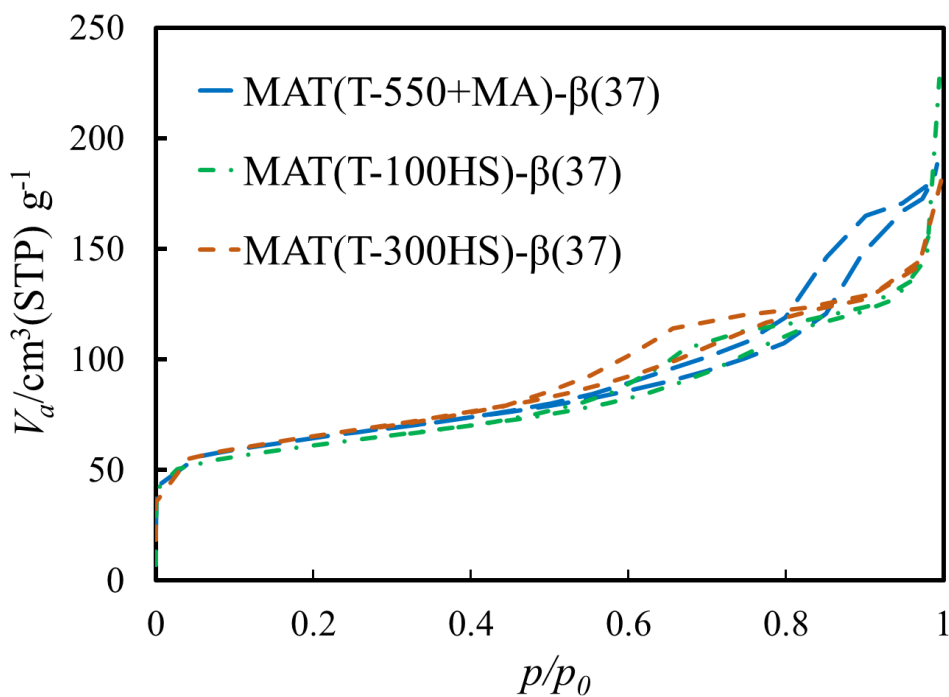


Figure 2.11 Nitrogen adsorption-desorption isotherms of GSR-silica-modified titania β -zeolite mixed catalysts and a titania β -zeolite mixed catalyst.

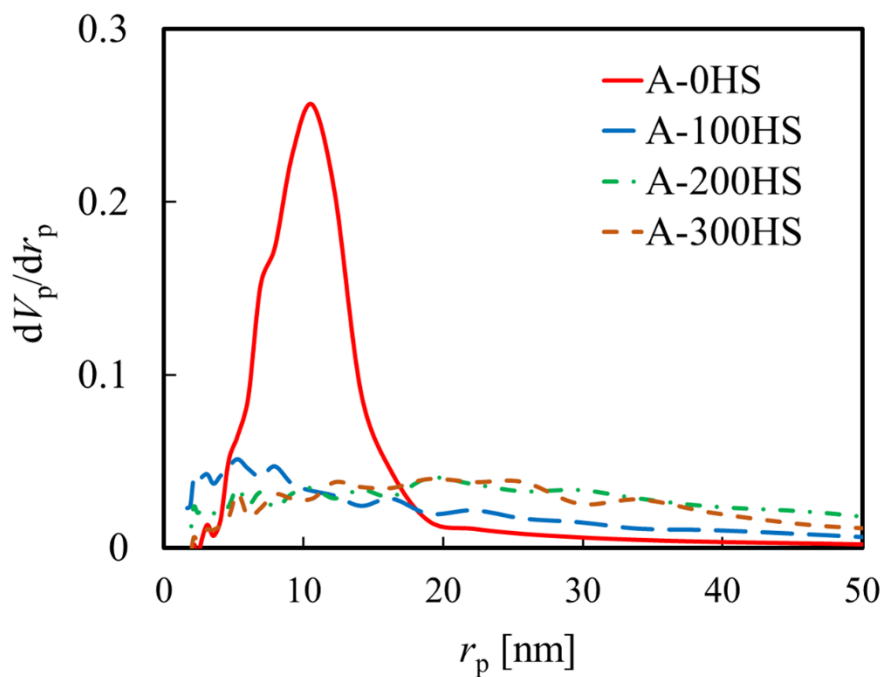


Figure 2.12 BJH pore-size distribution of GSR-silica-modified alumina and unmodified alumina.

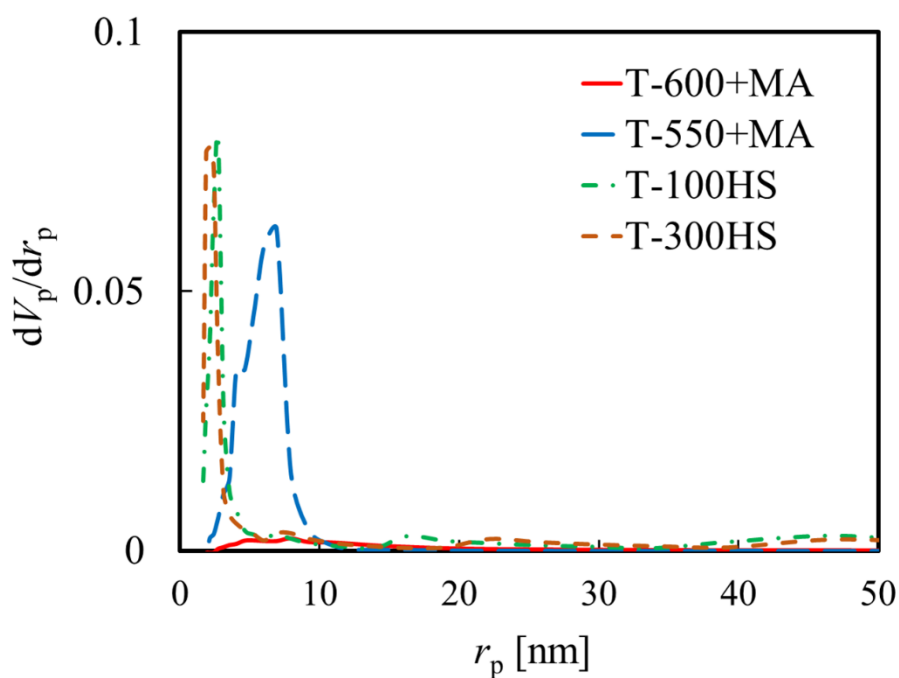


Figure 2.13 BJH pore-size distribution of GSR-silica-modified titania and titania prepared using the sol-gel method.

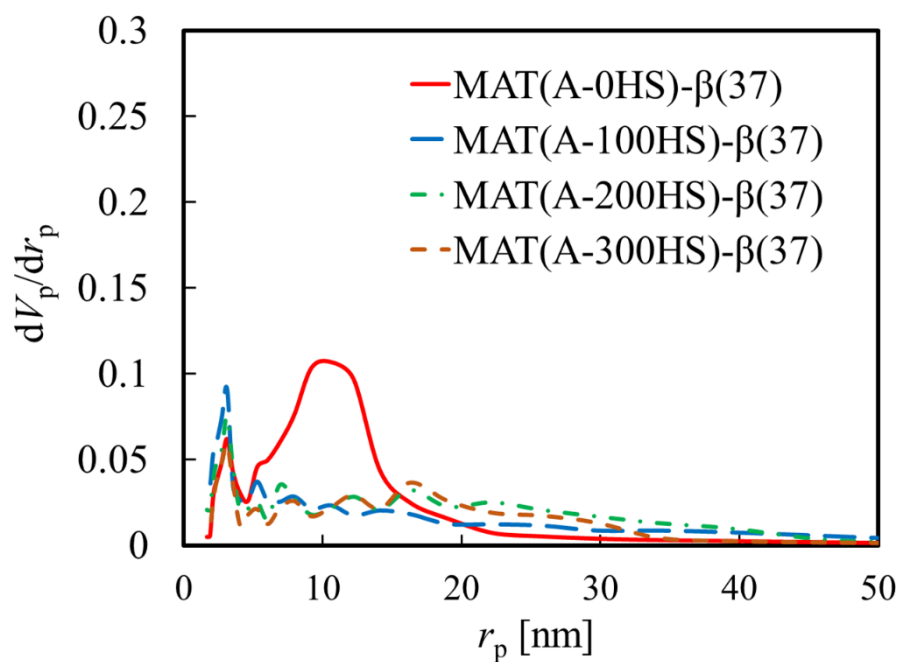


Figure 2.14 BJH pore-size distribution of the mixed catalysts using GSR-silica-modified alumina and unmodified alumina.

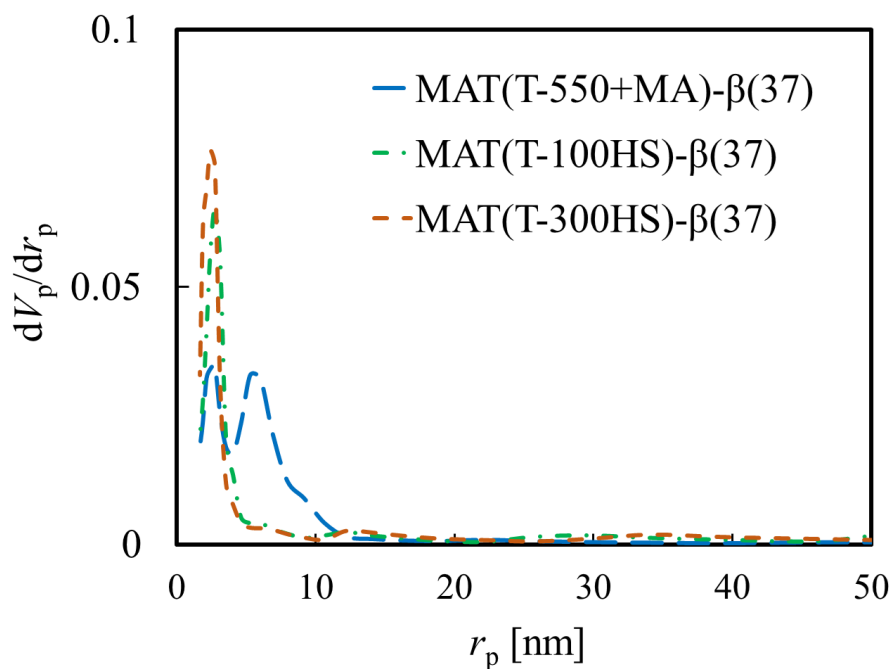


Figure 2.15 BJH pore-size distribution of the mixed catalysts using GSR-silica-modified titania and titania prepared using the sol-gel method.

Chapter 2

were very few effects of the amounts of GSR reagents on the pore properties.

Figure 2.16 shows the NH₃-TPD curve of the alumina mixed catalyst. Two clear peaks of β -zeolite single for the weak acid site and the strong acid site were observed around 260 °C and 390 °C, respectively. NH₃-TPD profiles for the alumina mixed catalysts exhibited somewhat broad peaks. When the amount of GSR reagents increased, the small peaks appeared at temperature higher than 390 °C. Larger the amount of the reagent was, at higher temperature the peaks appeared. The total amount of NH₃ desorbed was not so different each other, indicating that while the amounts of acid sites derived from β -zeolite were not changed by the addition of matrices, the small amounts of new acid sites would appear at the surface of matrices because the surface of alumina was modified by GSR-silica. Table 2.5 summarizes the amount of NH₃ desorbed on the mixed catalysts prepared and β -zeolite single. All the mixed catalysts contain only 26 wt% of β -zeolite. The amount of desorbed ammonia would change depending on the content of β -zeolite since the matrix may have only a few amounts of acid sites. However, the amounts of ammonia desorbed on the prepared alumina-mixed catalyst were about 40-66% of that for β -zeolite single, suggesting that there would be the formation of new acid sites other than β -zeolite [28]. Small NH₃-TPD peaks of the alumina mixed catalysts appeared at higher than 390 °C in Figure 2.16 and would correspond to the new acid sites.

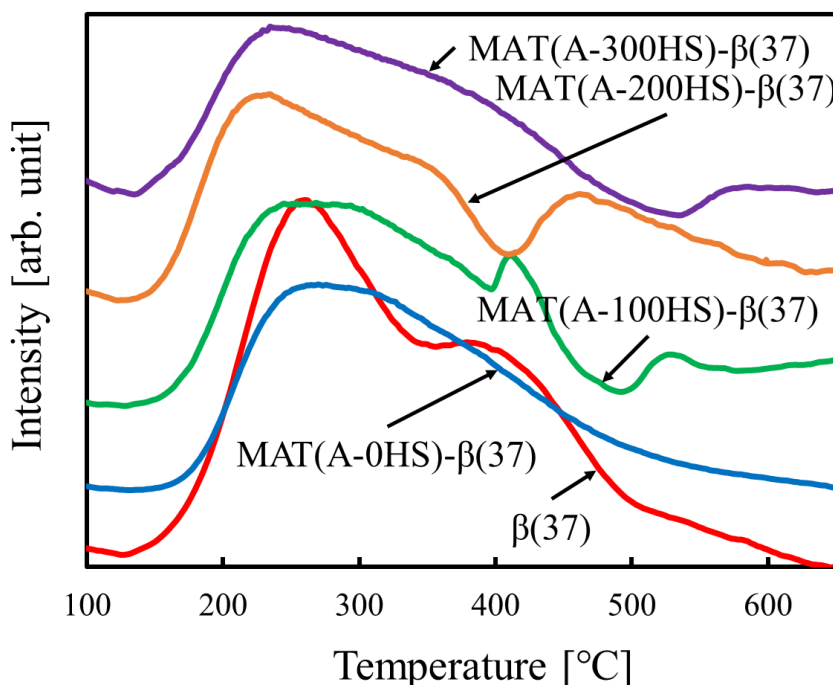


Figure 2.16 NH₃-TPD patterns of GSR-silica-modified alumina β -zeolite mixed catalysts and β -zeolite single.

Chapter 2

As described below, these alumina-mixed catalysts exhibited the superior activity to β -zeolite single in catalytic cracking of *n*-dodecane although the amount of desorbed NH_3 for the alumina mixed catalyst was smaller than that of β -zeolite single. MAT(A-100HS)- β and MAT(A-200HS)- β , which showed particularly high conversions, showed new small NH_3 -TPD peaks near 500 °C, suggesting that the new acid sites would have appeared at the surface of GSR-silica-modified alumina which play a decisive role to activate a hydrocarbon molecule. From these, it is considered that the primary cracking of *n*-dodecane may occur on the acid sites on the surface of the GSR-silica-modified alumina matrix contained in the mixed catalyst. Further, the presence of mesopores on the GSR-alumina matrices are advantageous for diffusion of intermediate molecules by the primary conversion, which would also progress the reaction effectively. As a result, the GSR-silica-modified alumina mixed catalyst exhibited the higher conversion than β -zeolite single.

The NH_3 -TPD curve of the titania mixed catalysts is shown in Figure 2.17. In contrast to the cases of the alumina mixed catalysts, no new peaks appeared and somewhat broad peaks appeared at the same peak position as that of β -zeolite single. Table 2.5 also shows the amount of NH_3 desorbed of the titania mixed catalysts. The values were smaller than that of β -zeolite single, which was consistent with the cases of the alumina mixed catalysts. As shown below, however,

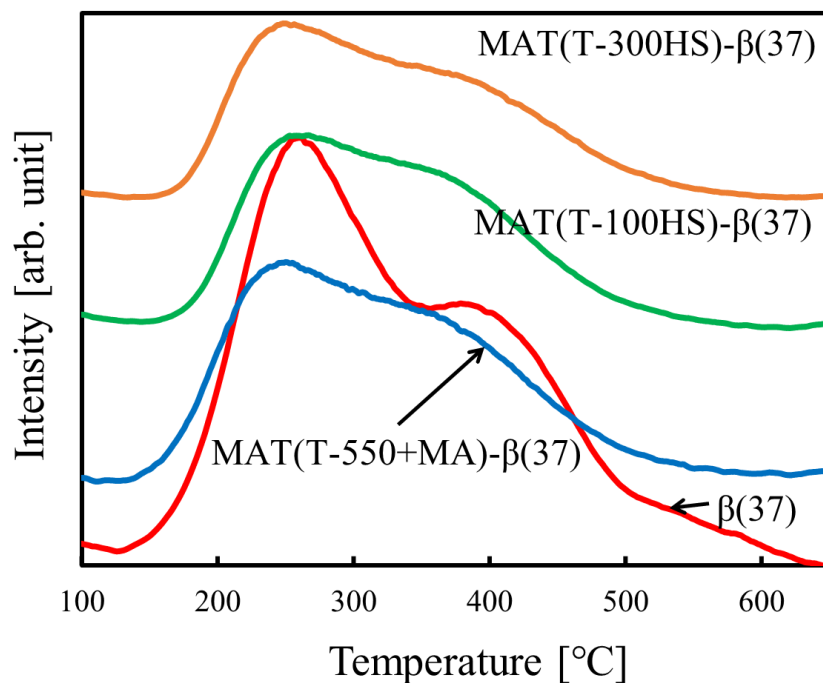


Figure 2.17 NH_3 -TPD patterns of GSR-silica-modified titania β -zeolite mixed catalysts, a titania β -zeolite mixed catalyst and β -zeolite single.

the conversion in catalytic cracking of *n*-dodecane using the titania mixed catalysts exhibited the activity similar to β -zeolite single although the amount of β -zeolite in the mixed catalysts was about one fourth. It seems that the presence of the mesopores would enable the efficient diffusion of the feed, intermediates and products into and out from the pores.

2.5.2 Catalytic cracking of *n*-dodecane using the GSR-silica-modified alumina and titania mixed catalysts

Figure 2.18 shows the paraffins, olefins, naphthenes and aromatics (PONA) distribution in the catalytic cracking of *n*-dodecane using GSR-silica-modified alumina mixed catalysts. All the prepared alumina mixed catalysts showed similar selectivity each other. However, the selectivity of paraffins and aromatics decreased, and the selectivity of olefin increased, indicating that the hydrogen transfer ability was suppressed in the presence of matrices [17,22,23,28,34,35]. This result tends to be seen regardless of the type of matrix [17,22,28,34] and the type of feed used, for examples, *n*-dodecane, atmospheric residue (AR), vacuum gas oil (VGO) and soybean oil [17,22,23,28,34,35]. It is considered that the use of the catalyst composed of β -zeolite and the matrix dispersed and diluted the β -zeolite crystals and lowered the acid density of the catalyst. Figure 2.19 shows the carbon number distribution in the catalytic cracking reaction using the alu-

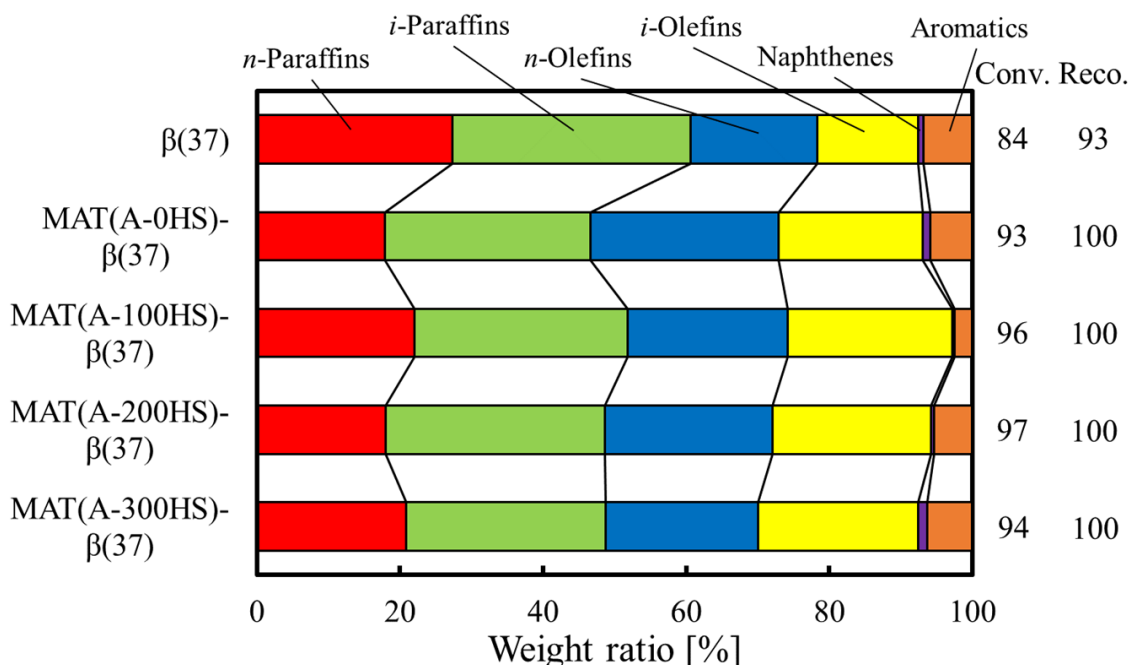


Figure 2.18 Selectivity for paraffins, olefins, naphthenes and aromatics in catalytic cracking of *n*-dodecane using the GSR-silica-modified alumina mixed catalysts.

Chapter 2

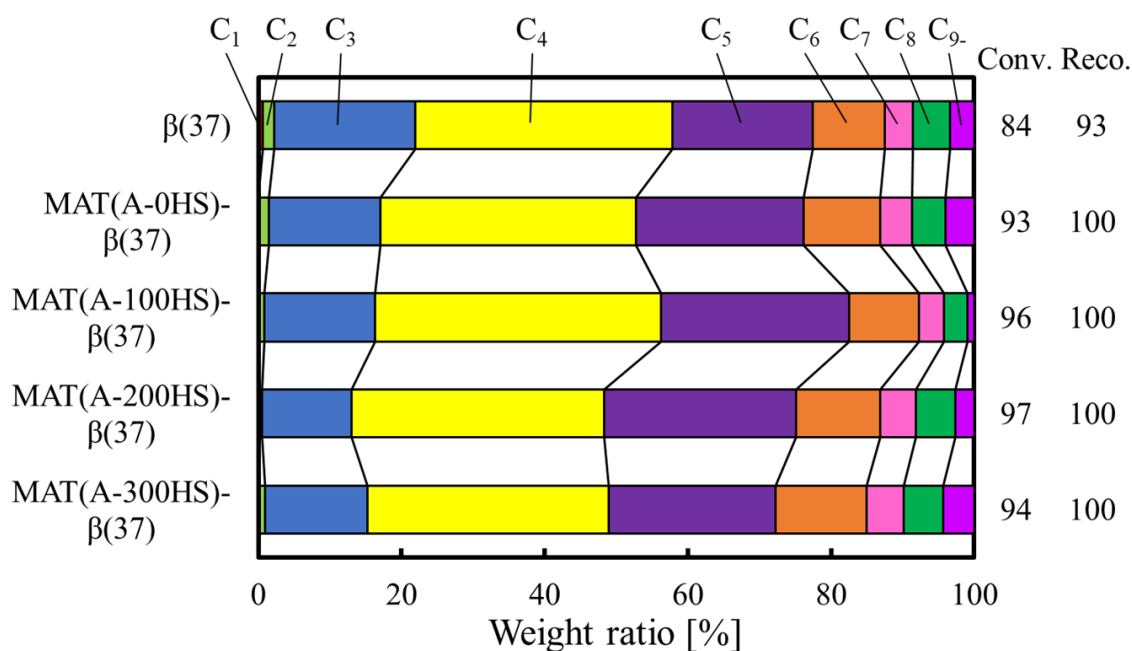


Figure 2.19 Distribution of carbon numbers in catalytic cracking of *n*-dodecane using the GSR-silica-modified alumina mixed catalysts.

mina mixed catalysts. The prepared alumina mixed catalyst gave less gas products (C₁-C₄) than β-zeolite single and suppressed over-cracking, suggesting that the mixed catalyst with large pores derived from alumina could effectively diffuse the gasoline fraction products with C₅ to C₁₁ generated in the β-zeolite pores out of the pores. Further, it is deduced that the dispersion and dilution of acid sites of β-zeolite with alumina would bring about the increase in the gasoline fraction. By controlling the acid site of β-zeolite by alumina matrix, it was possible to improve the conversion compared to β-zeolite single and increase the product selectivity of C₅-C₁₁ gasoline fraction.

Figure 2.20 shows the PONA distribution of products in the catalytic cracking of *n*-dodecane using titania mixed catalysts. The catalysts using T-550+MA [28] and GSR-silica-modified titania as matrices gave results similar to those of alumina mixed catalysts shown above, indicating that matrices would be effective for catalytic cracking of *n*-dodecane regardless of the type of oxide constituting the matrix. Further, as shown in the carbon number distribution of the titania mixed catalysts in Figure 2.21, the formation of C₃ and C₄ were slightly suppressed compared to the case of β-zeolite single. Since the mixed catalyst had mesopores derived from the matrix, it is considered that the multi-branched products generated in micropore of β-zeolite were desorbed by a shorter route than in the case of β-zeolite single. Therefore, the products of C₅ and more than C₅ were not excessively cracked, and the selectivity of the gasoline fraction increased.

Chapter 2

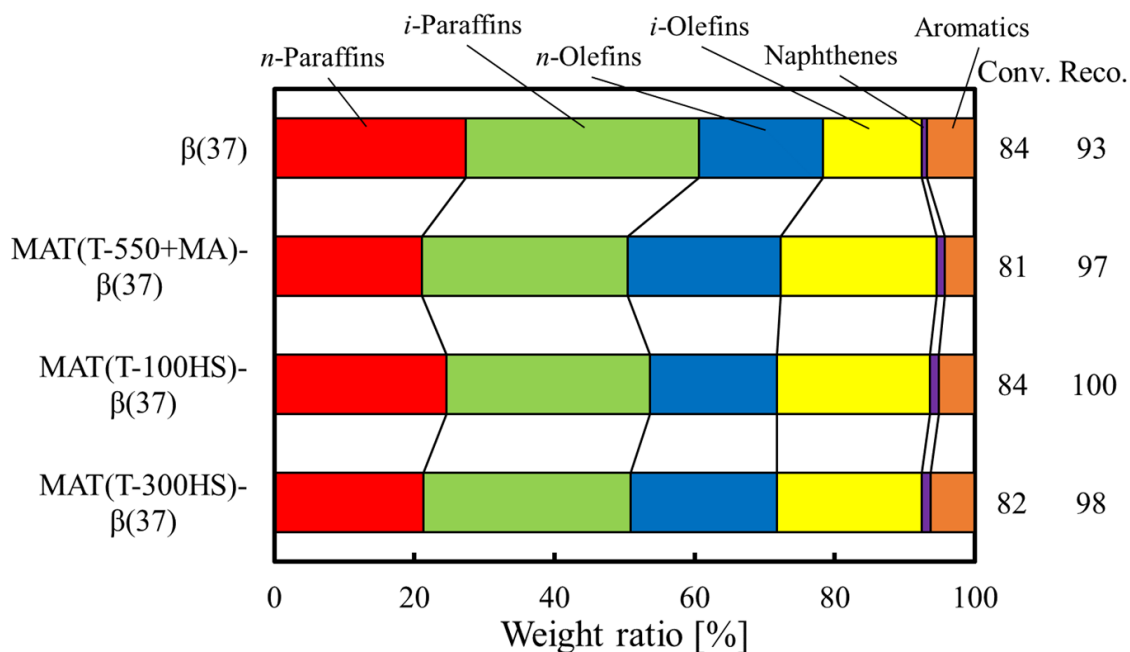


Figure 2.20 Selectivity for paraffins, olefins, naphthenes and aromatics in catalytic cracking of *n*-dodecane using the GSR-silica-modified titania mixed catalysts.

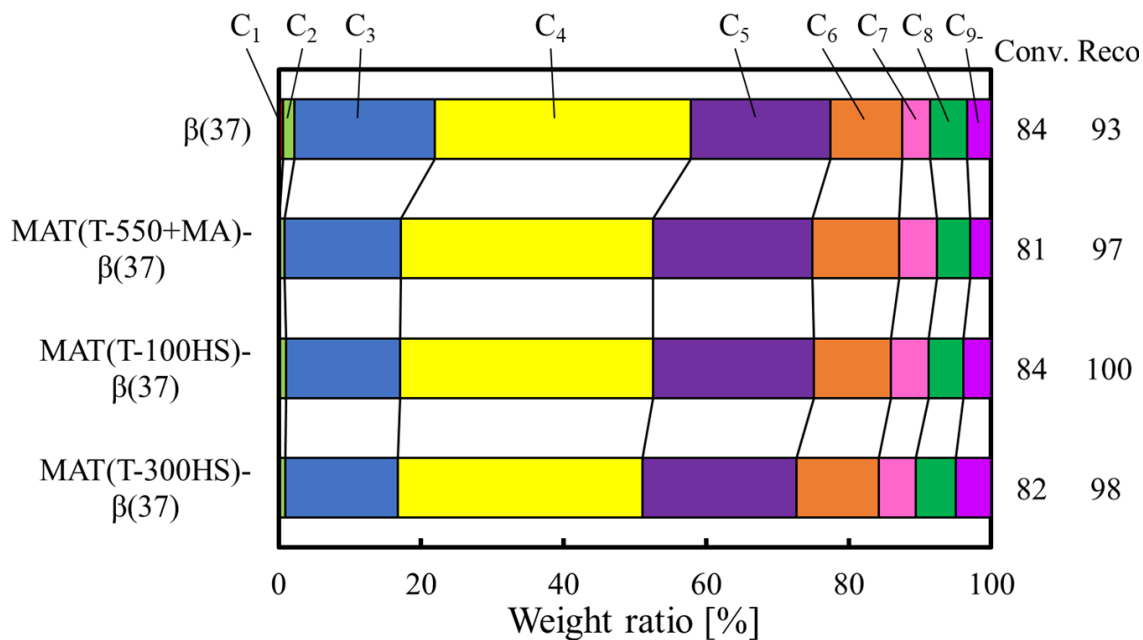


Figure 2.21 Distribution of carbon numbers in catalytic cracking of *n*-dodecane using the GSR-silica-modified titania mixed catalysts.

Chapter 2

Table 2.5 Product distribution, catalytic properties, parameters in gasoline fraction and amount of NH₃ desorbed.

Catalyst	Product distribution (wt. %)			Parameters in gasoline fraction				Amount of NH ₃ desorbed (10 ⁻⁴ mol/g)		
	C ₁ -C ₄	Gasoline (C ₅ -C ₁₁)	C ₁₂ -	Conv. (%)	Reco. (%)	O/P	iso-/ n-		M/S	RON
β(37)	58	42	0.48	84	93	0.46	2.17	0.06	86	6.1
MAT(A-0HS)-β(37)	53	47	0.43	93	100	0.59	1.91	0.08	87	3.6
MAT(A-100HS)-β(37)	56	44	0	96	100	0.70	1.95	0.08	89	3.9
MAT(A-200HS)-β(37)	48	52	0.06	97	100	0.60	1.95	0.11	86	4.0
MAT(A-300HS)-β(37)	49	51	0.45	94	100	0.69	1.99	0.08	86	3.5
MAT(T-550+MA)-β(37)	53	47	0.20	81	97	0.71	2.11	0.09	86	3.3
MAT(T-100HS)-β(37)	53	47	0.43	84	100	0.71	2.10	0.09	87	2.8
MAT(T-300HS)-β(37)	51	48	0.46	82	98	0.63	2.06	0.10	86	2.5

O/P: Olefin/Paraffin, M/S: Multi/Single branch.

Table 2.5 summarizes the product distribution, catalytic properties, parameters in gasoline fraction and amount of NH₃ desorbed for the alumina and titania mixed catalysts. The *iso*-/*n*-ratios for the alumina mixed catalysts were lower than that of β-zeolite single while the multi-branched/single-branched ratio (M/S) of the mixed catalysts were higher than that of β-zeolite single, indicating that that total amounts of branched products decreased because of the high activity of the mixed catalysts and that the isomerization reaction of single-branched products to multi-branched products would be promoted probably because the larger amount of mesoporous matrices existed and the restriction to the size of molecules decreased. Further, in the cases of titania mixed catalysts the *iso*-/*n*- ratios were maintained while the M/S ratios increased, indicating that the moderate cracking activity and the large mesopores of the matrices in the titania mixed catalysts would promote the desorption of branched products from the catalyst pores and the formation of multi-branched products simultaneously. However, in the case of β-zeolite single, the reactivity is originally higher, and the pore size is smaller than that of matrices. Therefore, it is considered that intermediates of the multi-branched products produced by the isomerization reaction are difficult to be eliminated. As a result, intermediates of multi-branched products were cracked before desorption to the outside of the pores, and the M/S ratio was lower than those of the alumina and titania mixed catalysts. A similar tendency has been observed in catalytic cracking using mixed catalysts with silica matrices [17,22] and catalytic cracking of AR and VGO using mixed catalysts with silica-alumina matrices [22,23]. In addition, the gasoline yields of all the mixed catalysts were higher than those of β-zeolite single. In particular, it exceeded 50 % for two

Chapter 2

mixed catalysts of MAT(A-200HS)- β (37) and MAT(A-300HS)- β (37). Although the conversion and the selectivity for gasoline fraction with alumina mixed catalysts were higher than those of β -zeolite single, the product selectivity shows a similar tendency between the mixed catalysts, indicating that the basic product selectivity of mixed catalysts would depend on that of β -zeolite. Although each mixed catalyst contained only 26 wt% of β -zeolite, the presence of alumina and titania matrices having pores larger than β -zeolite promoted the cracking reaction [17,22,23,33,34,36]. In other words, it is speculated that a micro-meso hierarchical structure is formed by the introduction of a matrix and β -zeolite, the diffusivity of the feed and products are improved, and the feed is easily accessible to acid sites of β -zeolite. Further, as shown in Figure 2.22, the gasoline yield linearly increased with the conversion, indicating that not only the gasoline yield could be improved with the increase in the activity, but also the type and characteristics of the matrix greatly influenced the activity [22,23,26,27,35]. The latter will be considered further in the next section.

Table 2.6 summarizes the coke yields of catalysts measured by TGA after the catalytic cracking of *n*-dodecane. It was found that about 2 % and 1 % of coke were formed in the alumina and titania mixed catalysts, respectively, suggesting that the presence of the matrix with mesoporosity would shorten the diffusion path of products, inhibit the further reaction of products, and suppress the hydrogen transfer reaction [22,23,33,37,38].

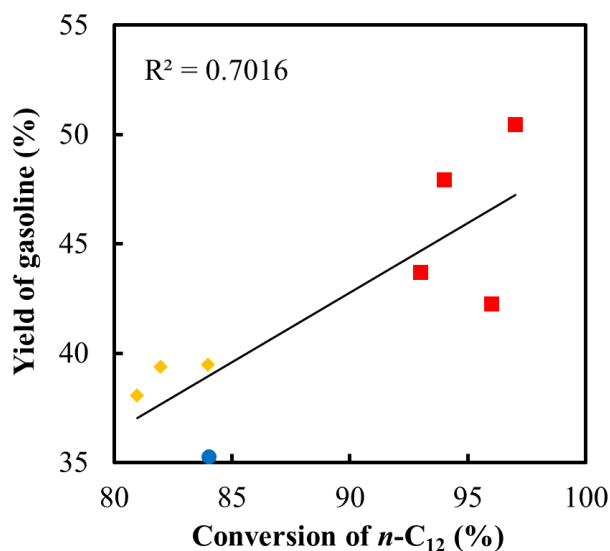


Figure 2.22 Relationship between yield of gasoline and conversions of *n*-dodecane (*n*-C₁₂). The square ■, diamond ◆ and circle ● show GSR-silica-modified alumina mixed catalyst, GSR-silica-modified titania mixed catalyst and β -zeolite single, respectively.

Table 2.6 Coke yields of catalysts measured by TGA after cracking.

Catalyst	Coke yield (mg)	Coke yield (wt.%)	Result of <i>n</i> -dodecane cracking		
			Conv. (%)	Reco. (%)	
				Gas + Liquid	+ coke
MAT(A-0HS)- β (37)	0.19	1.88	93	100	102
MAT(A-100HS)- β (37)	0.20	1.93	96	100	102
MAT(A-200HS)- β (37)	0.23	2.03	97	100	102
MAT(A-300HS)- β (37)	0.17	1.67	94	100	102
MAT(T-550+MA)- β (37)* ¹	1.00	1.00	81	97	98
MAT(T-100HS)- β (37)	0.12	1.31	84	100	101
MAT(T-300HS)- β (37)	0.12	1.09	82	98	99

Cat.: 10 mg, Temp.: 400-600 °C, Atmosphere: O₂, Programming rate: 10.0 °C/ min, Retention time at 600 °C: 0 h

*¹: Measured by electric furnace (Cat.: 0.1 g, Temp.: 120-500 °C, Atmosphere: Dry air)

2.5.3 Relationship between catalytic cracking of *n*-dodecane and catalyst texture

In order to investigate the influence of the pore characteristics and acid characteristics of the catalyst on the reactivity of *n*-dodecane, BET surface area (SA-BET), BJH surface area (SA-BJH), total pore volume (Total-PV), BJH pore volume (PV-BJH), and amounts of NH₃ desorbed (NH₃-TPD) were plotted against the conversion in Figure 2.23a-e, respectively. In each of Figure 2.23a-e, the correlation coefficient and the linear approximation line showing the strength of the correlation are indicated [28]. A weak correlation was found in Figures 2.23a and e (solid line), while a strong correlation was found in Figures 2.23b-d. From these facts, it was confirmed that the improvement in the diffusivity of *n*-dodecane due to the development of mesoporous volumes would contribute to the improvement of the conversion. It was reported that, in catalytic cracking of *n*-octane by β -zeolite catalyst with mesopores [39], the acidity would determine the activity as the reactants could easily diffuse in the pores. In the present study, it was also observed that, when compared between the catalysts prepared by the mixed catalysts (broken line in Figure 2.23e), there would be a tendency to depend on the acidity of the catalysts. However, when β -zeolite single was added to the plot, the correlation disappeared (solid line in Figure 2.23e).

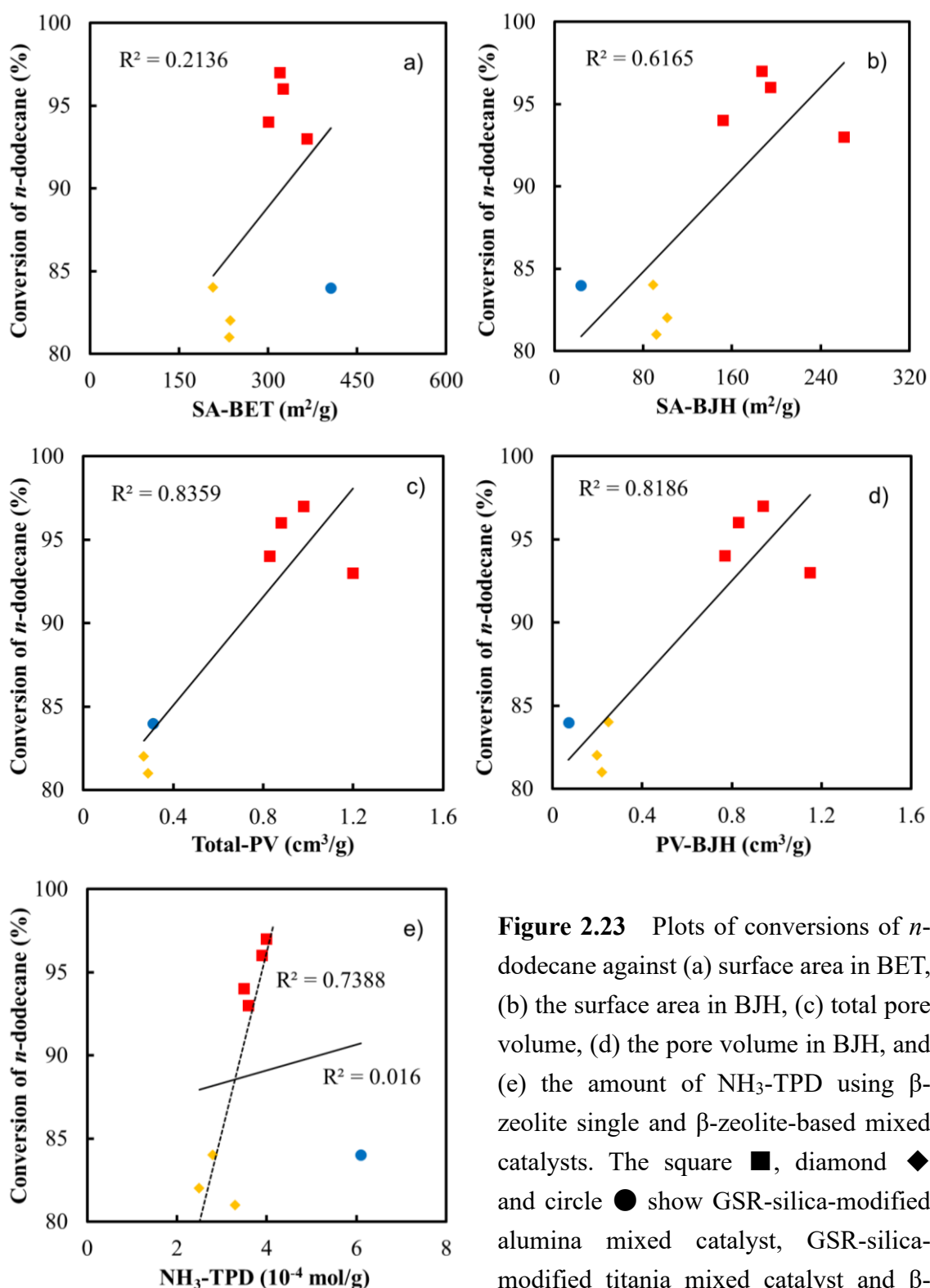


Figure 2.23 Plots of conversions of *n*-dodecane against (a) surface area in BET, (b) the surface area in BJH, (c) total pore volume, (d) the pore volume in BJH, and (e) the amount of NH_3 -TPD using β -zeolite single and β -zeolite-based mixed catalysts. The square ■, diamond ◆ and circle ● show GSR-silica-modified alumina mixed catalyst, GSR-silica-modified titania mixed catalyst and β -zeolite single, respectively.

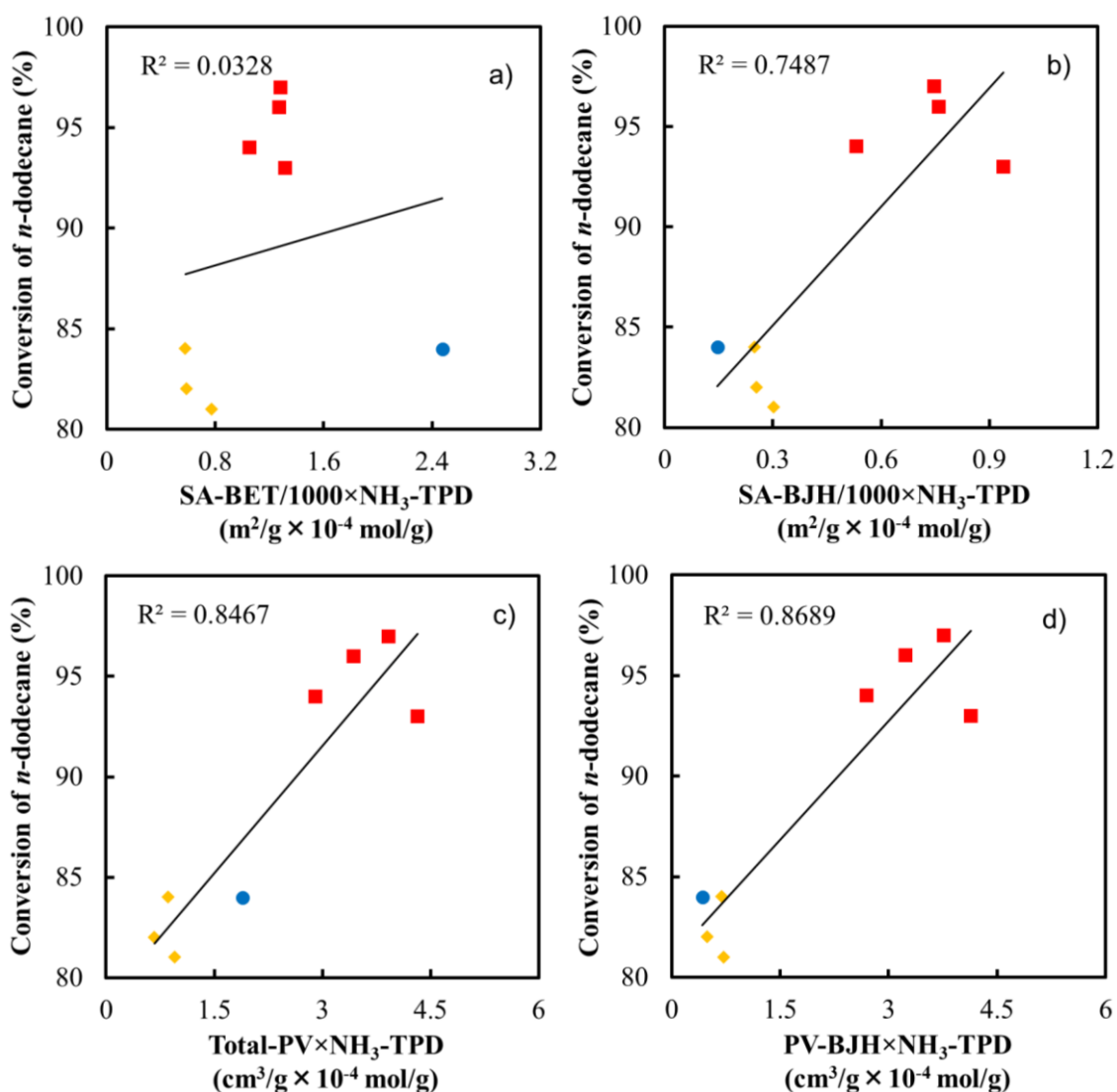


Figure 2.24 Plots of conversions of *n*-dodecane against (a) the product of surface area in BET and NH₃-TPD, (b) the product of surface area in BJH and NH₃-TPD, (c) the product of total pore volume and NH₃-TPD and (d) the product of pore volume in BJH and NH₃-TPD using β-zeolite single and β-zeolite-based mixed catalysts. The square ■, diamond ◆ and circle ● show GSR-alumina mixed catalyst, GSR-titania mixed catalyst and β-zeolite single, respectively.

To further discuss this result, Figure 2.24 denotes the relationships between the conversion of *n*-dodecane and the products of each parameter on the horizontal axis in Figures 2.23a-d and the amount of NH₃ desorbed (NH₃-TPD) [22,28]. As a result, strong correlations were found in Figures 2.24b-d, and specifically strong correlations were found in Figure 2.24c and d. Further, decision coefficients in Figure 2.23c and d increased those in Figure 2.24c and d, indicating that

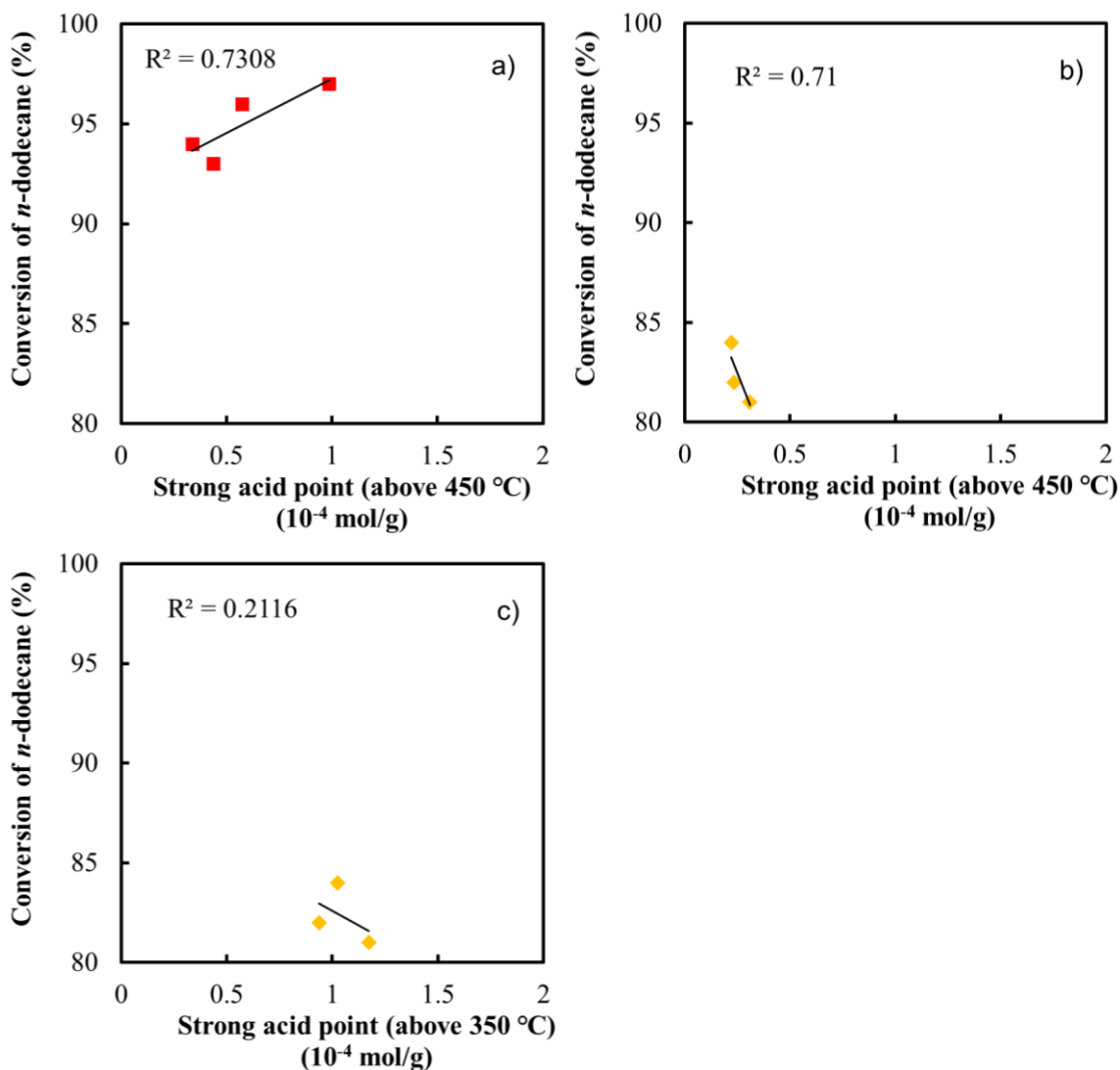


Figure 2.25 Plots of the amount of strong acid point and conversion of the β -zeolite-based mixed catalysts. The square ■ and diamond ◆ show GSR-alumina mixed catalyst and GSR-titania mixed catalyst, respectively.

there would be the synergy pore volumes and the acidity of the catalysts and that the activity of the catalyst would strongly depend on the combination of pore volume and acidity of the catalyst. This is a tendency [22,40] which is often seen in catalysts having a micro- and meso-porous structure. In addition, since a strong correlation was also found with the BJH specific surface area shown in Figures 2.23b and 2.24b, it was confirmed that the mesopore characteristics of the catalyst significantly contributed to the activity of the catalyst. Figures 2.25a-c shows plots of the amount of strong acid sites and conversion of the β -zeolite-based mixed catalysts. Since the GSR alumina mixed catalyst has a large surface area and the zeolite is well dispersed, a correlation can

Chapter 2

be seen between the amount of acid sites and the activity (Figure 2.25a). However, in the case of GSR titania mixed catalyst, due to the small surface area, low zeolite dispersibility, and small measurement points, there is not clear correlation between the amount of acid sites and the activity at the strong acid sites of above 350 °C (Figure 2.25b) or 450 °C (Figure 2.25c) or even the entire acid sites. Nevertheless, the correlation coefficient of alumina and titania combined does not decrease as compared with the correlation coefficient of alumina alone. Therefore, as a whole, it is considered that the amount of acidity of the catalyst, that is, the amount of effective acidity of zeolite affects the activity.

During the last decade, it has become to be known that hierarchical zeolites with mesopores or hierarchical catalysts including zeolites could exhibit the high activity in catalytic cracking of large molecules, and a lot of reports have appeared even within the last one year [22,41-54]. In these reports, the catalysts with the hierarchical structure increased the activity rather than the product selectivity, suggesting that the presence of hierarchical structure would closely be related to the activity. However, most of these catalysts were prepared to introduce mesoporous structures into zeolite skeletal and basically consisted of only zeolite, and it seems that there would still be the diffusion limitation to some extent when a large molecule is processed. Therefore, the structure with larger mesopores in the outside and smaller micropores of zeolite in the inside may be preferred as shown in the graphical abstract because cracking products like olefins, aromatics and branched paraffins are usually more reactive than reactants of saturated linear hydrocarbons.

2.6 Conclusions

During the preparation of alumina and titania by the sol-gel method, the silica-modification of alumina and titania surfaces by the GSR method using HMDS-AA system was performed. The prepared GSR-silica-modified alumina and titania were characterized and their reactivity as matrices in a mixed catalyst with β -zeolite was investigated in the catalytic cracking of n-dodecane in detail.

By applying the GSR method to the production of alumina matrices, GSR-silica-modified aluminas having a wider pore distribution than those from the conventional sol-gel method were produced. When a mixed catalyst was prepared using these aluminas, a novel acid property appeared due to the presence of silica-modification on the surface of the prepared alumina. In addition, the wide distribution of mesopores promoted the diffusion of both reactants and products, and improved the activity compared to a mixed catalyst using alumina without the GSR-silica-modification and β -zeolite single.

By applying the GSR-silica modification to titania, the anatase phase was stably formed even after calcining at 600 °C for 3 h, and it was confirmed that its thermal stability was higher than

Chapter 2

that of conventional titania prepared without the GSR-silica modification. It was found that the GSR-silica-modified titania retained the matrix pores even when used as a matrix for mixed catalysts. In catalytic cracking of *n*-dodecane using the mixed catalysts with GSR-silica-modified titania, the obtained products had the higher gasoline yield, olefin/paraffin ratio, *iso*-/*n*- ratio and multi/single blanch ratio compared with those from β -zeolite single.

References

- [1] M. Sobhani, H. Tavakoli, M.D. Chermahini, M. Kazazi, "Preparation of macro-mesoporous γ -alumina via biology gelatin assisted aqueous sol-gel process", *Ceram. Int.*, 45 (2019) 1385-1391, <https://doi.org/10.1016/j.ceramint.2018.09.056>
- [2] Q. Sun, Y. Zheng, Z. Li, Y. Zheng, Y. Xiao, G. Cai, "Synthesis of ordered mesoporous γ -alumina influenced by the interfacial protector", *Mater. Lett.*, 84 (2012) 44-47, <https://doi.org/10.1016/j.matlet.2012.06.035>
- [3] X. Ji, S. Tang, L. Gu, T. Liu, X. Zhang, "Synthesis of rod-like mesoporous γ -Al₂O₃ by an ionic liquid-assisted sol-gel method", *Mater. Lett.*, 151 (2015) 20-23, <https://doi.org/10.1016/j.matlet.2015.03.022>
- [4] M. Trueba, S.P. Trasatti, " γ -Alumina as a Support for Catalysts: A Review of Fundamental Aspects", *Eur. J. Inorg. Chem.*, 17 (2005) 3393-3403, <https://doi.org/10.1002/ejic.200500348>
- [5] H. Kondoh, K. Tanaka, Y. Nakasaka, T. Tago, T. Masuda, "Catalytic cracking of heavy oil over TiO₂-ZrO₂ catalysts under superheated steam conditions", *Fuel*, 167 (2016) 288-294, <https://doi.org/10.1016/j.fuel.2015.11.075>
- [6] F.J. Beltrán, M. Checa, "Comparison of graphene oxide titania catalysts for their use in photocatalytic ozonation of water contaminants: Application to oxalic acid removal", *Chem. Eng. J.*, 385 (1) (2020) 123922, <https://doi.org/10.1016/j.cej.2019.123922>
- [7] L.G. Devi, R. Kavitha, "A review on non metal ion doped titania for the photocatalytic degradation of organic pollutants under UV/solar light: Role of photogenerated charge carrier dynamics in enhancing the activity", *Appl. Catal. B*, 140-141 (2013) 559-587, <https://doi.org/10.1016/j.apcatb.2013.04.035>
- [8] P. Akhter, M.A. Farkhondehfal, S. Hernández, M. Hussain, A. Fina, G. Saracco, A.U. Khan, N. Russo, "Environmental issues regarding CO₂ and recent strategies for alternative fuels through photocatalytic reduction with titania-based materials", *J. Environ. Chem. Eng.*, 4 (2016) 3934-3953, <https://doi.org/10.1016/j.jece.2016.09.004>
- [9] A. Aguirre-Gutiérrez, J.A. Montoya de la Fuente, J.A. de los Reyes, P. del Angel, A. Vargas, "Palladium effect over Mo and NiMo/alumina-titania sulfided catalysts on the hydrodesulfurization of 4,6-dimethyldibenzothiophene", *J. Mol. Catal. A Chem.*, 346 (1-2) (2011) 12-19, <https://doi.org/10.1016/j.molcata.2011.06.005>
- [10] C.L. Wong, Y.N. Tan, A.R. Mohamed, "A review on the formation of titania nanotube photocatalysts by hydrothermal treatment", *J. Environ. Manage.*, 92 (7) (2011) 1669-1680, <https://doi.org/10.1016/j.jenvman.2011.03.006>
- [11] G. Centi, R. Passalacqua, S. Perathoner, "Advanced nanostructured titania photoactive materials for sustainable H₂ production", *Mater. Sci. Semicond. Process.*, 42 (1) (2016) 115-121,

Chapter 2

<https://doi.org/10.1016/j.mssp.2015.07.051>

- [12] J.M.O. Silveira, A.C.L. Ubiali, D.C. Baldini, K.J. Ciuffi, L.A. Rocha, E.J. Nassar, “Manganese-doped titania matrix obtained by sol-gel process: Magnetic properties”, *Microelectron. Eng.*, 196 (2018) 49-53, <https://doi.org/10.1016/j.mee.2018.04.014>
- [13] C. J. Brinker, G. W. Scherer, “Sol-Gel Science: The Physics and Chemistry of Sol-Gel Processing”, *Academic Press* (1990) 1-908, <https://doi.org/10.1016/C2009-0-22386-5>
- [14] J. D. Wright, N. A. J. M. Sommerdijk, “Sol-Gel Materials Chemistry and Applications”, *CRC Press* (2000) 1-129, <https://doi.org/10.1201/9781315273808>
- [15] M. Sharbatdaran, M.M. Amini, A. Majdabadi, “Effect of aluminium alkoxide with donor-functionalized group on texture and morphology of the alumina prepared by sol-gel processing”, *Mater. Lett.*, 64 (2010) 503-505, <https://doi.org/10.1016/j.matlet.2009.11.057>
- [16] E.M. Lucas, M.S. Doescher, D.M. Ebenstein, K.J. Wahl, D.R. Rolison, “Silica aerogels with enhanced durability, 30-nm mean pore-size, and improved immersibility in liquids”, *J. Non-Cryst. Solids*, 350 (2004) 244-252, <https://doi.org/10.1016/j.jnoncrysol.2004.07.074>
- [17] A. Ishihara, H. Oono, T. Hashimoto, H. Nasu, “Preparation of SiO₂ and SiO₂-Al₂O₃ catalysts by gel skeletal reinforcement using hexamethyldisiloxane (HMDS) and acetic anhydride and aluminum tri-sec-butoxide (ASB) systems and elucidation of their catalytic cracking properties as matrices”, *Microporous Mesoporous Mater.*, 233 (2016) 163-170, <https://doi.org/10.1016/j.micromeso.2016.01.025>
- [18] S. Smitha, P. Shajesh, P.R. Aravind, S.R. Kumar, P.K. Pillai, K.G.K. Warriar, “Effect of aging time and concentration of aging solution on the porosity characteristics of subcritically dried silica aerogels”, *Microporous Mesoporous Mater.*, 91 (2006) 286-292, <https://doi.org/10.1016/j.micromeso.2005.11.051>
- [19] T.B. Du, S.M. Jang, B.W. Chen, “Manufacture of mesoporous alumina of boehmite type via subcritical drying and application to purify liquid crystal”, *Chem. Eng. Sci.*, 62 (2007) 4864-4868, <https://doi.org/10.1016/j.ces.2006.12.073>
- [20] V. Durand, M. Drobek, M. Duchateau, A. Hertz, J.C. Ruiz, S. Sarrade, C. Guizard, A. Julbe, “Potential of sub- and supercritical CO₂ reaction media for sol-gel deposition of silica-based molecular sieve membranes”, *Sep. Purif. Technol.*, 121 (2014) 30-37, <https://doi.org/10.1016/j.seppur.2013.06.031>
- [21] J.Q. Albarelli, D.T. Santos, M.A.A. Meireles, M. Salgado, M. Rueda, “Techno-economic analysis of production of ammonia-borane confined in silica aerogel microparticles by subcritical CO₂ drying”, *J. Supercrit. Fluids*, 138 (2018) 147-153, <https://doi.org/10.1016/j.supflu.2018.04.012>
- [22] A. Ishihara, “Preparation and reactivity of hierarchical catalysts in catalytic cracking”, *Fuel Process. Technol.*, 194 (2019) 106116, <https://doi.org/10.1016/j.fuproc.2019.05.039>

Chapter 2

- [23] T. Sonthisawate, T. Nakanishi, H. Nasu, T. Hashimoto, A. Ishihara, “Catalytic cracking reaction of vacuum gas oil and atmospheric residue by zeolite-containing microporous and mesoporous composites using Curie point pyrolyzer”, *Fuel Process. Technol.*, 142 (2016) 337-344, <https://doi.org/10.1016/j.fuproc.2015.10.016>
- [24] A. Ishihara, D. Kawaraya, T. Sonthisawate, H. Nasu, T. Hashimoto, “Preparation and characterization of zeolite-containing silica-aluminas with three layered micro-meso-meso-structure and their reactivity for catalytic cracking of soybean oil using Curie point pyrolyzer”, *Fuel Process. Technol.*, 161 (2017) 8-16, <https://doi.org/10.1016/j.fuproc.2017.03.002>
- [25] A. Ishihara, T. Tsukamoto, T. Hashimoto, H. Nasu, “Catalytic cracking of soybean oil by ZSM-5 zeolite-containing silica-aluminas with three layered micro-meso-meso-structure”, *Catal. Today*, 303 (2018) 123-129, <https://doi.org/10.1016/j.cattod.2017.09.033>
- [26] A. Ishihara, K. Nakajima, M. Hirado, T. Hashimoto, H. Nasu, “Novel Method for Generating Large Mesopores in an Amorphous Silica–Alumina by Controlling the Pore Size with the Gel Skeletal Reinforcement and Its Catalytic Cracking Properties as a Catalyst Matrix”, *Chem. Lett.*, 40 (6) (2011) 558-560, <https://doi.org/10.1246/cl.2011.558>
- [27] A. Ishihara, S. Matsuura, F. Hayashi, K. Suemitsu, T. Hashimoto, “Estimation of Catalytic Cracking of Vacuum Gas Oil by a Y Zeolite-Containing Two-Layered Catalyst and a Novel Three-Layered Hierarchical Catalyst Using a Curie Point Pyrolyzer Method”, *Energy Fuels*, 34 (6) (2020) 7448-7454, <https://doi.org/10.1021/acs.energyfuels.0c00957>
- [28] A. Ishihara, K. Tatebe, T. Hashimoto, H. Nasu, “Preparation of Silica, Alumina, Titania, and Zirconia with Different Pore Sizes Using Sol–Gel Method and Their Properties as Matrices in Catalytic Cracking”, *Ind. Eng. Chem. Res.*, 57 (43) (2018) 14394-14405, <https://doi.org/10.1021/acs.iecr.8b03019>
- [29] M.K. Mardkhe, K. Keyvanloo, C.H. Bartholomew, W.C. Hecker, T.M. Alam, B.F. Woodfield, “Acid site properties of thermally stable, silica-doped alumina as a function of silica/alumina ratio and calcination temperature”, *Appl. Catal. A Gen.*, 482 (2014) 16-23, <https://doi.org/10.1016/j.apcata.2014.05.011>
- [30] K. Okada, N. Yamamoto, Y. Kameshima, A. Yasumori, K.J.D. MacKenzie, “Effect of Silica Additive on the Anatase-to-Rutile Phase Transition”, *J. Am. Ceram. Soc.*, 84 (7) (2001) 1591-1596, <https://doi.org/10.1111/j.1151-2916.2001.tb00882.x>
- [31] Y. Suyama, A. Kato, “Effect of Additives on the Formation of TiO₂ Particles by Vapor Phase Reaction”, *J. Am. Ceram. Soc.*, 68 (6) (1985) 154, <https://doi.org/10.1111/j.1151-2916.1985.tb15225.x>
- [32] J. Yang, J.M.F. Ferreira, “On the Titania Phase Transition by Zirconia Additive in a Sol-Gel-Derived Powder”, *Mater. Res. Bull.*, 33 (3) (1998) 389-394, [https://doi.org/10.1016/S0025-5408\(97\)00249-3](https://doi.org/10.1016/S0025-5408(97)00249-3)

Chapter 2

- [33] L. Jia, X. Sun, X. Ye, C. Zou, H. Gu, Y. Huang, G. Niu, D. Zhao, “Core–shell composites of USY@Mesosilica: Synthesis and application in cracking heavy molecules with high liquid yield”, *Microporous Mesoporous Mater.*, 176 (2013) 16-24, <https://doi.org/10.1016/j.micromeso.2013.03.029>
- [34] A. Ishihara, H. Negura, T. Hashimoto, H. Nasu, “Catalytic properties of amorphous silica-alumina prepared using malic acid as a matrix in catalytic cracking of n-dodecane”, *Appl. Catal. A Gen.*, 388 (2010) 68-76, <https://doi.org/10.1016/j.apcata.2010.08.027>
- [35] A. Ishihara, K. Kimura, Tadanori Hashimoto, H. Nasu, “Catalytic Cracking of VGO by Zeolite–kaolin Mixed Catalysts Using Curie Point Pyrolyzer”, *J. Jpn. Petrol. Inst.*, 58 (2015) 169-175, <https://doi.org/10.1627/jpi.58.169>
- [36] A. Palizdar, S.M. Sadrameli, “Catalytic upgrading of beech wood pyrolysis oil over iron- and zinc-promoted hierarchical MFI zeolites”, *Fuel*, 264 (2020) 116813, <https://doi.org/10.1016/j.fuel.2019.116813>
- [37] T. Imyen, W. Wannapakdee, J. Limtrakul, C. Wattanakit, “Role of hierarchical micro-mesoporous structure of ZSM-5 derived from an embedded nanocarbon cluster synthesis approach in isomerization of alkenes, catalytic cracking and hydrocracking of alkanes”, *Fuel*, 254 (2019) 115593, [10.1016/j.fuel.2019.06.001](https://doi.org/10.1016/j.fuel.2019.06.001)
- [38] Y. Wang, R. Otomo, T. Tatsumi, T. Yokoi, “Dealumination of organic structure-directing agent (OSDA) free beta zeolite for enhancing its catalytic performance in n-hexane cracking”, *Microporous Mesoporous Mater.*, 220 (2016) 275-281, <https://doi.org/10.1016/j.micromeso.2015.09.015>
- [39] W. Wang, W. Zhang, Y. Chen, X. Wen, H. Li, D. Yuan, Q. Guo, S. Ren, X. Pang, B. Shen, “Mild-acid-assisted thermal or hydrothermal dealumination of zeolite beta, its regulation to Al distribution and catalytic cracking performance to hydrocarbons”, *J. Catal.*, 362 (2018) 94-105, <https://doi.org/10.1016/j.jcat.2018.03.002>
- [40] E.V. Parkhomchuk, D.A. Sladkovskii, Y. Gunb, W. Wud, K.A. Sashkina, A.I. Lysikov, V.N. Parmon, “Catalytic Cracking of n-Hexane in the Presence of Zeolite ZSM-5 Micro- and Nanocrystals”, *Pet. Chem.*, 59 (3) (2019) 338-348, <https://doi.org/10.1134/S0965544119030113>
- [41] Y. Zang, J. Wang, J. Gu, J. Qu, F. Gao, M. Li, “Cost-effective synthesis of hierarchical HZSM-5 with a high Si/TPA⁺ ratio for enhanced catalytic cracking of polyethylene”, *J. Solid State Chem.*, 291 (2020) 121643, <https://doi.org/10.1016/j.jssc.2020.121643>
- [42] B. Meng, S. Ren, Z. Li, H. Duan, X. Gao, H. Zhang, W. Song, Q. Guo, B. Shen, “Intra-Crystalline Mesoporous Zeolite [Al,Zr]-Y for Catalytic Cracking”, *ACS Appl. Nano Mater.* (2020), <https://doi.org/10.1021/acsanm.0c01925>
- [43] N. Cui, H. Guo, J. Zhou, L. Li, L. Guo, Z. Hua, “Regulation of framework Al distribution of high-silica hierarchically structured ZSM-5 zeolites by boron-modification and its effect on

Chapter 2

- materials catalytic performance in methanol-to-propylene reaction”, *Microporous Mesoporous Mater.*, 306 (2020) 110411, <https://doi.org/10.1016/j.micromeso.2020.110411>
- [44] K.A. Tarach, K. Pyra, K. Gora-Marek, “Opening up ZSM-5 Hierarchical Zeolite’s Porosity through Sequential Treatments for Improved Low-Density Polyethylene Cracking”, *Molecules*, 25 (12) (2020) 2878, <https://doi.org/10.3390/molecules25122878>
- [45] A. Ishihara, M. Ninomiya, T. Hashimoto, H. Nasu, “Catalytic cracking of C₁₂-C₃₂ hydrocarbons by hierarchical β - and Y-zeolite-containing mesoporous silica and silica-alumina using Curie point pyrolyzer”, *J. Anal. Appl. Pyrol.*, 150 (2020) 104876, <https://doi.org/10.1016/j.jaap.2020.104876>
- [46] K. Zhang, S. Fernandez, E.S. Converse, S. Kobaslija, “Exploring the impact of synthetic strategies on catalytic cracking in hierarchical beta zeolites via hydrothermal desilication and organosilane-templated synthesis”, *Catal. Sci. Technol.*, 10 (14) (2020) 4602-4611, <https://doi.org/10.1039/d0cy01209b>
- [47] W. Kim, J.-C. Kim, S. Lee, J. Kim, R. Ryoo, “Mesopore-selective incorporation of strong Brønsted acid catalytic sites via aluminium grafting on hierarchically porous siliceous MFI zeolite”, *Microporous Mesoporous Mater.*, 305 (2020) 110353, <https://doi.org/10.1016/j.micromeso.2020.110353>
- [48] A. Talebian-Kiakalaieh, S. Tarighi, “Synthesis of hierarchical Y and ZSM-5 zeolites using post-treatment approach to maximize catalytic cracking performance”, *J. Ind. Eng. Chem.*, 88 (2020) 167-177, <https://doi.org/10.1016/j.jiec.2020.04.009>
- [49] L. Zhang, X. Sun, M. Pan, X. Yang, Y. Liu, J. Sun, Q. Wang, J. Zheng, Y. Wang, J. Ma, W. Li, R. Li, “Interfacial effects between carbon nanotube templates and precursors on fabricating a wall-crystallized hierarchical pore system in zeolite crystals”, *J. Mater. Sci.*, 55 (24) (2020) 10412-10426, <https://doi.org/10.1007/s10853-020-04708-1>
- [50] Y. Liu, B. Qin, H. Gao, W. Ning, L. Zhang, J. Zheng, Y. Du, Y. Wang, W. Li, R. Li, “A core-shell Y zeolite with a mono-crystalline core and a loosely aggregated polycrystalline shell: a hierarchical cracking catalyst for large reactants”, *Catal. Sci. Technol.*, 10 (7) (2020) 2303-2312, <https://doi.org/10.1039/c9cy02577d>
- [51] M.A. Sanhoob, U. Khalil, E.N. Shafei, K.-H. Choi, T. Yokoi, O. Muraza, “Steam cracking of green diesel (C₁₂) to BTX and olefins over silane-treated hierarchical BEA”, *Fuel*, 263 (2020) 116624, <https://doi.org/10.1016/j.fuel.2019.116624>
- [52] S. Hu, H. Jia, J. Ma, W. Hao, R. Li, “A hierarchical zeolite microsphere prepared by an eco-friendly and practical route for efficient reaction of bulky molecules”, *Microporous Mesoporous Mater.*, 294 (2020) 109931, <https://doi.org/10.1016/j.micromeso.2019.109931>
- [53] C. Peng, Z. Liu, Y. Yonezawa, N. Linares, Y. Yanaba, C.A. Trujillo, T. Okubo, T. Matsumoto, J. Garcia-Martinez, T. Wakihara, “Testing the limits of zeolite structural flexibility: ultrafast

Chapter 2

introduction of mesoporosity in zeolites”, *J. Mater. Chem. A*, 8 (2) (2020) 735-742, <https://doi.org/10.1039/c9ta10570k>

[54] M. Alonso-Doncel, A. Peral, M. Shamzhy, J. Cejka, R. Sanz, D.P. Serrano, “Untangling the role of the organosilane functional groups in the synthesis of hierarchical ZSM-5 zeolite by crystallization of silanized protozeolitic units”, *Catal. Today*, 345 (2020) 27-38, <https://doi.org/10.1016/j.cattod.2019.11.031>

Chapter 2

Chapter 3

Preparation of novel zeolite-containing hierarchical two-layered catalysts with large mesopores by gel skeletal reinforcement and their reactivities in catalytic cracking of *n*-dodecane

In order to crack hydrocarbons with a large molecular weight, it is necessary to diffuse those substrates deeply into the inside of a catalyst. Catalysts having the hierarchical structure including not only micropores of zeolites in the inner side but also large mesopores in the outer side could crack large molecules of hydrocarbons quite effectively. To prepare such hierarchical catalysts, in this study, ZSM-5, Y and β zeolites were uniformly dispersed in silicas with large mesopores generated by the gel skeletal reinforcement (GSR) method. It was observed by XRD measurement that these catalysts maintained the framework of zeolite. Nitrogen adsorption and desorption measurement exhibited that the maximum pore volume and pore diameter of catalysts reached 5 cm³/g and 50 nm, respectively. These results indicated that silica having large mesopores would be present around the zeolite. When catalytic cracking of *n*-dodecane using these catalysts was performed, the ZSM-5-containing hierarchical catalysts exhibited 30% higher conversions than that of zeolite single. When catalysts containing β - and Y-zeolites were used, the ratios of multi-branched hydrocarbons/single-branched hydrocarbons (m/s) and olefin/paraffin (O/P) ratios in the gasoline fraction were about 1.5–2 times higher than those of ZSM-5-containing catalysts. The O/P ratios and conversions increased as the mesoporous diameter increased while the *iso*-/*n*-ratio of the gasoline fraction tended to depend on the microporous sizes of the zeolites.

3.1 Introduction

Fluid catalytic cracking (FCC) is a major petroleum refining process that cracks large hydrocarbon molecules to produce fuels and petrochemical raw materials. The functions required for FCC catalysts are changing year by year in response to changes in treatment targets such as the discovery of unconventional oils, the use of biomass resources, and changes in gasoline

Chapter 3

demand. A typical FCC catalyst consists of crystalline Y-zeolite (main active component), an active matrix, a low activity filler, a binder and other additives [1,2]. The FCC process with such catalysts treats hydrocarbon molecules with various carbon numbers and boiling points. The larger molecular diameter of hydrocarbon molecules makes themselves difficult to enter zeolite micropores directly and therefore the size of zeolite micropores limits the diffusion in many catalytic reactions [1,3]. Large molecules that cannot enter the zeolite micropores are cracked by the outer surface of zeolite and matrix components with weak active sites and introduced into the zeolite pores [1]. Only by going through such a process, an efficient cracking reaction would become possible. Research on zeolites as catalytic cracking catalysts is extensive and there are many studies, for example, post-treatment with an acid or base [3,4], a hierarchical structure by a method such as using a different structure-determining agent when producing zeolite [5-9], a core-shell structure [10], a surface modification [9,11-13], etc. On the other hand, research on matrix components is limited [2,14-29], and few reports have been used for catalytic cracking [2,14-16,29].

In previous studies and chapter, the gel skeletal reinforcement (GSR) method, one kind of sol-gel methods, has been used to prepare the matrix components [30-32]. In this preparation process, a porous material having new properties was developed by performing alkoxide modification of prepared silica-gel [30]. Further, a porous material having large mesopores (pore volume of 5 cm³/g and average pore diameter of 40 nm) [31] and new characteristics [32] were developed by applying the GSR method using a silylating agent of hexamethyldisiloxane and acetic anhydride. When these materials were used as matrix components with zeolites in catalytic cracking reactions [30-32], it was found that the catalysts generated exhibited the significantly high activity. In a recent study, the GSR method was examined in the presence of a two-layered structure catalyst [33-35], and it was also found that high activity was obtained by catalytic cracking of VGO and that there was clear relationship between the size of mesopore and the activity [34].

Therefore, the simple idea of examining the formation of GSR silica around zeolite single rather than that around two-layered catalysts was came up. The investigation was performed in the structure, acid properties and catalytic cracking properties of the prepared catalysts with changing the type of zeolite. In this chapter, to prepare zeolite-containing hierarchical two-layered catalysts (ZC2L) in which various zeolites were uniformly dispersed in large mesoporous silica matrix components using the GSR method were attempted. In addition, a catalytic cracking reaction of *n*-dodecane using these catalysts was carried out, and the effects of pore structure and acid properties on catalytic activity and product selectivity were evaluated.

3.2 Catalyst preparation

The following reagents were used to prepare ZC2L catalysts: Tetraethyl orthosilicate (TEOS; $\text{Si}(\text{OCH}_2\text{CH}_3)_4$, Nacalai Tesque, Inc.) was used for silica source. Ethanol (EtOH; $\text{CH}_3\text{CH}_2\text{OH}$, Nacalai Tesque, Inc.) and 2-propanol (2-PrOH; $\text{CH}_3\text{CH}(\text{OH})\text{CH}_3$, Nacalai Tesque, Inc.), 35 wt% hydrochloric acid (HCl aq., Nacalai Tesque, Inc.) and 28 wt% ammonia water (NH_3 aq., Nacalai Tesque, Inc.) were used for solvents and hydrolysis of TEOS in preparation of catalysts, respectively. Hexamethyldisiloxane (HS; $\text{O}(\text{Si}(\text{CH}_3)_3)_2$, Nacalai Tesque, Inc.) and acetic anhydride (AA; $(\text{CH}_3\text{CO})_2\text{O}$, Nacalai Tesque, Inc.) were reinforcing agent and solvent for GSR. ZSM-5 (HSZ-822HOA; $\text{SiO}_2/\text{Al}_2\text{O}_3 = 24$ mol/mol), Y (JRC-HY5.5; $\text{SiO}_2/\text{Al}_2\text{O}_3 = 5.5$ mol/mol, reference catalyst of Catalysis Society of Japan) and β (HSZ-940HOA; $\text{SiO}_2/\text{Al}_2\text{O}_3 = 37$ mol/mol) zeolites were produced by Tosoh Corp.

Kaolin (white clay; Practical Grade, Wako Pure Chemical Corp.) and alumina-sol (Cataloid AP-1; JGC Catalysts and Chemicals Ltd.) were utilized as filler and binder for the preparation of kaolin mixed catalysts.

3.2.1 Preparation of zeolite-containing hierarchical two-layered catalysts by gel skeletal reinforcement method

The ZC2L catalyst was prepared according to the flowchart shown in Figure 3.1 with reference to the previous reports [17,30,31,33,34]. The typical procedure is as follows: EtOH (15.00 g) and zeolite (1.30 g, weight of 26 wt% of the catalysts after calcining [31-35]) were added to a 200 mL PP beaker with a stir bar, and the mixture was stirred for 30 min. After TEOS (12.83 g) was added and was stirred for 30 min, 0.5 wt% HCl aq. (17.25 g) was added and stirred for 30 min. Then, pH was adjusted to 5 with 2.5 wt% NH_3 aq. and the temperature was raised to 50 °C. After the stir bar stopped, it was allowed to stand for 3 h. The gel was taken out and was immersed in a beaker containing 100 mL of ion-exchanged water for 18 h. After 18 h, the ion-exchanged water was removed with a pipette, and the gel was cut to about 5 mm cube. To remove water in the gel, replace the gel solvent with 2-PrOH using the following procedure: Added 30 mL of 2-PrOH (50 °C), allowed to stand for 5 min, and then drain using a pipette. This procedure was repeated 5 times. After replace of solvent, the gel is immersed in a reinforcing solution (a mixed solution of HS and AA, TEOS: HS = 1: 1 or 2, HS: AA = 1: 1 mol/mol) prepared in a sealed container made of PFA. Then, it was placed in an oven at 50 °C for 48 h. The solvent was changed again with 30 mL of 2-PrOH for 5 times and allowed to stand at 70 °C for 72 h. The resulted gel was calcined in 600 mL/min of dried air at 600 °C for 3 h (2.5 °C/min of programmed rate). The calcined material without molding was sieved to a particle size of 125 to 355 μm before use. The

Chapter 3

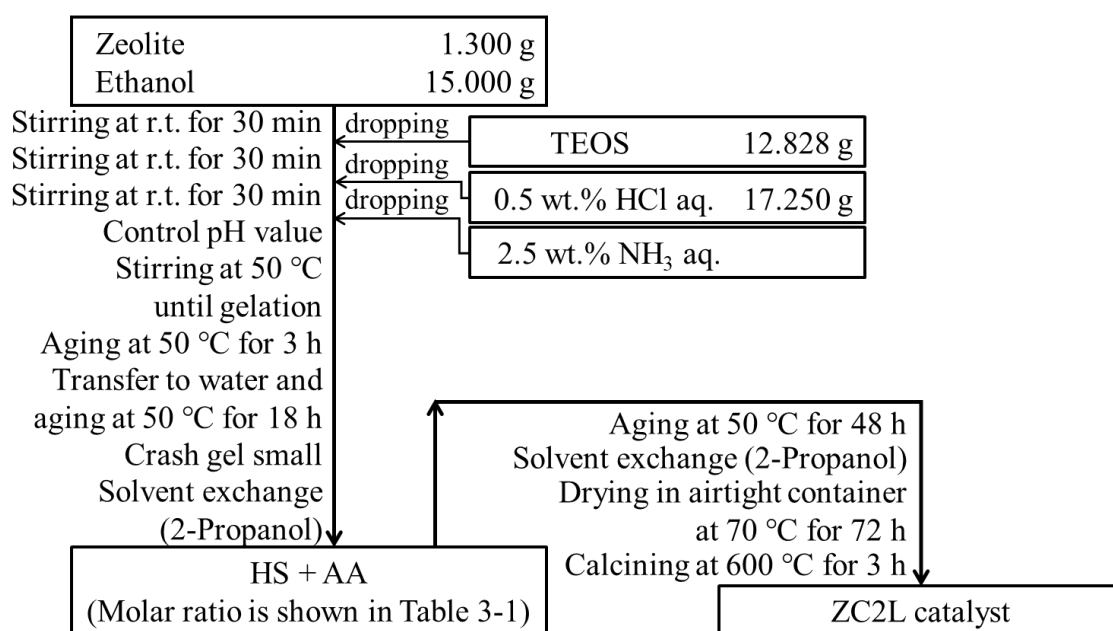


Figure 3.1 Flowchart for preparation of ZC2L catalyst.

Table 3.1 Catalyst name and composition of reinforcement solution of ZC2L catalyst.

Catalyst name	Molar ratio			$\frac{\text{HS (mol)}}{\text{TEOS (mol)}} \times 100$
	TEOS	HS	AA	
S-100HS-Zeolite	1.0	1.0	1.0	100
S-200HS-Zeolite	1.0	2.0	2.0	200

Zeolite: ZSM-5, β or Y

molar ratio of the reagents used to prepare each catalyst were shown in Table 3.1. For an example, a catalyst is named as S-100HS-ZSM-5 in which S indicates silica derived from TEOS and 100 indicates the molar ratio of HS/TEOS \times 100. In addition, the type of zeolite used is shown at the end.

3.2.2 Preparation of kaolin mixed catalyst with zeolite

The kaolin mixed catalyst was prepared by the method of kneading the mixture of kaolin (58 wt%), alumina-sol (16 wt%) and zeolite (26 wt%, ZSM-5, Y or β) described in the previous section while adding water little by little. The clay-like mixture made by kneading was pelletized to 0.5 mm diameter by a sodium press (NP-1; Sanki Seisakusho Co., Ltd.). The catalyst pellets

were calcined under the same conditions as that of the ZC2L catalyst. For example, a sample name is written as Kaolin-ZSM-5. The mixed catalysts were sieved to a particle size of 125 to 355 μm before catalytic test.

3.3 Characterization of zeolite-containing hierarchical two-layered catalysts

Characterizations of the prepared catalysts were carried out according to methods previously reported [32].

X-ray diffraction (XRD) patterns of prepared catalyst powder were measured by using a diffractometer Ultima IV (Rigaku Corp.) equipped with an X-ray tube with a Ni filter. About 0.1 g of the prepared catalyst was fixed to a glass sample holder so that the irradiation surface was flat, and set in the center of the measurement chamber. The tube voltage and tube current of the X-ray tube were set to 40 kV and 20 mA, respectively, and the $\text{CuK}\alpha$ ray ($\lambda = 1.5405 \text{ nm}$) generated was irradiated on the sample surface, and the diffraction pattern was acquired in the range of $2\theta = 3^\circ$ - 70° . The crystal state of the catalyst was confirmed from the obtained XRD pattern.

The pore characteristics of the prepared catalyst were obtained by nitrogen adsorption/desorption measurement using BELSORP-mini II (MicrotracBEL Corp.). Prior to this measurement, approximately 0.02 g of catalyst was treated in vacuum at 350 $^\circ\text{C}$ for 3 h using pretreatment device BELPERP-vac II (MicrotracBEL Corp.). The data obtained were analyzed using two methods. The BET method was used to calculate the total surface area (BET-SA), total pore volume (TPV) and average pore diameter (APD). For mesopores with pore diameters larger than 3.3 nm, the surface area, pore volume and pore diameter were calculated using the BJH method, and the mesopore distribution was also estimated.

The acid properties of the prepared catalyst were clarified by performing NH_3 temperature-programmed desorption (NH_3 -TPD) measurement by the ammonia pulse method. NH_3 adsorption was carried out by introducing a certain amount of gaseous NH_3 dehydrated by a cooling trap into 40 mg of a catalyst fixed with quartz wool (fine, 2–6 μm , Tosoh Corp.) in the center of the flow reactor connected to the gas chromatograph with thermal conductivity detector (GC-TCD). NH_3 adsorbed on the catalyst was desorbed by raising the temperature from 100 to 650 $^\circ\text{C}$ at a rate of 10 $^\circ\text{C}/\text{min}$ under He flow. Desorbed ammonia was detected by the connected GC-TCD. The conditions of GC-TCD are as follows: detector 170 $^\circ\text{C}$, column oven: 140 $^\circ\text{C}$, current: 100 mA, column flow rate: 50 mL/ min.

3.4 Activity test of zeolite-containing hierarchical catalysts in catalytic cracking of *n*-dodecane

The reaction apparatus is shown in Figure 2.3 [32]. The catalyst of 1.0 g was packed in a fixed bed down flow reactor (300 mm length and 8 mm internal diameter) with quartz wool and quartz sand (Wako Pure Chemical Corp.) in its top and bottom. Prior to the catalytic cracking reaction, the catalyst layer was heated to 500 °C at 5 °C/min while flowing N₂ (about 30 mL/min). At the same time as stopping the N₂ flow, *n*-dodecane (CH₃(CH₂)₁₀CH₃, Nacalai Tesque, Inc.) was fed to the reactor at about 1.3 mL/min for 80 s, then switched to the N₂ flow again and allowed to flow at about 30 mL/min for 30 min. The gas product was recovered with N₂ in a Tedlar bag, and the liquid product was recovered to the test tube by cool trap for the first 15 min with - 50 °C EtOH and for the next 15 min with 15 °C water, respectively.

The recovered gases and liquids were determined by a GC (GC-2014, GC-2010 Plus; Shimadzu Corp.) equipped with a flame ionization detector (FID). Product peaks detected by FID were identified by retention time of GC. Detailed analysis conditions for GC-FID measurement are described in the previous reports [31,32]. The catalyst was recovered to measure the weight of coke deposited by thermogravimetric-differential thermal analysis (TG-DTA, DTG-60AH, Shimadzu Corp.). The measurement was carried out by raising the temperature from 25 to 600 °C at a rate of 10 °C/min.

3.5 Results and discussion

3.5.1 Characterization of zeolite-containing hierarchical catalysts prepared by gel skeletal reinforcement method

The reaction mechanism in which large mesopores are formed by the GSR method was described elsewhere [31]. Figure 3.2 shows XRD patterns of ZC2L catalysts. As all the ZC2L catalysts exhibited characteristic diffraction peaks derived from the type of zeolite, it was confirmed that all ZC2L catalysts maintained the original zeolite crystal structure. However, the intensities of zeolite crystals became smaller than those of zeolite single because of their low contents. All ZC2L catalysts also had broad peaks derived from amorphous silica.

Figure 3.3 shows the mesopore size distribution of the ZC2L catalyst by nitrogen adsorption/desorption measurement. The respective nitrogen adsorption and desorption isotherms are shown in Figure 3.4. A type IV hysteresis loop indicating the presence of mesopores was observed.

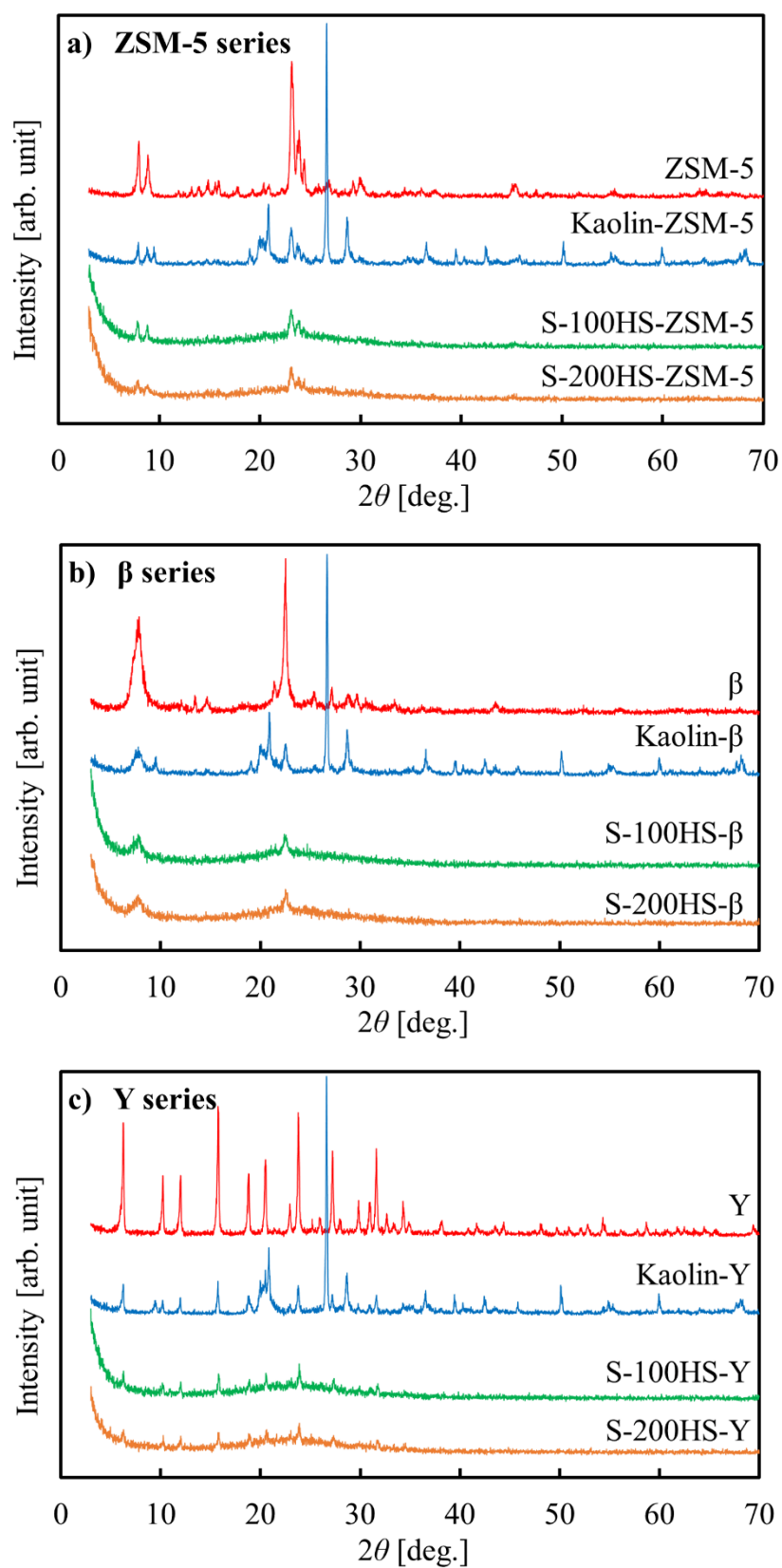


Figure 3.2 XRD patterns of ZC2L catalyst.

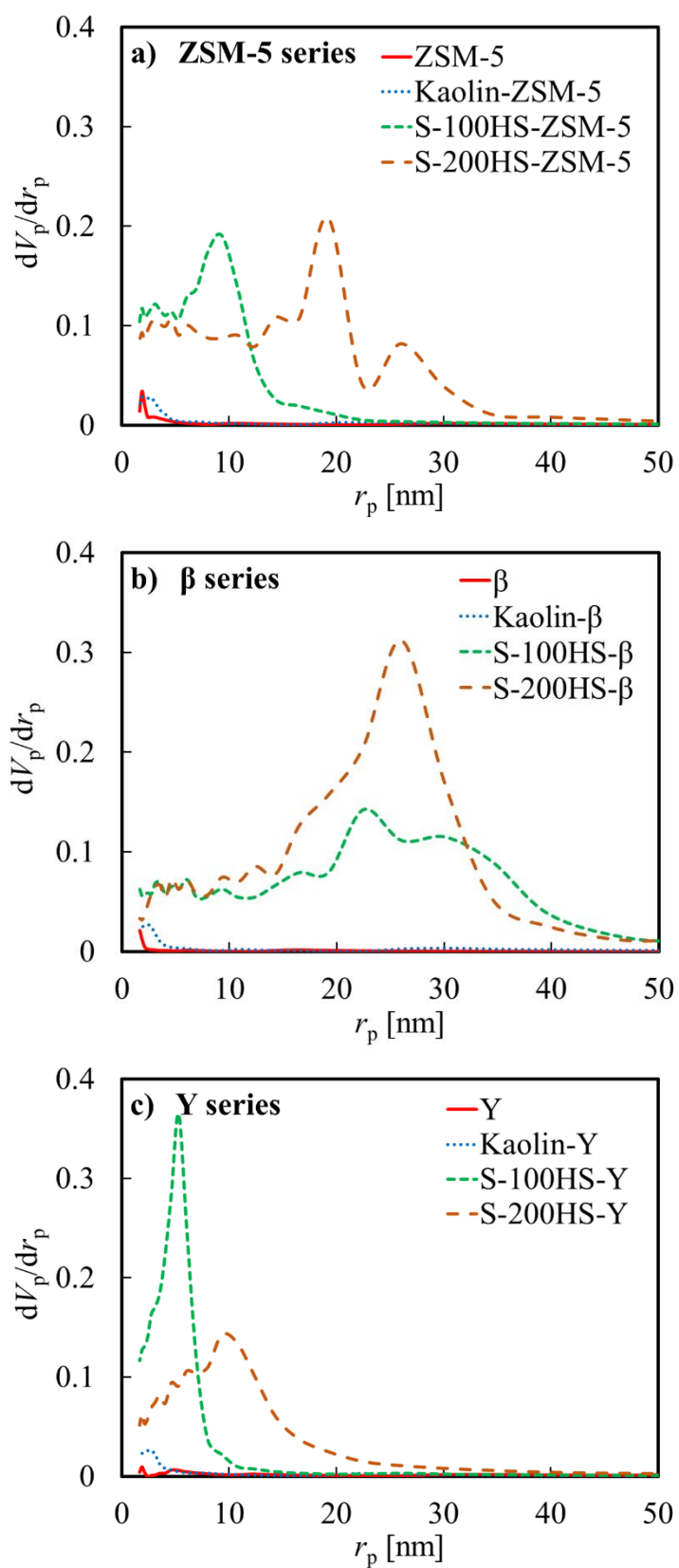


Figure 3.3 BJH pore-size distribution of ZC2L catalyst.

Chapter 3

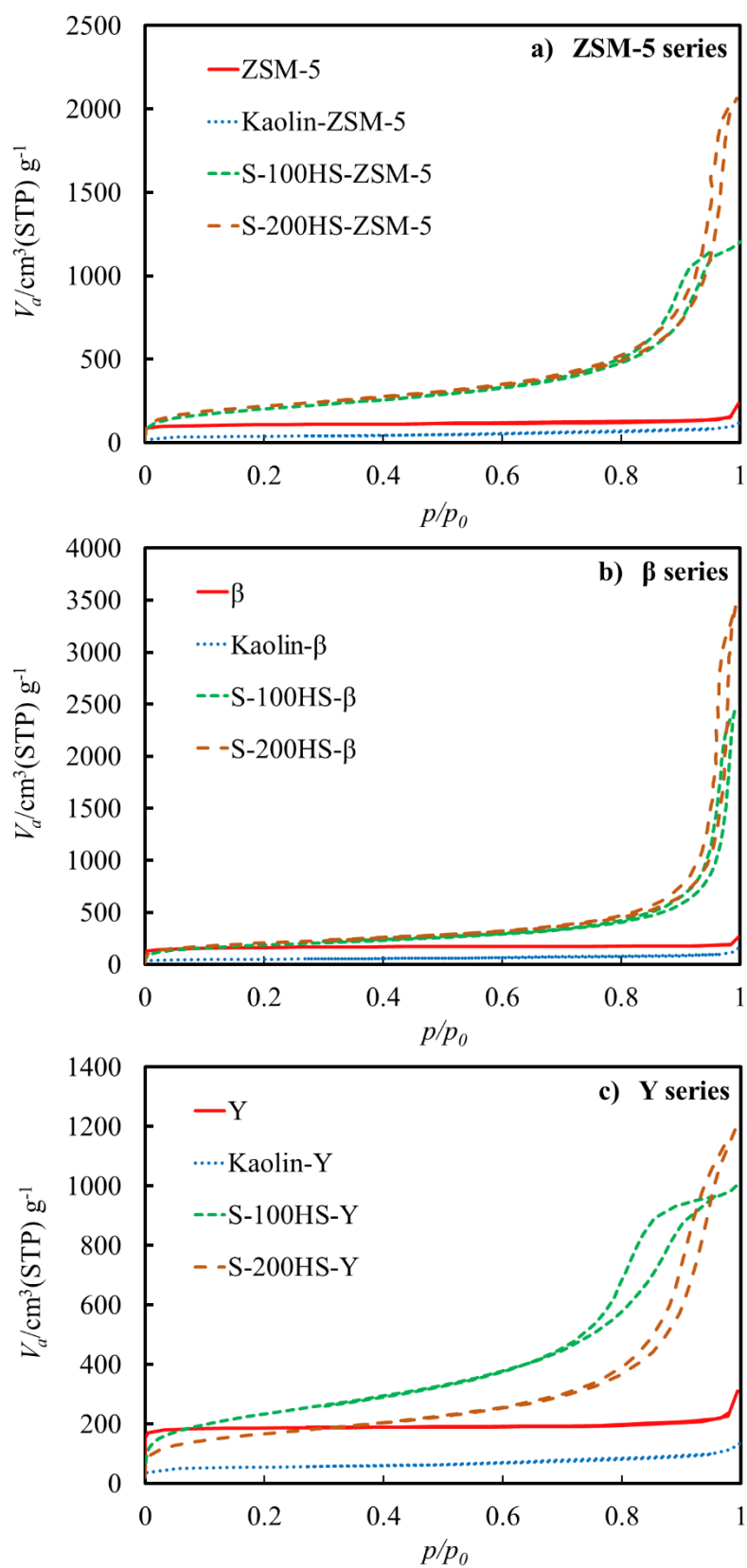


Figure 3.4 Nitrogen adsorption/desorption isotherms.

Chapter 3

rved in all the prepared catalysts except the kaolin mixed catalyst (Figure 3.4). This mesoporous profile was not changed regardless of the absence and presence of zeolite [31]. In Figure 3.3, the pore size increased as the HS/TEOS molar ratio increased. Further, the structures of various zeolites were maintained as shown in the XRD measurement of Figure 3.2. From these results, it was confirmed that the ZC2L catalysts produced in this study had both micropores and mesopores. In S-200HS- β , it seems that highly developed mesopores would develop around the zeolite. Although smaller than ZSM-5 and β , the Y series also had both zeolite micropores and large mesopores derived from TEOS and HS.

Table 3.2 shows the pore characteristics (BET-SA, TPV, APD, BJH-SA, BJH-PV and BJH-PD) of the ZC2L catalysts. It was found that most of the pores of ZC2L catalysts consisted of mesopores because the differences between the values of BET-SA and BJH-SA or the values of TPV and BJH-PV were very small. Further, as the HS/TEOS molar ratio increased, the pore volume and pore diameter increased [31,32]. Specifically, it was confirmed that S-200HS- β had BJH-PV of 5.1 cm³/g and BJH-PD of 25 nm and 52 nm. Relatively large mesopores were formed in the ZSM-5 and β series, however, the mesopore sizes of the Y series catalysts were not so large as those for the ZSM-5 and β series catalysts. The pore size of the ZC2L catalyst decreased in the

Table 3.2 Pore properties of ZC2L catalysts obtained by nitrogen adsorption/desorption measurement.

Catalyst	BET Surface area (m ² /g)	Total Pore volume (cm ³ /g)	Average Pore diameter (nm)	BJH		
				Surface area (m ² /g)	Pore volume (cm ³ /g)	Pore diameter (nm)
ZSM-5	388	0.30	3.1	34	0.14	3.7
Kaolin-ZSM-5	131	0.16	4.9	56	0.14	3.7
S-100HS-ZSM-5	730	1.82	10.0	552	1.72	18.6 (6.2)
S-200HS-ZSM-5	790	3.15	16.0	590	3.02	38.5 (6.2)
β	406	0.31	3.1	24	0.07	3.3
Kaolin- β	202	0.20	4.0	55	0.14	3.7
S-100HS- β	679	3.74	22.1	481	3.61	44.9 (60.2)
S-200HS- β	755	5.20	27.5	600	5.13	52.1 (24.8)
Y	668	0.45	2.7	20	0.16	3.7 (9.2)
Kaolin-Y	225	0.22	4.0	55	0.16	3.7
S-100HS-Y	847	1.54	7.3	628	1.41	10.6
S-200HS-Y	607	1.84	12.1	434	1.75	18.6 (12.1)

Chapter 3

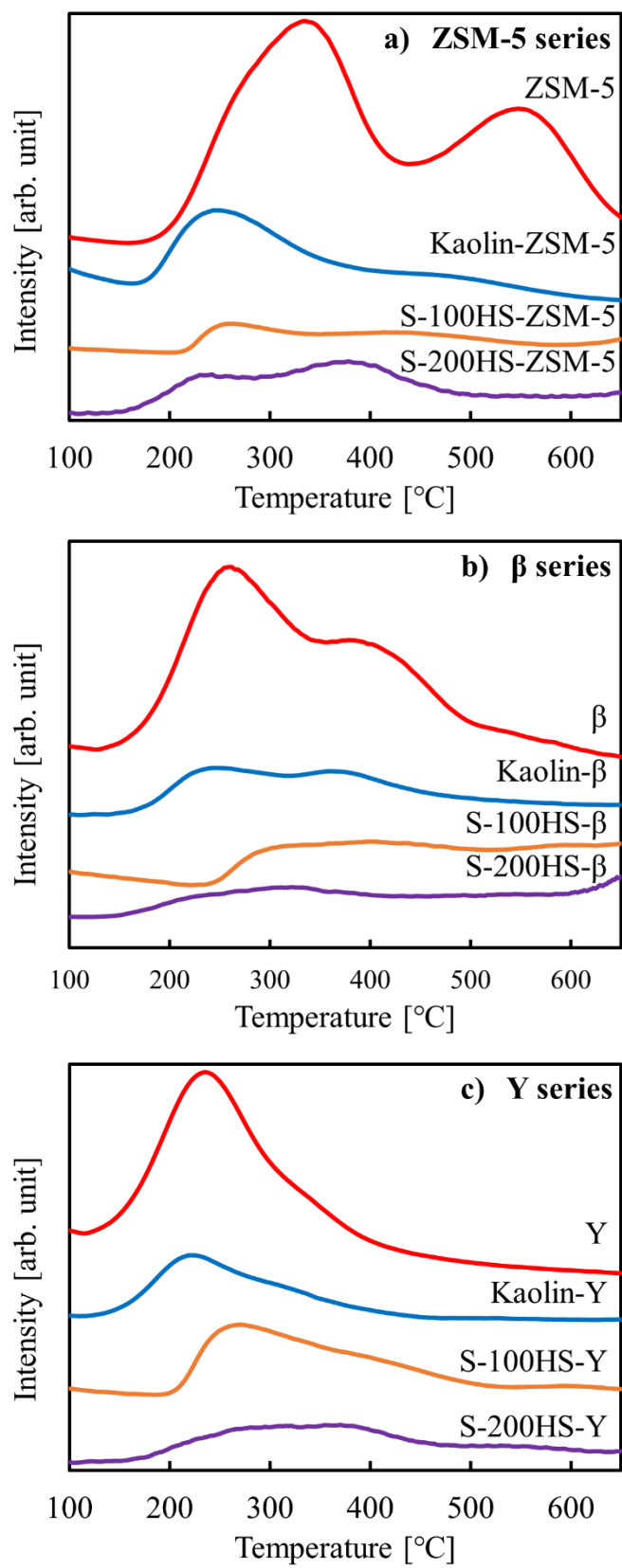


Figure 3.5 NH₃-TPD patterns of ZC2L catalyst.

Chapter 3

order of $\beta > \text{ZSM-5} > \text{Y}$ although the micropore size of zeolite decreases in a different order of $\text{Y} > \beta > \text{ZSM-5}$. On the other hand, the $\text{SiO}_2/\text{Al}_2\text{O}_3$ molar ratio of zeolite and extra-skeletal alumina may affect the size of the mesopores formed. It seems that since zeolite is present in the solvent (EtOH) from the first step at the preparation method of this study (Figure 3.1), acid sites derived from zeolite and elution of extra-skeletal alumina could affect the hydrolysis reaction of TEOS. As a result, it is likely that the characteristics of the mesopores would change depending on the type of zeolite used.

Figure 3.5 and Table 3.3 show TPD curves and values measured by NH_3 -TPD of the ZC2L catalyst. The low and high temperature peaks indicate desorption of NH_3 from weak and strong acid sites, respectively [9,37]. The amount of desorption decreased in all the prepared kaolin mixed catalysts and ZC2L catalysts as compared with the measurement results of zeolite single because of the low contents of zeolites for the prepared kaolin mixed catalysts and ZC2L catalysts.

For the ZSM-5 containing catalysts, the amounts of NH_3 desorption were the smallest probably because of the strong acidity of ZSM-5. Since the β series has a larger pore volume than other ZC2L catalysts, it is considered that more NH_3 was adsorbed (Table 3.3).

In our previous studies, when GSR-silica-gel was directly mixed with zeolite-containing two-layered catalyst, it was confirmed by TEM measurement after calcination that this two-layer-

Table 3.3 Product distribution, catalytic properties, parameters in gasoline fraction coke yield and amount of NH_3 desorbed.

Catalyst	Product distribution (wt%)					Parameters in gasoline fraction				Amount of NH_3 desorbed (10^{-4} mol/g)
	$\text{C}_1\text{-C}_4$	Gasoline ($\text{C}_5\text{-C}_{11}$)	C_{12} -	Coke yield (wt%)	Conv. (%)	O/P	iso- / n-	M/S	RON	
ZSM-5	74	25	1.03	1.56	60 (61) ^a	0.06	2.58	0.07	106	8.1
Kaolin-ZSM-5	69	31	0.17	0.50	96 (96) ^a	0.56	1.37	0.15	91	2.8
S-100HS-ZSM-5	79	21	0.13	0.65	98 (98) ^a	0.39	1.31	0.07	93	1.1
S-200HS-ZSM-5	65	34	0.65	0.73	99 (100) ^a	0.18	1.74	0.07	99	2.2
β [30]	58	42	0.48	6	84 (90) ^a	0.46	2.17	0.06	86	6.1
Kaolin- β [30]	54	46	0.25	0	67 (67) ^a	0.67	1.86	0.07	86	2.0
S-100HS- β	56	44	0.07	1.23	70 (71) ^a	0.95	2.27	0.13	88	2.4
S-200HS- β	59	41	0	2.90	70 (73) ^a	0.99	2.17	0.12	87	1.7
Y [30]	50	49	0.55	9	56 (65) ^a	0.13	4.44	0.06	85	7.8
Kaolin-Y [30]	46	54	0.31	1	47 (48) ^a	0.36	3.59	0.08	87	2.3
S-100HS-Y	56	44	0.20	2.44	58 (60) ^a	0.25	3.85	0.05	87	3.2
S-200HS-Y	56	44	0.38	2.42	54 (56) ^a	0.44	4.28	0.12	89	2.6

^aThe value in parenthesis represents total conversion which includes the conversion to coke.

ed catalyst was dispersed further in the resultant three-layered catalyst [36]. In the present study, although TEM was not measured, the silica matrix precursor solution was constantly stirred and the zeolite also remains uniform in the solution until gelation (a state in which the viscosity was spiked and whole solution was retained uniformly in the gel network). Therefore, it is considered that zeolites in the catalyst after calcination were also uniform.

3.5.2 Catalytic cracking of *n*-dodecane using zeolite-containing hierarchical two-layered catalysts

Figures 3.6 and 3.7 show the paraffins, olefins, naphthenes and aromatics (PONA) distribution and carbon number distribution in the catalytic cracking reaction, respectively. Table 3.3 shows the product distribution, the coke yield, the conversion of *n*-dodecane and some parameters in the gasoline fraction, where O/P means the ratio of olefins to paraffins, *iso*/*n* means the ratio of branched hydrocarbons to straight-chained hydrocarbons, m/s means the ratio of multi-branched hydrocarbons to single-branched hydrocarbons and RON means the research octane number. The conversions of the ZSM-5 series catalysts were very high because of the strong acidity of ZSM-5. The significant amounts of gaseous products were formed and the select-

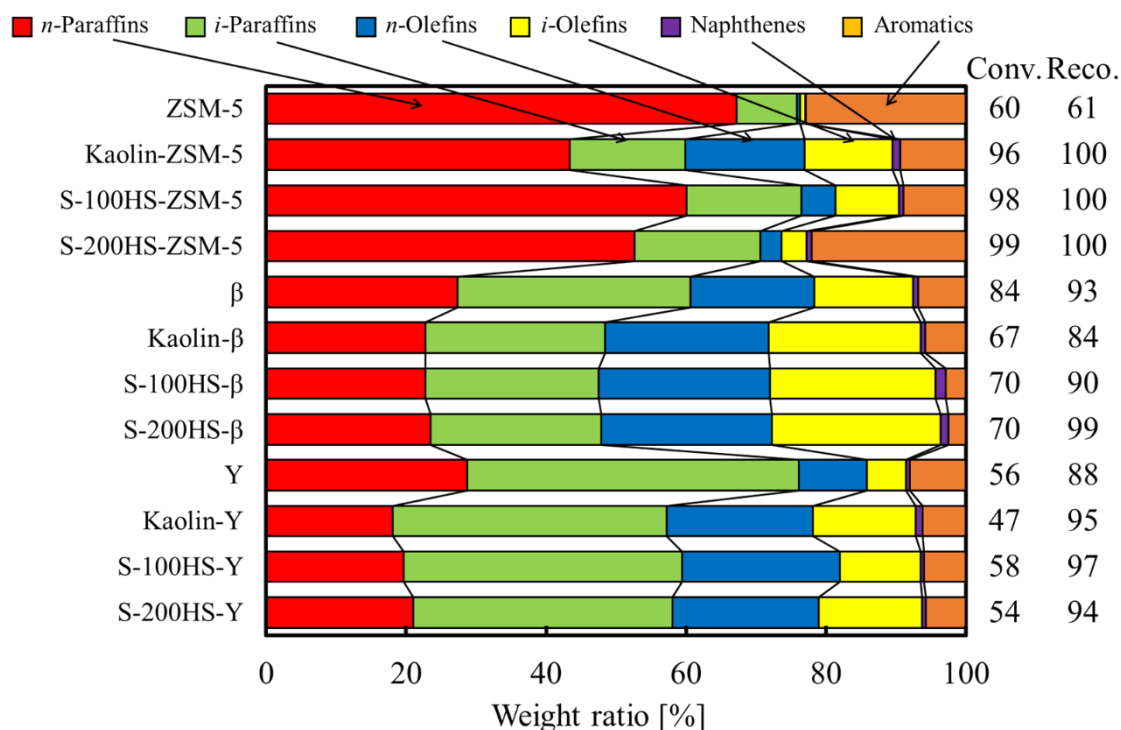


Figure 3.6 Selectivity for paraffins, olefins, naphthenes and aromatics in catalytic cracking of *n*-dodecane using ZC2L catalysts.

Chapter 3

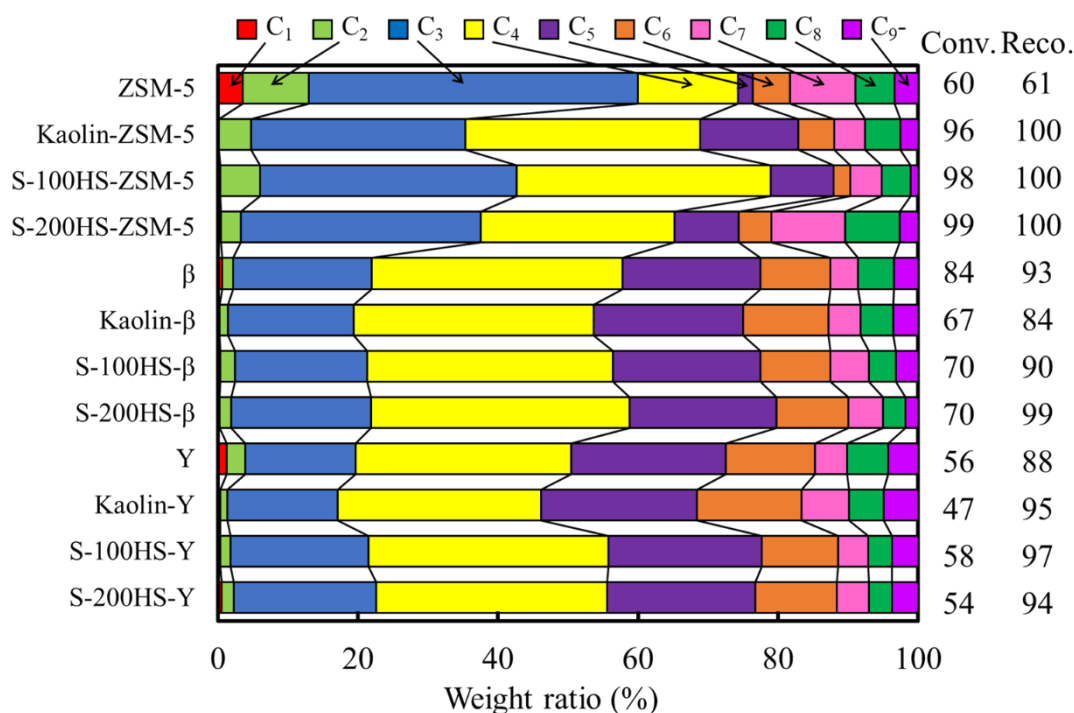


Figure 3.7 Distribution of carbon numbers in catalytic cracking of *n*-dodecane using ZC2L catalysts.

ivity for C₁-C₄ fraction exceeded 65 %. As Figure 3.6 includes hydrocarbons from C₁ to C₁₂, the selectivities of *n*-paraffin in hierarchical S-100HS-ZSM-5 and S-200HS-ZSM-5 were much higher than those of other catalysts except for single zeolites. Since zeolites themselves usually have the high ability of hydrogen transfer, the selectivity of paraffins for zeolite singles is high compared to those of catalysts with smaller amounts of zeolites. Since S-100HS-ZSM-5 and S-200HS-ZSM-5 have significant amounts of mesopores, it is likely that the acid sites would be diluted by the dispersion of ZSM-5 and that the diffusivity of substances into the micropores of ZSM-5 would have been improved by the primary cracking of *n*-dodecane in the mesopores. Therefore, it is considered that the cracking reaction is efficiently carried out and the conversion is improved as compared with the ZSM-5 single. The excessive hydrogen transfer reaction from paraffins to olefins was inhibited with the use of the hierarchical catalysts and the O/P ratios increased as shown in Table 3.3 [2,32]. On using the S-200HS-ZSM-5 prepared with the higher molar ratio of HS/TEOS, significant decrease in olefins and increase in aromatics were observed, indicating that dehydrocyclization of olefins to aromatics would proceed selectively [1,8]. Since ZSM-5 single exhibited the similar selectivity of PONA distribution, it seems that S-200HS-ZSM-5 catalyst would maintain the original characteristics of ZSM-5 zeolite. The β- and Y-zeolite containing catalysts also exhibited the suppressed hydrogen transfer reaction and the olefin

Chapter 3

selectivity in PONA distribution and the higher O/P ratio in the gasoline fraction were observed in comparison with those of single β - and Y-zeolite. In contrast to results from ZSM-5-containing catalysts, the formation of aromatics was suppressed and the higher olefin selectivity was observed, suggesting that aromatics could not be formed through cyclization of lower olefins using β -zeolite and Y-zeolite, different from ZSM-5.

In the carbon number distribution (Figure 3.7), the selectivity of C_3 for ZSM-5-containing catalysts was much higher than those of β - and Y-zeolite containing catalysts. The selectivity of C_7 fraction was high for S-200HS-ZSM-5, which may be related to the high selectivity of aromatics. In dehydrocyclization of *n*-pentane using ZnZSM-5- and GaZSM-5-containing composite catalysts, it was suggested that toluene could be formed by the reaction of propene with C_4 olefins through Diels–Alder reaction [38,39]. The selectivity for C_3 and C_4 fractions also decreased in this S-200HS-ZSM-5 catalyst, indicating that this type of cyclization would occur on ZSM-5. In contrast, the decreases in C_3 and C_4 fractions were not observed in the β - and Y-zeolite-containing catalysts, indicating that cyclization of propene with C_4 olefins could hardly occur on β - and Y-zeolite.

When ZSM-5-series ZC2L catalysts were used, RON was higher than those of β - and Y-series ZC2L catalysts probably because of the high selectivity of aromatics. In the β series, the larger mesopores of the prepared ZC2L catalyst became a reaction field capable of converting *n*-dodecane into a multi-branch product, which was considered to have improved the gasoline fraction characteristics. In addition, the *iso/n*-ratios of the Y series were larger than those of other zeolite series, indicating that the presence of the super cage of Y could bring about the increase in the formation of branched products. On the other hand, in the β series ZC2L catalyst, the *iso/n*-ratio and the *m/s* ratio are relatively high. The cracking reaction mainly proceeded in the ZSM-5 series ZC2L catalyst because of its high reactivity, and it seems that the structure of microporous ZSM-5 could play an important role to produce aromatics from lower olefins [9].

The coke yield was measured after catalytic cracking of *n*-dodecane and the results are shown in the middle column of Table 3.3. Using ZSM-5 single, 1.56 wt% of coke was deposited, but with ZSM-5-series ZC2L catalysts, there was a tendency for each catalyst to form about 0.7 wt% of coke, suggesting that the presence of mesopores could rapidly diffuse the reactive cracking products, precursors of coke, to the outside of pores [5,8,9]. In addition, it is considered that the distribution of acid sites was effectively adjusted [9]. Since the ZSM-5-series ZC2L catalysts had the high cracking activity, it did not generate a lot of coke [15,16]. In the β - and Y-zeolite-series ZC2L catalysts, about 1 to 3 wt% of coke was formed. Since extra-skeletal alumina is present in Y and is dispersed in the silica derived from TEOS during the catalyst preparation, new acid sites formed would yield a lot of coke.

In the present study, various hierarchical ZC2L catalysts with large mesopores were prepared

Chapter 3

by preparing zeolite-containing gel, and higher activity was obtained in catalytic cracking of *n*-dodecane at 500 °C. It was found that a catalyst with the high catalytic activity could be produced by combining a small amount of zeolite with large mesoporous silica prepared by the gel skeletal reinforcement method.

3.6 Conclusions

In this study, to prepare various ZC2L catalyst having a more uniform microporous and mesoporous hierarchical structure, zeolite was dispersed in the sol-gel process to prepare mesoporous silica by the GSR method. As a result, a hierarchical composite of zeolite and mesoporous silica (ZC2L catalyst) could be prepared by a simpler procedure than before. Using these catalysts, a catalytic cracking of *n*-dodecane was carried out in a fixed bed reactor, and the effects of the microporous and mesoporous hierarchical structure on the reactivity were evaluated. ZSM-5-, β - and Y-zeolite-series ZC2L catalysts exhibited the better activity and product selectivity than zeolite single and kaolin mixed catalysts due to presence of their large mesopores.

Acknowledgements

A part of this work was supported by the Alumni Association of Graduate School of Engineering in Mie University. The authors also thank Mr. Koudai Mizuno for his helpful work.

References

- [1] E. T. C. Vogt, B. M. Weckhuysen, “Fluid catalytic cracking: recent developments on the grand old lady of zeolite catalysis”, *Chem. Soc. Rev.*, 44 (2015) 7342-7370, <https://doi.org/10.1039/c5cs00376h>
- [2] M. S. Aghakhani, A. A. Khodadadi, Sh. Najafi, Y. Mortazavi, “Enhanced triisopropylbenzene cracking and suppressed coking on tailored composite of Y-zeolite/amorphous silica–alumina catalyst”, *J. Ind. Eng. Chem.*, 20, 5 (2014) 3037-3045, <https://doi.org/10.1016/j.jiec.2013.11.040>
- [3] Q. Yu, H. Sun, H. Sun, L. Li, X. Zhu, S. Ren, Q. Guo, B. Shen, “Highly mesoporous IM-5 zeolite prepared by alkaline treatment and its catalytic cracking performance”, *Microporous Mesoporous Mater.*, 273 (2019) 297-306, <https://doi.org/10.1016/j.micromeso.2018.08.016>
- [4] Z. Qin, B. Shen, X. Gao, F. Lin, B. Wang, C. Xu, “Mesoporous Y zeolite with homogeneous aluminum distribution obtained by sequential desilication–dealumination and its performance in the catalytic cracking of cumene and 1,3,5-triisopropylbenzene”, *J. Catal.*, 278 (2011) 266-275, <https://doi.org/10.1016/j.jcat.2010.12.013>
- [5] X. Zhang, D. Cheng, F. Chen, X. Zhan, “n-Heptane catalytic cracking on hierarchical ZSM-5 zeolite: The effect of mesopores”, *Chem. Eng. Sci.*, 168 (2017) 352-359, <https://doi.org/10.1016/j.ces.2017.05.012>
- [6] T. Odedairo, R. J. Balasamy, S. Al-Khattaf, “Influence of mesoporous materials containing ZSM-5 on alkylation and cracking reactions”, *J. Mol. Catal. A: Chem.*, 345 (2011) 21-36, <https://doi.org/10.1016/j.molcata.2011.05.015>
- [7] P. Sazama, B. Wichterlova, J. Dedecek, Z. Tvaruzkova, Z. Musilova, L. Palumbo, S. Sklenak, O. Gonsiorova, “FTIR and 27Al MAS NMR analysis of the effect of framework Al- and Si-defects in micro- and micro-mesoporous H-ZSM-5 on conversion of methanol to hydrocarbons”, *Microporous Mesoporous Mater.*, 143 (2011) 87-96, <https://doi.org/10.1016/j.micromeso.2011.02.013>
- [8] T. Zhao, F. Li, H. Yu, S. Ding, Z. Li, X. Huang, X. Li, X. Wei, Z. Wang, H. Lin, “Synthesis of mesoporous ZSM-5 zeolites and catalytic cracking of ethanol and oleic acid into light olefins”, *Appl. Catal. A: Gen.*, 575 (2019) 101-110, <https://doi.org/10.1016/j.apcata.2019.02.011>
- [9] Y. Sang, H. Li, “Effect of phosphorus and mesopore modification on the HZSM-5 zeolites for n-decane cracking” *J. Solid State Chem.*, 271 (2019) 326-333, <https://doi.org/10.1016/j.jssc.2019.01.016>
- [10] M. Pan, J. Zheng, Y. Liu, W. Ning, H. Tian, R. Li, “Construction and practical application of a novel zeolite catalyst for hierarchically cracking of heavy oil”, *J. Catal.*, 369 (2019) 72-85, <https://doi.org/10.1016/j.jcat.2018.10.032>
- [11] X. Hou, W. Zhu, Y. Tian, Y. Qiu, Z. Diao, F. Feng, X. Zhang, G. Liu, “Superiority of ZrO₂

Chapter 3

surface enrichment on ZSM-5 zeolites in n-pentane catalytic cracking to produce light olefins”, *Microporous Mesoporous Mater.*, 276, 1 (2019) 41-51, <https://doi.org/10.1016/j.micromeso.2018.09.019>

[12] T. Wu, G. Yuan, S. Chen, D. Zhao, J. Xu, T. Fan, Y. Cao, “Butylene catalytic cracking to propylene over a hierarchical HZSM-5 zeolite: Location of acid sites controlling the reaction pathway”, *Mole. Catal.*, 453 (2018) 161-169, <https://doi.org/10.1016/j.mcat.2018.04.026>

[13] Y. Ji, H. Yang, Q. Zhang, W. Yan, “Phosphorus modification increases catalytic activity and stability of ZSM-5 zeolite on supercritical catalytic cracking of n-dodecane”, *J. Solid State Chem.*, 251 (2017) 7-13, <https://doi.org/10.1016/j.jssc.2017.03.023>

[14] B. Wang, C. Han, Q. Zhang, C. Li, C. Yang, H. Shan, “Studies on the Preliminary Cracking of Heavy Oils: The Effect of Matrix Acidity and a Proposal of a New Reaction Route”, *Energy Fuels*, 29, 9 (2015) 5701-5713, <https://doi.org/10.1021/acs.energyfuels.5b01280>

[15] B. T. Holland, V. Subramani, S. K. Gangwal, “Utilizing Colloidal Silica and Aluminum-Doped Colloidal Silica as a Binder in FCC Catalysts: Effects on Porosity, Acidity, and Microactivity”, *Ind. Eng. Chem. Res.*, 46, 13 (2007) 4486-4496, <https://doi.org/10.1021/ie0702734>

[16] S. Al-Khattaf, “The Influence of Alumina on the Performance of FCC Catalysts during Hydrotreated VGO Catalytic Cracking”, *Energy Fuels*, 17, 1 (2003) 62-68, <https://doi.org/10.1021/ef020066a>

[17] P. R. Aravind, P. Mukundan, P. K. Pillai, K. G. K. Warriar, “Mesoporous silica–alumina aerogels with high thermal pore stability through hybrid sol–gel route followed by subcritical drying”, *Microporous Mesoporous Mater.*, 96 (2006) 14-20. <https://doi.org/10.1016/j.micromeso.2006.06.014>

[18] Y. Jiang, X. Ding, J. Zhao, H. Bala, X. Zhao, Y. Tian, K. Yu, Y. Sheng, Y. Guo, Z. Wang, “A facile route to synthesis of hollow SiO₂/Al₂O₃ spheres with uniform mesopores in the shell wall”, *Mater. Lett.*, 59 (2005) 2893-2897, <https://doi.org/10.1016/j.matlet.2005.04.037>

[19] Y. Jiang, J. Zhao, H. Bala, H. Xu, N. Tao, X. Ding, Z. Wang, “Synthesis of stable hollow spheres of Si/Al composite oxide with controlled pore size in the shell wall”, *Mater. Lett.*, 58 (2004) 2401-2405, <https://doi.org/10.1016/j.matlet.2004.02.046>

[20] R. Takahashi, S. Sato, T. Sodesawa, M. Yabuki, “Silica–Alumina Catalyst with Bimodal Pore Structure Prepared by Phase Separation in Sol–Gel Process”, *J. Catal.*, 200 (2001) 197-202, <https://doi.org/10.1006/jcat.2001.3196>

[21] H. Izutsu, F. Mizukami, T. Sashida, K. Maeda, Y. Kiyozumi, Y. Akiyama, “Effect of malic acid on structure of silicon alkoxide derived silica”, *J. Non-Cryst. Solids*, 212 (1997) 40-48, [https://doi.org/10.1016/S0022-3093\(96\)00620-5](https://doi.org/10.1016/S0022-3093(96)00620-5)

[22] P. Padmaja, G.M. Anilkumar, P. Mukundan, G. Aruldas, K.G.K. Warriar, “Characterisation

Chapter 3

- of stoichiometric sol–gel mullite by fourier transform infrared spectroscopy”, *Int. J. Inorg. Mater.*, 3 (2001) 693-698, [https://doi.org/10.1016/S1466-6049\(01\)00189-1](https://doi.org/10.1016/S1466-6049(01)00189-1)
- [23] B. Dragoi, A. Gervasini, E. Dumitriu, A. Auroux, “Calorimetric determination of the acidic character of amorphous and crystalline aluminosilicates”, *Thermochim. Acta*, 420 (2004) 127-134, <https://doi.org/10.1016/j.tca.2003.10.031>
- [24] A. Carati, G. Ferraris, M. Guidotti, G. Moretti, R. Psaro, C. Rizzo, “Preparation and characterisation of mesoporous silica–alumina and silica–titania with a narrow pore size distribution”, *Catal. Today*, 77 (2003) 315-323, [https://doi.org/10.1016/S0920-5861\(02\)00376-0](https://doi.org/10.1016/S0920-5861(02)00376-0)
- [25] C. J. Brinker, G. W. Scherer, “Sol-Gel Science: The Physics and Chemistry of Sol-Gel Processing”, *Academic Press* (1990) 1-908, <https://doi.org/10.1016/C2009-0-22386-5>
- [26] J. D. Wright, N. A. J. M. Sommerdijk, “Sol-Gel Materials, chemistry and application”, *CRC Press* (2000) 1-129, <https://doi.org/10.1201/9781315273808>
- [27] E. M. Lucas, M. S. Doescher, D. M. Ebenstein, K. J. Wahl, D. R. Rolison, “Silica aerogels with enhanced durability, 30-nm mean pore-size, and improved immersibility in liquids”, *J. Non-Cryst. Solids*, 350 (2004) 244-252, <https://doi.org/10.1016/j.jnoncrsol.2004.07.074>
- [28] P. B. Sarawade, J. K. Kim, A. Hilonga, H. T. Kim, “Production of low-density sodium silicate-based hydrophobic silica aerogel beads by a novel fast gelation process and ambient pressure drying process”, *Solid State Sci.*, 12 (2010) 911-918, <https://doi.org/10.1016/j.solidstatesciences.2010.01.032>
- [29] M. Falco, E. Morgado, N. Amadeo, U. Sedran, “Accessibility in alumina matrices of FCC catalysts”, *Appl. Catal. A: Gen.*, 315, 23 (2006) 29-34, <https://doi.org/10.1016/j.apcata.2006.08.028>
- [30] A. Ishihara, K. Tatebe, T. Hashimoto, H. Nasu, “Preparation of Silica, Alumina, Titania, and Zirconia with Different Pore Sizes Using Sol–Gel Method and Their Properties as Matrices in Catalytic Cracking”, *Ind. Eng. Chem. Res.*, 57, 43 (2018) 14394-14405, <https://doi.org/10.1021/acs.iecr.8b03019>
- [31] A. Ishihara, H. Oono, T. Hashimoto, H. Nasu, “Preparation of SiO₂ and SiO₂-Al₂O₃ catalysts by gel skeletal reinforcement using hexamethyldisiloxane (HMDS) and acetic anhydride and aluminum tri-sec-butoxide (ASB) systems and elucidation of their catalytic cracking properties as matrices”, *Microporous Mesoporous Mater.*, 233 (2016) 163-170, <https://doi.org/10.1016/j.micromeso.2016.01.025>
- [32] S. Matsuura, T. Hashimoto, A. Ishihara, “Preparation of β-zeolite mixed catalysts using alumina and titania matrices modified by silication of gel skeletal reinforcement and their reactivity for catalytic cracking of n-dodecane”, *Appl. Catal. A, Gen.*, 610 (2021) 117959, <https://doi.org/10.1016/j.apcata.2020.117959>
- [33] A. Ishihara, M. Ninomiya, T. Hashimoto, H. Nasu, “Catalytic cracking of C₁₂-C₃₂

Chapter 3

- hydrocarbons by hierarchical β - and Y-zeolite-containing mesoporous silica and silica-alumina using Curie point pyrolyzer”, *J. Anal. Appl. Pyrol.*, 150 (2020) 104876, <https://doi.org/10.1016/j.jaap.2020.104876>
- [34] A. Ishihara, S. Matsuura, F. Hayashi, K. Suemitsu, T. Hashimoto, “Estimation of Catalytic Cracking of Vacuum Gas Oil by a Y Zeolite-Containing Two-Layered Catalyst and a Novel Three-Layered Hierarchical Catalyst Using a Curie Point Pyrolyzer Method”, *Energy Fuels*, 34 (2020) 7448–7454, <https://doi.org/10.1021/acs.energyfuels.0c00957>
- [35] B. C. Gates, J. R. Katzer, G. C. A. Schuit, “Chemistry of Catalytic Process”, *McGraw-Hill* (1979) Catalytic reforming, Chapter 3, <https://doi.org/10.1002/aic.690250427>
- [36] A. Ishihara, T. Tsukamoto, T. Hashimoto, H. Nasu, “Catalytic cracking of soybean oil by ZSM-5 zeolite-containing silica-aluminas with three layered micro-meso-meso-structure”, *Catal. Today*, 303 (2018) 123-129, <https://doi.org/10.1016/j.cattod.2017.09.033>
- [37] H. Li, S. He, K. Ma, Q. Wu, Q. Jiao, K. Sun, “Micro-mesoporous composite molecular sieves H-ZSM-5/MCM-41 for methanol dehydration to dimethyl ether: Effect of $\text{SiO}_2/\text{Al}_2\text{O}_3$ ratio in H-ZSM-5”, *Appl. Catal. A, Gen.*, 450 (2013) 152-159, <https://doi.org/10.1016/j.apcata.2012.10.014>
- [38] A. Ishihara, K. Takai, T. Hashimoto, H. Nasu, “Effects of a Matrix on Formation of Aromatic Compounds by Dehydrocyclization of n-Pentane Using ZnZSM-5– Al_2O_3 Composite Catalysts”, *ACS Omega*, 5 (2020) 11160-11166, <https://doi.org/10.1021/acsomega.0c01147>
- [39] A. Ishihara, Y. Kodama, T. Hashimoto, “Effect of matrix on aromatics production by cracking and dehydrocyclization of n-pentane using Ga ion-exchanged ZSM-5-alumina composite catalysts”, *Fuel Processing Technology*, 213 (2021) 106679, <https://doi.org/10.1016/j.fuproc.2020.106679>

Chapter 4

Catalytic cracking of low-density polyethylene over zeolite-containing hierarchical two-layered catalyst with different mesopore size using Curie point pyrolyzer

Zeolite-containing hierarchical two-layered (ZC2L) catalysts were prepared by the gel skeletal reinforcement method. Their reactivity was estimated in catalytic cracking of low-density polyethylene (LDPE) at 590 °C using a Curie point pyrolyzer method. In addition, the “relative activity” per amount of zeolite in the catalyst was calculated, and the relationship between the pore and acid properties of each catalyst was investigated. The results suggested that the presence of both mesopores and the strong acid sites of zeolite would be closely related to the increase in activity. ZSM-5-ZC2L catalysts showed much higher aromatics selectivity especially for toluene and *p*-xylene than ZSM-5 single and kaolin-mixed catalysts. In contrast to the cases of ZSM-5-containing catalysts, β -zeolite-containing catalysts and Y-zeolite-containing catalysts selectively produced *i*-olefins and *i*-paraffins, respectively. The product selectivity of the ZC2L catalyst was influenced by the size of the micropores of the zeolite while the hierarchical ZC2L catalysts with a small amount (26 wt%) of zeolite exhibited the higher activity than zeolite single catalysts.

4.1 Introduction

Polyethylene is used in large quantities in various fields for applications such as containers and packaging, and is an important material indispensable for today's life [1]. In industrial applications, polyethylene is used as a packaging material to prevent damage during transportation of industrial products [1], and is often discarded after transportation, and thus the product life is relatively short. For the effective use of limited petroleum resources, it is important to recycle such waste. In recent years, many studies have been conducted in order to recycle waste plastic products, and one of technologies includes their conversion to transportation fuels and petrochemical raw materials using catalysts [2-19]. When polyethylene is pyrolyzed, linear

Chapter 4

hydrocarbons having about 1-40 carbon atoms are mainly produced [20]. Transportation fuel and petrochemical raw materials can be obtained by further cracking the pyrolyzed hydrocarbons in the presence of a catalyst to increase product selectivity. The catalyst for catalytic cracking process mainly has the ability to crack heavy hydrocarbons such as vacuum gas oil (VGO) having about 20-45 carbon atoms and atmospheric residue (AR) with carbon atoms similar to and higher than those of VGO [21-23]. Therefore, it is considered that the catalyst for catalytic cracking process works effectively even on the pyrolysis products of polyethylene having a wide carbon number distribution of 1-40, and many studies using spent fluid catalytic cracking catalysts have been conducted [7,10,13,14,16]. It has been shown that catalytic cracking of low-density polyethylene (LDPE) produced not only paraffins and aromatic compounds [7] but also gas products [14]. On the other hand, HZSM-5 produced gases with high C₃ content while H- β yielded gases with high C₄₋₅ content [11]. Further, it was confirmed that in catalytic cracking of high-density polyethylene (HDPE), a characteristic pattern of product distribution was observed depending on the structure of the zeolite used [18]. When ZSM-5/MCM-41 was used in the catalytic cracking of HDPE, the product distribution was similar to that of HZSM-5 while a higher amount of light hydrocarbons, especially C₃₋₅ olefins, was obtained [19].

In our previous studies, it was found that novel hierarchical catalysts with a matrix having large mesoporous silica as well as microporous zeolite could be prepared using the gel skeletal reinforcement (GSR) method, and that these catalysts were effective in catalytic cracking of linear hydrocarbons (such as *n*-dodecane), AR, VGO and soybean oil [24-37]. Further, it was also found that the Curie point pyrolyzer (CPP) method could also be very useful for small-scale and rapid estimation of catalytic cracking of high boiling compounds such as VGO, AR, and soybean oil [27, 31-37]. In these studies, it was shown that the proper distribution of large mesopores and acid sites is necessary for efficient conversion of large size molecules [24-37]. In this study, in order to obtain olefins and aromatic compounds as petrochemical feedstocks, catalytic cracking of LDPE was performed using zeolite-containing hierarchical two-layered (ZC2L) catalysts [29] prepared by the GSR method and their catalytic activity and selectivity of products were evaluated using the CPP method.

4.2 Catalyst preparation and characterization

The catalyst was prepared according to the procedure shown in Figure 3.1 [29]. The zeolites used were ZSM-5 (HSZ-822HOA; SiO₂/Al₂O₃ (mol/mol) = 24, Tosoh Corp.), β (HSZ-940HOA; SiO₂/Al₂O₃ (mol/mol) = 37, Tosoh Corp.) and Y (JRC-HY5.5; SiO₂/Al₂O₃ (mol/mol) = 5.5, reference catalyst of Catalysis Society of Japan), and the amount of these zeolites was adjusted to 26 wt% of the catalyst weight after calcination [26,28,29]. The zeolite was added to ethanol

Chapter 4

(EtOH; CH₃CH₂OH, Nacalai Tesque, Inc.), and tetraethyl orthosilicate (TEOS; Si(OCH₂CH₃)₄, Nacalai Tesque, Inc.) was added dropwise into a suspension of zeolite. After stirring for 30 min., 0.5 wt% hydrochloric acid (HCl aq.; 35 wt% hydrochloric acid, Nacalai Tesque, Inc.) was subsequently added and the mixture was further stirred for 30 min. The temperature was raised to 50 °C, 2.5 wt% ammonia water (NH₃ aq.; 28 wt% ammonia water, Nacalai Tesque, Inc.) was added, and a gel was formed. The preparation method of gel was referred to the conventional sol-gel process [38]. After aging the gel in water at 50 °C, the gel was divided into about 5 mm cube-like, and the solvent was exchanged with 2-propanol (2-PrOH; CH₃CH(OH)CH₃, Nacalai Tesque, Inc.). Subsequently, the gel was added to a predetermined concentration of hexamethyldisiloxane (HS; O(Si(CH₃)₃)₂, Nacalai Tesque, Inc.) and acetic anhydride (AA, (CH₃CO)₂O, Nacalai Tesque, Inc.) solution in the GSR method and was held at 50 °C for 48 h [26,28,29,36,37]. After the similar solvent exchange process, the gel was dried in airtight container at 70 °C for 72 h. The resultant gel was calcined at 600 °C for 3 h under dry air. The ZC2L catalyst name was shown as “S-100HS-ZSM-5” by combining the ratio (%) of HS (mol) to TEOS (mol) and the zeolite name. Details of the catalyst name of the ZC2L catalyst and the composition of the HS-AA solution were shown in Table 3.1. For comparison with and without mesopores, the kaolin mixed catalyst by the kneading method was also prepared using kaolin (white clay; Practical Grade, Wako Pure Chemical Corp.), alumina-sol (Cataloid AP-1; JGC Catalysts and Chemicals Ltd.) and above-mentioned zeolite [29]. The kaolin mixed catalyst was shown as “Kaolin-ZSM-5”.

An X-ray diffractometer (UltimaIV, Rigaku Corp.) was used to measure the XRD patterns of each catalyst. Nitrogen adsorption-desorption was performed on BELSORP-mini II (MicrotracBEL Corp.) for measuring pore properties of catalysts. Ammonia temperature programmed desorption (NH₃-TPD) was also performed by ammonia pulse method using GC equipped with TCD detector (GC-8A, Shimadzu Corp.) to elucidate acid properties of catalysts. To estimate the amount of coke formed on spent catalysts, thermogravimetric analysis (TGA; DTG-60AH, Shimadzu Corp.) was operated. The method of these characterizations was mentioned in detail elsewhere [28,29].

4.3 Catalytic cracking of LDPE using the CPP method

The reaction apparatus of CPP was shown in Figure 4.1. 0.20 mg of LDPE (Polyethylene powder, low density, 500 μm, melt flow index: 17.5-23.5 g/ 10 min, Thermo Fisher Scientific Inc.) and 1.00 mg of catalysts were put together in ferromagnetic pyrolysis foil (Pyro-foil, F590, Japan Analytical Industry Co., Ltd.). Then, Pyro-foil was set into Curie point injector (JCI-22, Japan Analytical Industry Co., Ltd.). The injector of the CPP apparatus was preheated at 150 °C and the needle of the injector was introduced into the injection port of GC-FID (GC-2010 plus,

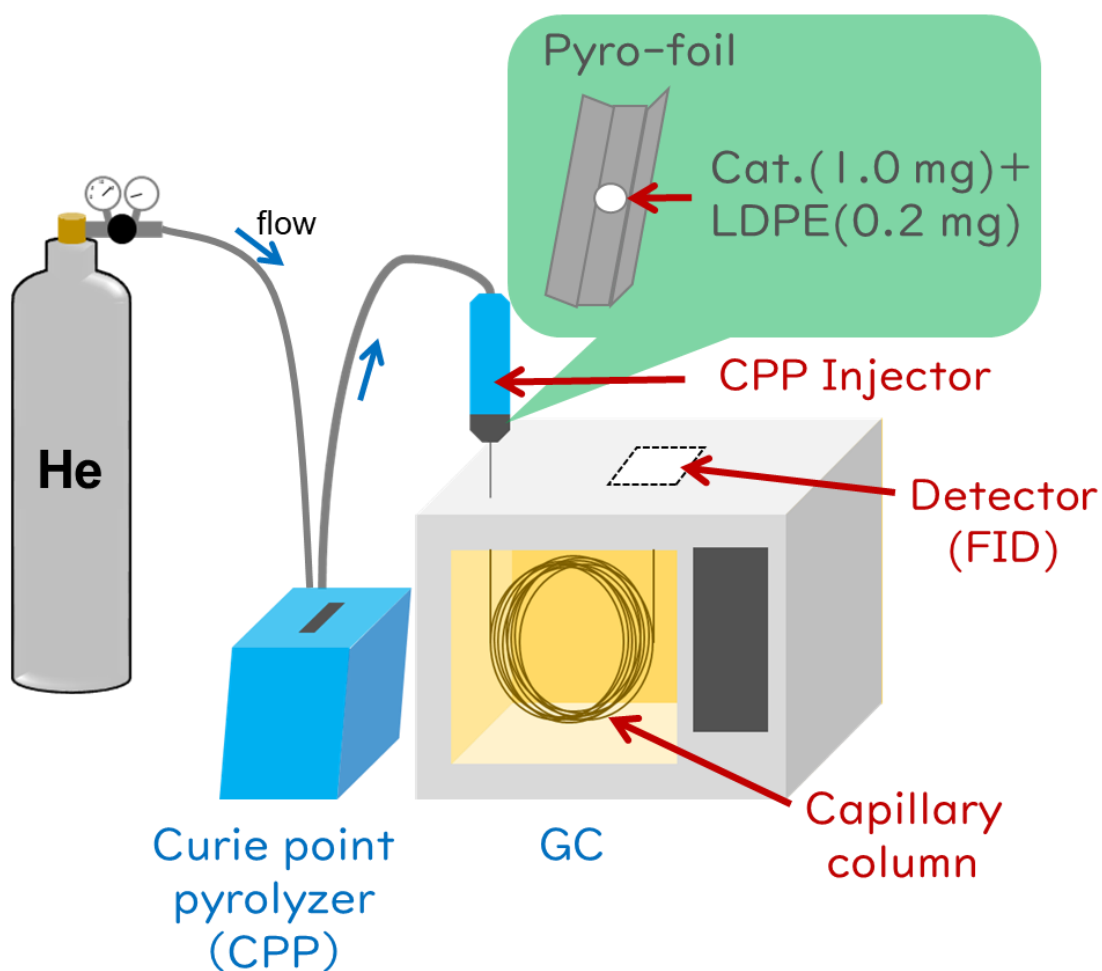


Figure 4.1 Schematic diagram of catalytic activity evaluation in catalytic pyrolysis of LDPE using CPP.

Shimadzu Corp.). Pyrolysis was carried out at 590 °C, 5 s, under He flow (0.6 MPa). Products were directly analyzed by the GC-FID. The detail of products identification was mentioned by previous reports [27-29,31-36]. In the catalytic cracking of LDPE, the amount of product and conversion was calculated by the following equation (1) using the peak area of the total product and the peak area of toluene (0.2 μ L of 1 wt% toluene ($C_6H_5CH_3$, Nacalai Tesque, Inc.)/*n*-dodecane ($CH_3(CH_2)_{10}CH_3$, Nacalai Tesque, Inc.) solution).

$$\text{Conversion of LDPE (\%)} = \frac{P_P \times C_T}{P_T \times C_L} \times 100 \quad (1)$$

In equation (1), P_P means total peak area of all products detected by FID, P_T means peak

Chapter 4

area of toluene (1 wt% toluene solution), C_T means amount of carbon in 1 wt% toluene used, C_L means amount of carbon in LDPE used.

The “relative activity”, defined by the following equation (2), was derived to estimate the activity per contained zeolite crystals. This relative activity was plotted against various parameters of the catalyst to show the correlation between catalytic activity and pore structure, and its decision coefficient was determined.

$$\text{Relative activity (-)} = \frac{C_C}{C_Z} \times \frac{I_Z}{I_C} \quad (2)$$

In equation (2), C_Z is the conversion of LDPE by each zeolite (%); C_C is the conversion of LDPE by each catalyst (%); I_Z is the integrated intensity from XRD measurement of each zeolite (Figure 3.2) over the range where the specific peaks of zeolite were detected (ZSM-5: $2\theta = 22.5$ - 25.0° , β : $2\theta = 22.0$ - 23.5° and Y: $2\theta = 15.0$ - 16.5°); I_C is the integrated intensity from XRD measurement of each catalyst (Figure 3.2) in the same range as I_Z .

4.4 Results and discussion

4.4.1 Characterization of catalysts

Figure 3.2 shows the XRD patterns of each catalyst [29]. Peaks characteristic of zeolite were observed, confirming that the structure of zeolite was maintained. Figure 3.3 and Table 3.2 show the results of nitrogen adsorption-desorption measurements. From the mesopore distribution in Figure 3.3, it could be seen that all ZC2L catalysts have large mesopores other than zeolite pores. From Table 3.2, it was confirmed that all ZC2L catalysts had a mesopore volume of more than $1.4 \text{ cm}^3/\text{g}$ and a mesopore diameter of more than 10 nm, with a maximum of $5 \text{ cm}^3/\text{g}$ and a large mesopore of about 50 nm by Barrett-Joyner-Hallenda (BJH) method. Therefore, the results of XRD and nitrogen adsorption-desorption measurements suggest that the ZC2L catalysts have a hierarchical structure of zeolite-derived micropores and GSR silica-derived mesopores. The acid properties of prepared catalysts were investigated by NH_3 -TPD and the results are shown in Figure 3.5 and Table 4.1. From the TPD curve in Figure 3.5, regardless of the type of zeolite, the zeolite single showed the largest peak, while the ZC2L catalysts and kaolin mixed catalysts with less zeolite content showed smaller peaks. The amounts of NH_3 desorbed for zeolite singles were in the range 6.1 - $8.1 \times 10^{-4} \text{ mol/g}$. The kaolin mixed catalysts had amounts of NH_3 desorbed in the range 2.0 - $2.8 \times 10^{-4} \text{ mol/g}$, which was about one third of those of the zeolite singles. The amounts of NH_3 desorbed of the β -ZC2L catalysts were very similar to those of the kaolin mixed catalysts,

however the amounts of NH₃ desorbed for the ZSM-5-ZC2L catalysts decreased and those for the Y-ZC2L catalysts increased. These may be due to the difficulty of NH₃ adsorption by the generation of mesoporous silica and the successive partial blockage of micropores in the ZSM-5-ZC2L catalysts, and the formation of new acid sites on the TEOS-derived mesoporous silica by extra-framework alumina of Y-zeolite in the Y-ZC2L catalysts [29].

4.4.2 Catalytic cracking of LDPE using various ZC2L catalysts, kaolin mixed catalysts and zeolite singles

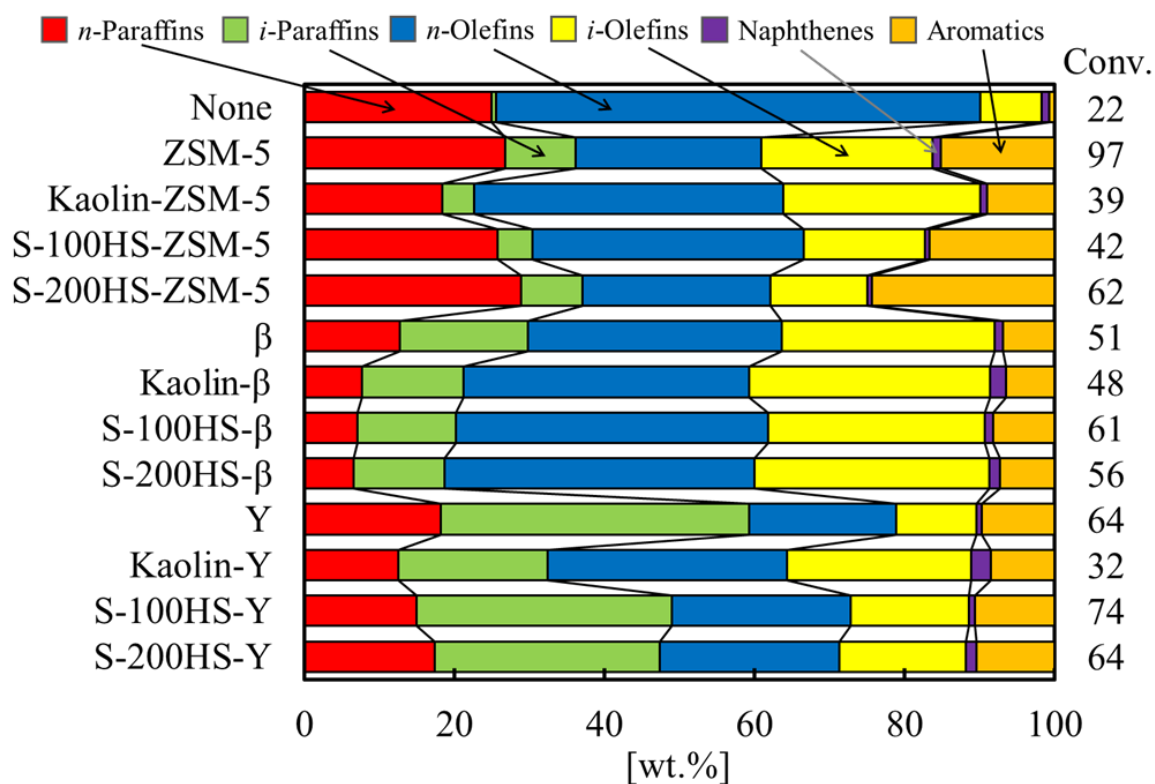
Using these ZC2L catalysts, kaolin mixed catalysts and zeolite singles, catalytic cracking of LDPE was performed at a reaction temperature of 590 °C by the CPP method. Table 4.1 shows the product distribution in the catalytic cracking of LDPE, some parameters of the gasoline fraction (C₅₋₁₁) and the amount of NH₃ desorbed of the fresh catalyst, and Figure 4.2 shows the selectivity for paraffins, olefins, naphthenes and aromatics (PONA) at all products detected (C₁₋₁₈) including gas products (C₁₋₄) and liquid products (C₅₋₁₈). In Table 4.1, in pyrolysis without a

Table 4.1 Product distribution, catalytic properties, parameters in gasoline fraction, coke yield and amount of NH₃ desorbed.

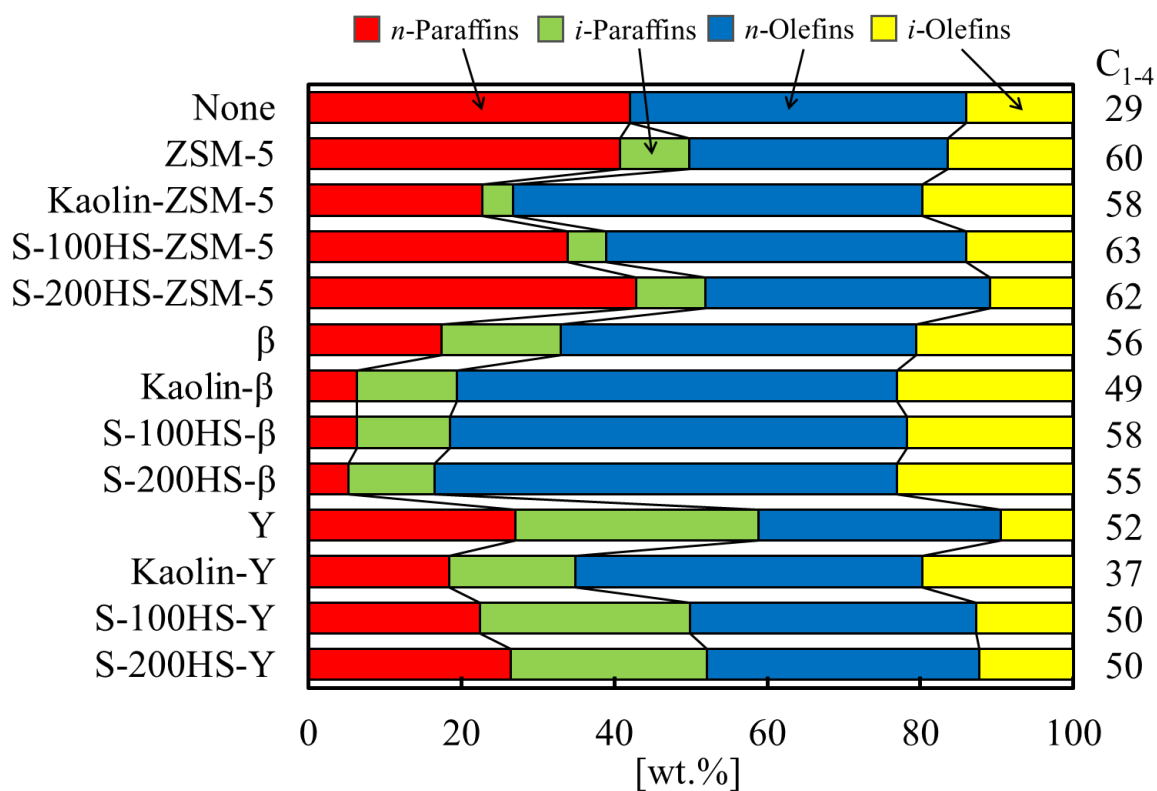
Catalyst	Product distribution (wt%)			Amount of coke* ¹ (%)	Conv. (+Coke) (%)	Parameters in gasoline fraction				Amount of NH ₃ desorbed* ² (10 ⁻⁴ mol/ g)	Relative activity (-)
	C ₁₋₄	Gasoline (C ₅₋₁₁)	C ₁₂₋₁₈			O/P	iso-/n-	m/s	RON		
None	29	49	22	-	22 (-)	4.44	0.11	1.72	84	-	-
ZSM-5	60	40	0.3	2.8	97 (107)	2.90	2.58	0.23	102	8.1	1.00
Kaolin-ZSM-5	58	38	4	2.2	39 (49)	4.38	1.42	0.30	100	2.8	1.41
S-100HS-ZSM-5	63	34	2	3.5	42 (57)	2.72	1.02	0.26	101	1.1	2.08
S-200HS-ZSM-5	62	38	0.3	3.4	62 (77)	1.76	1.97	0.19	103	2.2	4.05
β	56	44	0.4	2.3	51 (61)	2.20	2.32	0.16	98	6.1	1.00
Kaolin-β	49	49	2	2.2	48 (58)	2.76	2.16	0.24	97	2.0	4.35
S-100HS-β	58	41	0.7	3.8	61 (76)	2.53	2.26	0.14	100	2.4	6.51
S-200HS-β	55	44	1	4.7	56 (76)	2.91	2.20	0.18	99	1.7	7.11
Y	52	48	0.6	6.5	64 (89)	0.31	4.21	0.07	90	7.8	1.00
Kaolin-Y	37	60	3	2.2	32 (42)	1.74	1.72	0.45	93	2.3	2.73
S-100HS-Y	50	49	1	7.4	74 (99)	0.61	3.63	0.10	93	3.2	6.23
S-200HS-Y	50	49	1	7.7	64 (94)	0.79	2.98	0.14	93	2.6	6.20

*¹: Amount of coke (%) = {(Weight Loss at 400-600 °C [mg]) / (Weight at 600 °C [mg])} × 100, *²: Adapted from ref. [29], O/P: the ratio of olefins to paraffins, iso-/n-: the ratio of branched hydrocarbons to straight-chained hydrocarbons, m/s: the ratio of multibranch hydrocarbons to single-branched hydrocarbons, RON: the research octane number.

Chapter 4



a) All products (C_{1-18})



b) Gas products (C_{1-4})

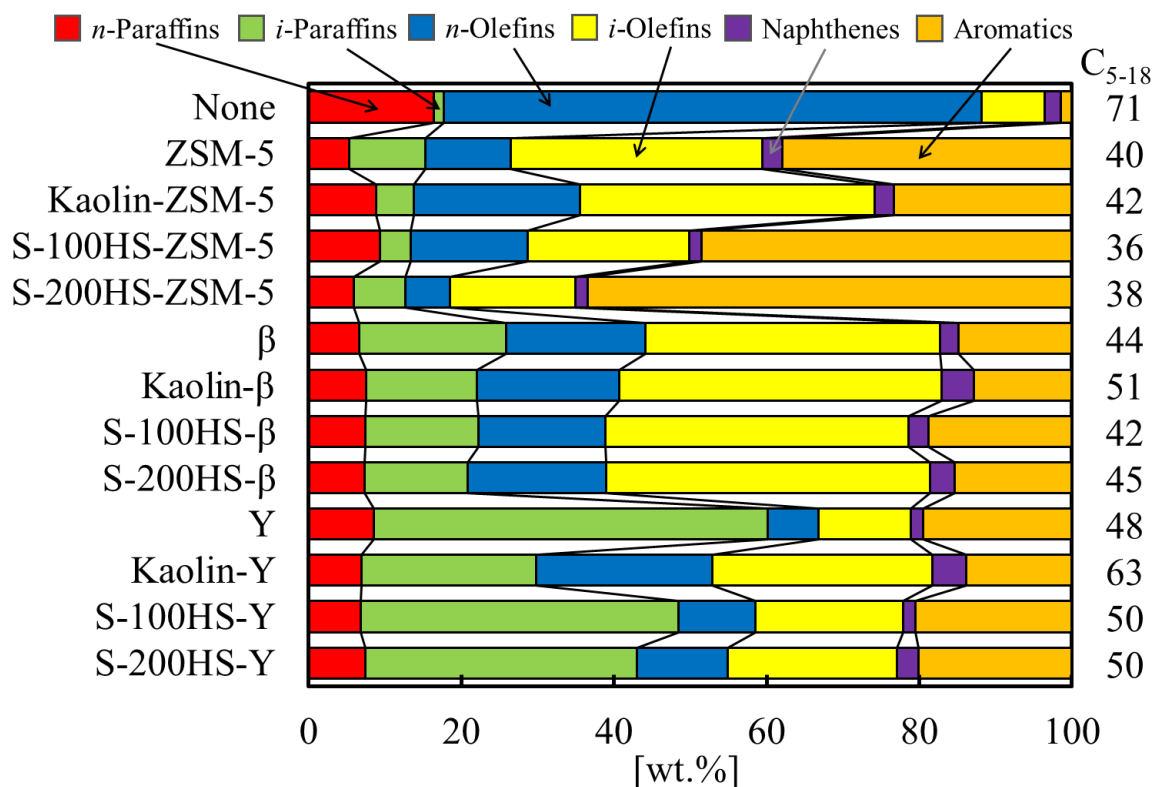
c) Liquid products (C₅₋₁₈)

Figure 4.2 Selectivity for paraffins, olefins, naphthenes and aromatics in catalytic cracking of LDPE using ZC2L catalysts.

catalyst (None), the conversion was 22 wt%, and straight-chained hydrocarbons (alkanes, alkenes, alkadienes) with each carbon number of C₁₋₁₈ were mainly detected. This is consistent with the appearance pattern of the pyrogram of polyethylene shown in some reports [9,14,17], and it was confirmed that the reaction and analytical conditions of this study were appropriate. The value of relative activity, calculated from equation (2), was ZC2L catalyst > Kaolin mixed catalyst > zeolite single for all zeolites (ZSM-5, Y, β). ZC2L catalysts and kaolin mixed catalysts showed the higher activity than the zeolite single although these hierarchical catalysts had the zeolite content of 26 wt% (Table 4.1). Therefore, it was likely that the acid site of the zeolite could be diluted with the matrix component as in the FCC catalyst to achieve the sufficient diffusion to acid sites of zeolite. The activity of kaolin mixed catalysts with zeolite content of 26 wt% similar to those of ZC2L was lower than the activities of ZC2L catalysts probably because the kaolin mixed catalysts hardly had mesopores. These results indicated that ZC2L catalysts was able to effectively work in catalytic cracking of LDPE with less amount of zeolite by the presence of mesoporous silica. Therefore, the activity per zeolite of ZC2L catalysts was improved due to the

Chapter 4

enhanced diffusion caused by the presence of mesopores and the appropriate acid strength caused by the dilution of the acid site of the zeolite. In comparison with the effect of the zeolite type on the cracking reactivity, it was showed that the relative activity and gasoline fraction selectivity decreased in the order of Y-series > β -series > ZSM-5-series. This result of selectivity was consistent with the results of previous studies where the selectivity of gasoline fractions was strongly influenced by the type of zeolite, i.e., the size of zeolite micropores [31,32,35]. The ZSM-5-ZC2L catalyst produced more aromatic compounds in the gasoline fraction than the Y- and β -ZC2L catalysts while they reduced the proportion of olefins (Figure 4.2c). The selectivity of paraffins produced by ZSM-5-ZC2L catalysts were similar to that of pyrolysis. Therefore, it was considered that the olefins produced in the pyrolysis of LDPE would be used in the cyclization-dehydrogenation reaction to aromatic compounds by Diels-Alder reaction [2,29,39,40]. In S-200HS-ZSM-5 with an increased HS/TEOS ratio, more olefins reduced, and aromatics increased. In the conversion of LDPE to fuel fractions of C₅₋₁₈ with ZSM-5-zeolite, it has been reported that the cyclization of polymer pyrolysis products was accelerated at a higher temperature of about 600 °C [8]. Similar results were obtained with ZSM-5-series in this study. On the other hand, some parameters in the gasoline fraction of the β - and Y-ZC2L catalysts showed the opposite trend to that of the ZSM-5-ZC2L catalyst with increasing HS/TEOS. The β and Y-ZC2L catalysts did not have as high selectivity for aromatic compounds as ZSM-5-ZC2L catalysts. It seems that even if the relative activity increased due to the improvement of mesopore properties by increasing the HS/TEOS ratio, the more pronounced product selectivity of the zeolite would not change. For ZSM-5-ZC2L catalysts, the cyclization-dehydrogenation of olefins was promoted, which led to a decrease in olefins or olefin/paraffin (O/P) ratio and an increase in aromatics. Therefore, it seems that the hydrogen produced by the cyclization of olefins and successive dehydrogenation would be transferred to paraffins produced by the cracking reaction. For the β and Y-ZC2L catalysts, isomerization of paraffins was promoted, resulting in an increase in multi-branched products and a relative increase in olefins in the gasoline fraction.

Figure 4.3 shows plots of relative activity against the product of surface area in BJH method (SA-BJH) and amount of NH₃ desorbed (NH₃-des.), and the product of pore volume in BJH method (PV-BJH) and NH₃-des. Figure 4.3 indicates that there was a strong correlation between relative activity and (a) product of SA-BJH and NH₃-des. and (b) product of PV-BJH and NH₃-des. With a coefficient of determination of more than 0.70 for all zeolites. Therefore, as both mesopore properties and ammonia desorption increased, relative activity increased, and it was inferred that both the acid strength of zeolite and the presence of mesopores would contribute to the increase in activity [26,35,41]. This tendency was common in catalysts with micro- and mesopores, and was confirmed in this study as well. On the other hand, plots of relative activity against surface area in Brunauer-Emmett-Teller (BET) method (BET-SA) (Figure 4.4) shows a

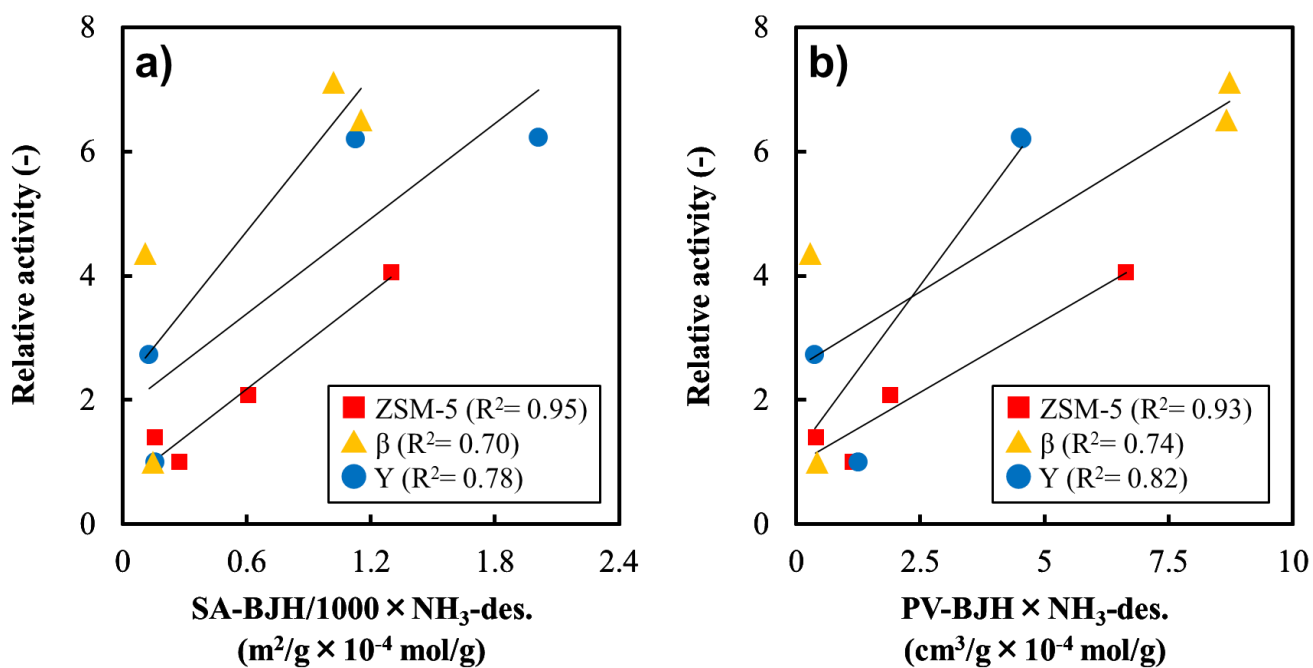


Figure 4.3 Plots of relative activity of catalysts for all zeolite series against (a) the product of surface area in BJH method and amount of NH₃ desorbed, and (b) the product of pore volume in BJH method and amount of NH₃ desorbed.

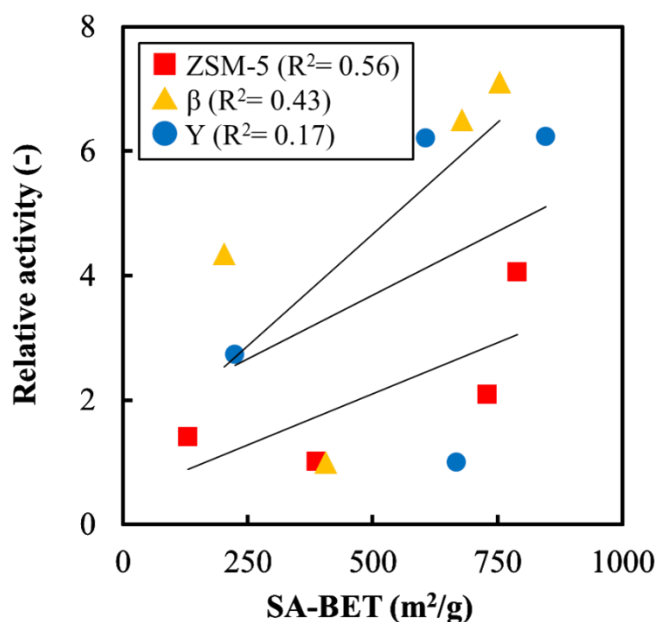


Figure 4.4 Plots of relative activity of catalysts for all zeolite series against surface area in BET method.

low coefficient of determination for all zeolites, indicating that they did not contribute much to the activity. ZC2L catalysts, like the FCC catalyst, consisted of zeolite and a matrix component that disperses the zeolite, and had the larger mesopores on the outside of the zeolite than the catalyst with mesopores introduced into the zeolite framework [2,5,6]. Therefore, ZC2L catalysts were less restrictive in the diffusion of reactants than those catalysts and might be more suitable for processing large molecules such as pyrolysis products of LDPE. It was also expected that cracking products such as olefins, branched paraffins, and aromatics, which were more reactive than the linear paraffins produced in the micropores of the zeolite, would diffuse quickly out of the reaction system due to the presence of mesopores, and as a result, it was suggested that over-cracking could be suppressed.

From the PONA distribution of all the detected products shown in Figure 4.2a, it is considered that the cracking reaction would proceed in the ZSM-5-single due to its high conversion, and that the selectivity of paraffins would increase compared to other ZSM-5-series due to the effect of hydrogen transfer reaction. These paraffins were confirmed to be mostly gas

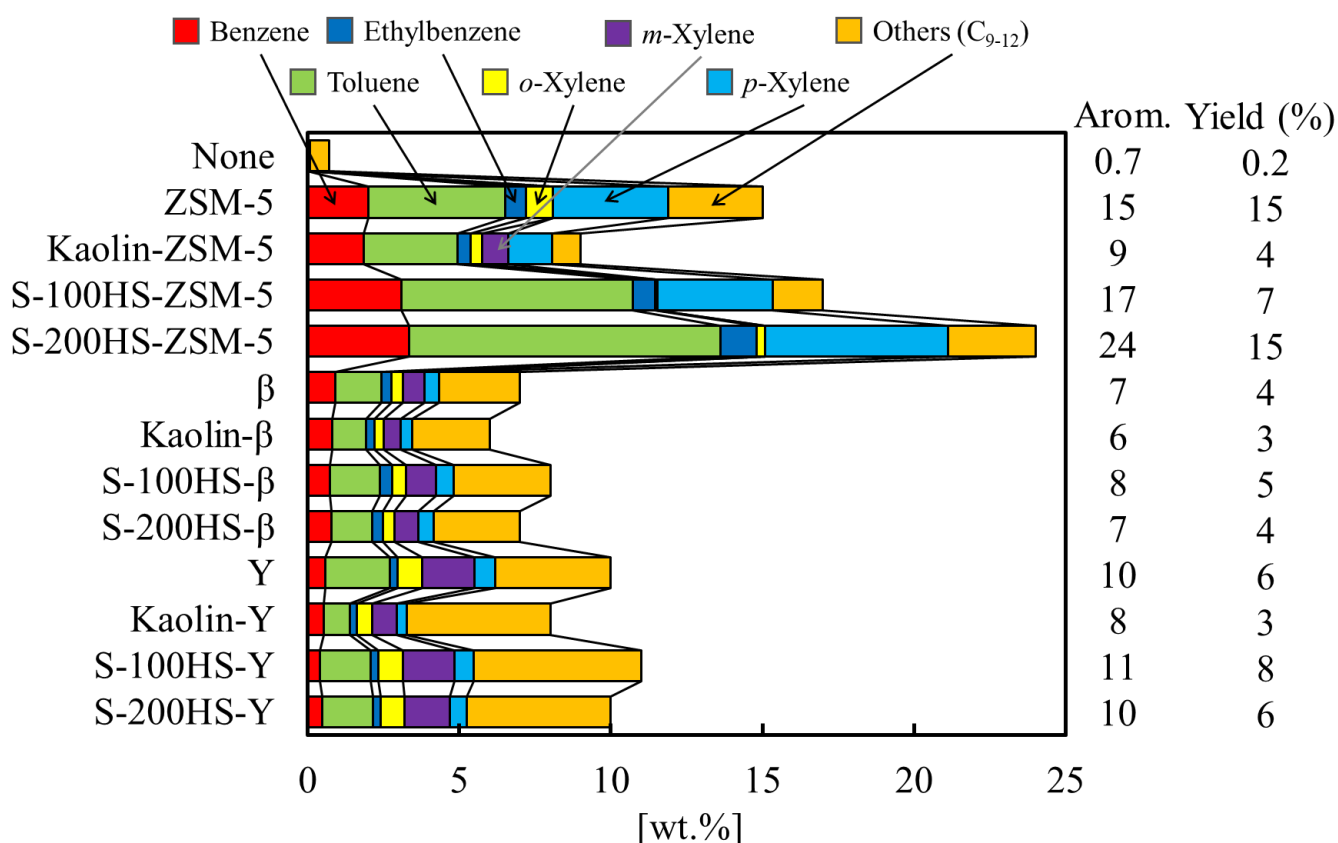


Figure 4.5 Selectivity for benzene, toluene, ethylbenzene, xylene (BTEX) and other aromatics (C₉₋₁₂) in catalytic cracking of LDPE using ZC2L catalysts.

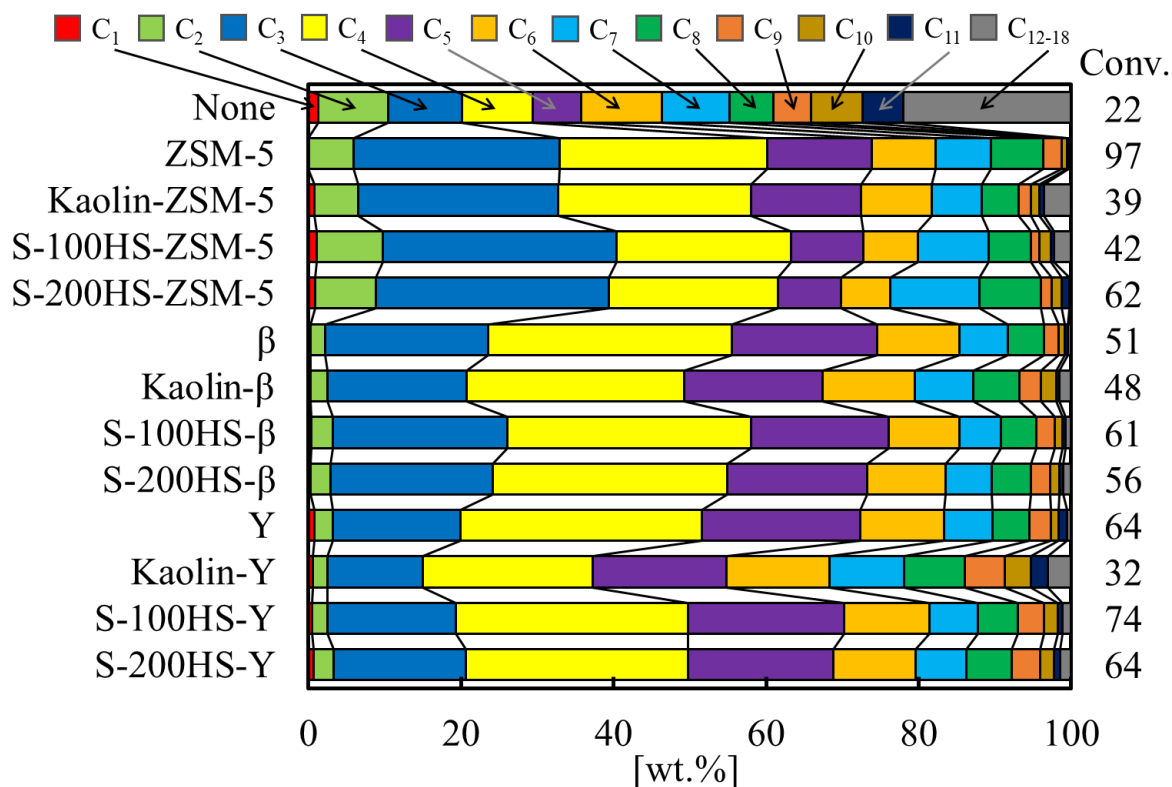


Figure 4.6 Distribution of carbon numbers in catalytic cracking of LDPE using ZC2L catalysts.

products from the PONA distribution of gas and liquid products in Figure 4.2b and c. When β -series was used as a catalyst, *n*-olefin tended to be more abundant in the gas product, but the aromatic compounds in the liquid product were not as abundant as in the ZSM-5-series, and *i*-olefin was more abundant, indicating that the isomerization reaction would proceed. In the case of Y-series, there were more *i*-paraffins and more aromatics than in the β -series, indicating that the isomerization and hydrogen transfer reactions would proceed.

The selectivity of each aromatic compound (benzene, toluene, ethylbenzene, xylene (BTEX) and others (C_{9-12})) shown in Figure 4.5 was characteristic of the micropores of the zeolite used. ZSM-5-series exhibited the high selectivity for toluene and *p*-xylene while *m*-xylene was not detected except for Kaolin-ZSM-5. Catalysts using Y-zeolite, which has the largest micropores among the zeolites used in this study, produced more aromatic compounds of C_{9-12} than that of C_{6-8} (BTEX).

Figure 4.6 shows the distribution of carbon numbers in catalytic cracking of LDPE using ZC2L catalysts. In Figure 4.6, pyrolysis without catalyst (None) resulted in almost the same proportion of each carbon number, since straight chain hydrocarbons (alkanes, alkenes, and alkadienes) of each carbon number in C_{1-18} were mainly detected as above-mentioned. In catalytic

Chapter 4

reactions, the cracking occurs by β -cleavage via carbenium ions, which was characteristic of catalytic cracking reactions [8,17], and the distribution of hydrocarbons with C_3 and more than C_3 was higher. When ZSM-5-zeolite was used as a catalyst, the selectivity of C_4 - and C_5 -hydrocarbons was slightly lower than those of β - and Y-series because of the higher cracking activity and the consumption of C_4 - and C_5 -hydrocarbons through cyclization-dehydrogenation reaction as described above. There was also an increase in selectivity for C_2 - and C_3 -hydrocarbons, which are considered to be cracking products, and C_7 - and C_8 -hydrocarbons, which contain aromatics from cyclization-dehydrogenation reactions. The *i*-paraffin in the gas fraction in Figure 4.2b shows isobutane (*i*- C_4), which accounts for about 10 % or less of the gas in ZSM-5- and β -series, but about 25 % of the gas in Y-series, and about 50 % of the C_4 product in Y-series was isobutane.

The weight loss between 400 and 600 °C, where the exothermic phenomenon was detected in the TGA measurement of the catalyst after the reaction, was regarded as the amount of coke deposited on the catalyst (Figure 4.7 and Table 4.1). The conversion of LDPE to coke was calculated from this value and was added into Table 4.1 in parentheses as the conversion including coke. The conversion to coke decreased in the order $Y > \beta > \text{ZSM-5}$, similar order of the selectivity for gasoline fraction described above, suggesting that the formation of coke would also be affected by the micropores of the zeolite. The conversion into coke of each Kaolin mixed catalyst was the lowest 10 %, presumably because kaolin mixed catalysts have the lower conversion and selectivity for aromatics of coke precursor than other catalysts (Figure 4.2c). On the other hand, ZC2L catalysts deposited the highest amount of coke when compared to other catalysts using the same zeolite, including zeolite single. The ZC2L catalyst showed the higher selectivity for aromatics than the zeolite single and Kaolin mixed catalysts, which may lead to the higher amount of coke because aromatics could be precursors of coke.

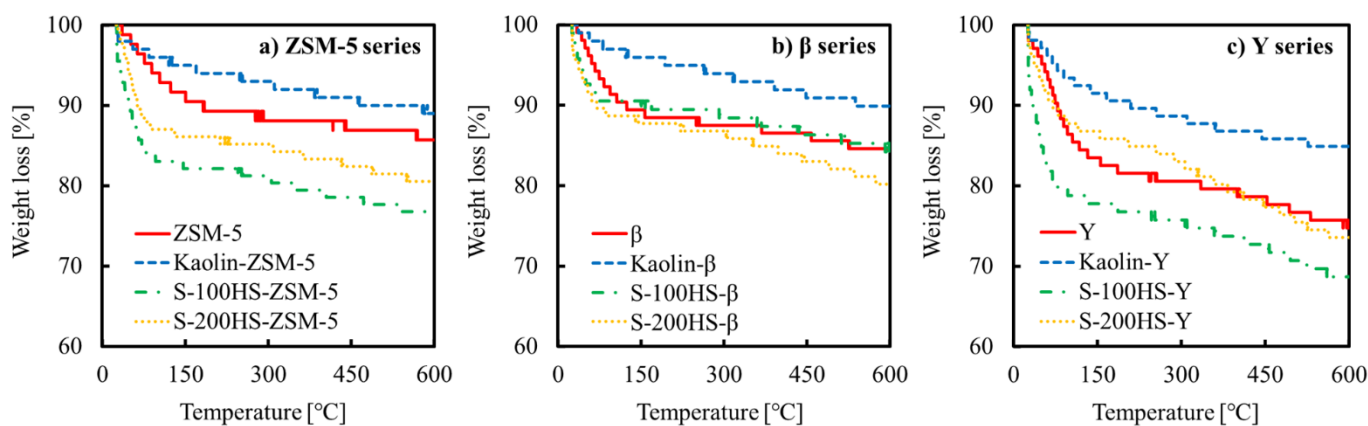


Figure 4.7 Weight loss of each catalyst after catalytic cracking of LDPE by TGA measurement.

4.4.3 Comparison of the results of catalytic cracking of LDPE and *n*-dodecane

When catalytic cracking of LDPE using ZC2L catalysts was compared with catalytic cracking of *n*-dodecane using the same catalysts, the selectivity for olefins was higher in the case of LDPE, while the selectivity for paraffins was higher in the case of *n*-dodecane [29]. Since *n*-dodecane has a shorter carbon chain than LDPE, the olefins produced by cracking were considered to become paraffins through hydrogen transfer reactions. On the other hand, LDPE has a long carbon chain, and it was inferred that the relatively long carbon-chained olefins produced by the cracking tended to increase more olefins because the adsorption equilibrium of a longer chain would be higher and its cracking reaction was repeated more rapidly than the hydrogen transfer reaction. Since the *iso*/*n*- ratios in the gasoline fractions were comparable between cracking of *n*-dodecane and LDPE, the selectivity of the isomerization reactions also suggested to be comparable. However, the *m*/*s* ratio was higher for LDPE. This might also be because hydrocarbons with long carbon chains derived from LDPE were more susceptible to isomerization reactions than *n*-dodecane. The higher *m*/*s* ratios, especially for ZSM-5- and β -ZC2L catalysts with larger mesopores, suggest that the mesopore size would contribute to the increase in *m*/*s* ratio significantly.

4.5 Conclusions

In this study, a hierarchical catalyst containing a small amount of zeolite in mesoporous silica was applied to the catalytic cracking of LDPE. For both types of zeolites, zeolite-containing hierarchical two-layered catalysts showed higher activity than kaolin mixed catalysts without mesopores and zeolite singles. Among the zeolite-containing hierarchical two-layered catalysts, the S-200HS-ZSM-5 catalyst with an increased HS/TEOS ratio showed the highest selectivity for aromatics (63 % of liquid products) among ZSM-5-containing catalysts, and the selectivity for toluene and *p*-xylene tended to be higher. The selectivity for gasoline fractions and aromatics strongly reflected the micropore characteristics of the zeolites used, but the prepared ZSM-5, β or Y-zeolite-containing hierarchical two-layered catalyst showed high conversions and high relative activities despite the low zeolite content of 26 wt%, indicating that the micro-meso-porous hierarchical structured catalyst would be effective for catalytic cracking of LDPE. The more detail study of the reaction mechanism and acid properties of the zeolite-containing hierarchical two-layered catalysts found in this study will be performed in the future.

Acknowledgements

This work was supported by the Alumni Association of Department of Engineering in Mie University. The authors also thank Mr. Koudai Mizuno for his helpful work.

References

- [1] O. Horodytska, F. J. Valdés, A. Fullana, “Plastic flexible films waste management – A state of art review”, *Waste Manag.*, 77 (2018) 413-425, <https://doi.org/10.1016/j.wasman.2018.04.023>.
- [2] H. Yu, F. Li, W. He, C. Song, Y. Zhang, Z. Li, H. Lin, “Synthesis of micro–mesoporous ZSM-5 zeolite with microcrystalline cellulose as co-template and catalytic cracking of polyolefin plastics”, *RSC Adv.*, 10 (2020) 22126, <https://doi.org/10.1039/d0ra03082a>.
- [3] E. Rodríguez, R. Palos, A. Gutiérrez, J. M. Arandes, J. Bilbao, “Production of Non-Conventional Fuels by Catalytic Cracking of Scrap Tires Pyrolysis Oil”, *Ind. Eng. Chem. Res.*, 58 (2019) 5158–5167, <https://doi.org/10.1021/acs.iecr.9b00632>.
- [4] D. P. Serrano, J. Aguado, J. M. Escola, “Developing Advanced Catalysts for the Conversion of Polyolefinic Waste Plastics into Fuels and Chemicals”, *ACS Catal.*, 2 (2012) 1924-1941, <https://doi.org/10.1021/cs3003403>.
- [5] Y.-M. Kim, J. Jeong, S. Ryu, H. W. Lee, J. S. Jung, M. Z. Siddiqui, S.-C. Jung, J.-K. Jeon, J. Jae, Y.-K. Park, “Catalytic pyrolysis of wood polymer composites over hierarchical mesoporous zeolites”, *Energy Convers. Manag.*, 195 (2019) 727-737, <https://doi.org/10.1016/j.enconman.2019.05.034>.
- [6] K. A. Tarach, K. Pyra, S. Siles, I. M.-Cabrera, K. G.-Marek, “Operando Study Reveals the Superior Cracking Activity and Stability of Hierarchical ZSM-5 Catalyst for the Cracking of Low-Density Polyethylene”, *ChemSusChem*, 12 (2019) 633-638, <https://doi.org/10.1002/cssc.201802190>.
- [7] K. H. Lee, N. S. Noh, D. H. Shin, Y. Seo, “Comparison of plastic types for catalytic degradation of waste plastics into liquid product with spent FCC catalyst”, *Polym. Degrad. Stab.*, 78 (2002) 539-544, [https://doi.org/10.1016/S0141-3910\(02\)00227-6](https://doi.org/10.1016/S0141-3910(02)00227-6).
- [8] S. L. Wong, N. Ngadi, T. A. T. Abdullah, I. M. Inuwa, “Conversion of low density polyethylene (LDPE) over ZSM-5 zeolite to liquid fuel”, *Fuel*, 192 (2017) 71-82, <https://doi.org/10.1016/j.fuel.2016.12.008>.
- [9] D. S. Achilias, C. Roupakiasa, P. Megalokonomos, A. A. Lappas, E. V. Antonakou, “Chemical recycling of plastic wastes made from polyethylene (LDPE and HDPE) and polypropylene (PP)”, *J. Hazard. Mater.*, 149 (2017) 536-542, <https://doi.org/10.1016/j.jhazmat.2007.06.076>.
- [10] Y.-H. Lin, M.-H. Yang, “Tertiary recycling of commingled polymer waste over commercial FCC equilibrium catalysts for producing hydrocarbons”, *Polym. Degrad. Stab.*, 94 (2009) 25-33, <https://doi.org/10.1016/j.polymdegradstab.2008.10.018>.
- [11] A. Marcilla, A. G.-Siurana, F. Valdés, “Catalytic pyrolysis of LDPE over H-beta and HZSM-5 zeolites in dynamic conditions: Study of the evolution of the process”, *J. Anal. Appl. Pyrolysis*, 79 (2007) 433-442, <https://doi.org/10.1016/j.jaap.2006.09.006>.

Chapter 4

- [12] A. L. Figueiredo, A. S. Araujo, M. Linares, Á. Peral, R. A. García, D. P. Serrano, V. J. Fernandes Jr., “Catalytic cracking of LDPE over nanocrystalline HZSM-5 zeolite prepared by seed-assisted synthesis from an organic-template-free system”, *J. Anal. Appl. Pyrolysis*, 117 (2016) 132-140, <https://doi.org/10.1016/j.jaap.2015.12.005>.
- [13] Y.-H. Lin, M.-H. Yang, “Catalytic conversion of commingled polymer waste into chemicals and fuels over spent FCC commercial catalyst in a fluidised-bed reactor”, *Appl. Catal. B: Environ.*, 69 (2007) 145-153, <https://doi.org/10.1016/j.apcatb.2006.07.005>.
- [14] A. Marcilla, M. R. Hernández, Á. N. García, “Degradation of LDPE/VGO mixtures to fuels using a FCC equilibrium catalyst in a sand fluidized bed reactor”, *Appl. Catal. A: Gen.*, 341 (2008) 181-191, <https://doi.org/10.1016/j.apcata.2008.02.041>.
- [15] F. J. Passamonti, U. Sedran, “Recycling of waste plastics into fuels. LDPE conversion in FCC”, *Appl. Catal. B: Environ.*, 125 (2012) 499-506, <https://doi.org/10.1016/j.apcatb.2012.06.020>.
- [16] E. T. Aisien, I. C. Otuya, F. A. Aisien, “Thermal and catalytic pyrolysis of waste polypropylene plastic using spent FCC catalyst”, *Environ. Technol. Innov.*, 22 (2021) 101455, <https://doi.org/10.1016/j.eti.2021.101455>.
- [17] X. Zhang, H. Lei, G. Yadavalli, L. Zhu, Y. Wei, Y. Liu, “Gasoline-range hydrocarbons produced from microwave-induced pyrolysis of low-density polyethylene over ZSM-5”, *Fuel*, 144 (2015) 33-42, <https://doi.org/10.1016/j.fuel.2014.12.013>.
- [18] G. Manos, A. Garforth, J. Dwyer, “Catalytic Degradation of High-Density Polyethylene over Different Zeolitic Structures”, *Ind. Eng. Chem. Res.*, 39 (2000) 1198-1202, <https://doi.org/10.1021/ie990512q>.
- [19] R. A. García, D. P. Serrano, D. Otero, “Catalytic cracking of HDPE over hybrid zeolitic–mesoporous materials”, *J. Anal. Appl. Pyrolysis*, 74 (2005) 379–386, <https://doi.org/10.1016/j.jaap.2004.11.002>.
- [20] S. Tsuge, H. Ohtani, W. Chuichi, “Pyrolysis - GC/MS Data Book of Synthetic Polymers: Pyrograms, Thermograms and MS of Pyrolyzates”, *Elsevier* (2011) 1-390, <https://doi.org/10.1016/B978-0-444-53892-5.10001-X>.
- [21] K. H. Altgelt, “Composition and Analysis of Heavy Petroleum Fractions (1st ed.)”, *CRC Press* (1993) 1-512, <https://doi.org/10.1201/b16931>.
- [22] M. Pan, J. Zheng, Y. Liu, W. Ning, H. Tian, R. Li, “Construction and practical application of a novel zeolite catalyst for hierarchically cracking of heavy oil”, *J. Catal.*, 369 (2019) 72-85, <https://doi.org/10.1016/j.jcat.2018.10.032>.
- [23] W. Chen, D. Han, X. Sun, C. Li, “Studies on the preliminary cracking of heavy oils: Contributions of various factors”, *Fuel*, 106 (2013) 498-504, <https://doi.org/10.1016/j.fuel.2012.12.090>.

Chapter 4

- [24] A. Ishihara, H. Negura, T. Hashimoto, H. Nasu, “Catalytic properties of amorphous silica-alumina prepared using malic acid as a matrix in catalytic cracking of n-dodecane”, *Appl. Catal. A: Gen.*, 388 (2010) 68-76, <https://doi.org/10.1016/j.apcata.2010.08.027>.
- [25] A. Ishihara, K. Tatebe, T. Hashimoto, H. Nasu, “Preparation of Silica, Alumina, Titania, and Zirconia with Different Pore Sizes Using Sol–Gel Method and Their Properties as Matrices in Catalytic Cracking”, *Ind. Eng. Chem. Res.*, 57 (2018) 14394-14405, <https://doi.org/10.1021/acs.iecr.8b03019>.
- [26] A. Ishihara, H. Oono, T. Hashimoto, H. Nasu, “Preparation of SiO₂ and SiO₂-Al₂O₃ catalysts by gel skeletal reinforcement using hexamethyldisiloxane (HMDS) and acetic anhydride and aluminum tri-*sec*-butoxide (ASB) systems and elucidation of their catalytic cracking properties as matrices”, *Microporous Mesoporous Mater.*, 233 (2016) 163-170 <https://doi.org/10.1016/j.micromeso.2016.01.025>.
- [27] A. Ishihara, M. Ninomiya, T. Hashimoto, H. Nasu, “Catalytic cracking of C₁₂-C₃₂ hydrocarbons by hierarchical β - and Y-zeolite containing mesoporous silica and silica-alumina using Curie point pyrolyzer”, *J. Anal. Appl. Pyrolysis*, 150 (2020) 104876, <https://doi.org/10.1016/j.jaap.2020.104876>.
- [28] S. Matsuura, T. Hashimoto, A. Ishihara, “Preparation of β -zeolite mixed catalysts using alumina and titania matrices modified by silication of gel skeletal reinforcement and their reactivity for catalytic cracking of n-dodecane”, *Appl. Catal. A Gen.*, 610 (2021) 117959, <https://doi.org/10.1016/j.apcata.2020.117959>.
- [29] S. Matsuura, T. Hashimoto, A. Ishihara, “Preparation of novel zeolite-containing hierarchical two-layered catalysts with large mesopores by gel skeletal reinforcement and their reactivities in catalytic cracking of n-dodecane”, *J. Porous Mater.*, 28 (2021) 1935-1944, <https://doi.org/10.1007/s10934-021-01133-w>.
- [30] A. Ishihara, K. Inui, T. Hashimoto, H. Nasu, “Preparation of hierarchical β and Y zeolite-containing mesoporous silica–aluminas and their properties for catalytic cracking of n-dodecane”, *J. Catal.*, 295 (2012) 81-90, <https://doi.org/10.1016/j.jcat.2012.07.027>.
- [31] A. Ishihara, K. Kimura, A. Owaki, K. Inui, T. Hashimoto, H. Nasu, “Catalytic cracking of VGO by hierarchical ZSM-5 zeolite containing mesoporous silica-aluminas using a Curie point pyrolyzer”, *Catal. Commun.*, 28 (2012) 163-167, <https://doi.org/10.1016/j.catcom.2012.08.023>.
- [32] A. Ishihara, D. Kawaraya, T. Sonthisawate, K. Kimura, T. Hashimoto, H. Nasu, “Catalytic cracking of soybean oil by hierarchical zeolite containing mesoporous silica-aluminas using a Curie point pyrolyzer”, *J. Mol. Catal. A Chem.*, 396 (2015) 310-318, <https://doi.org/10.1016/j.molcata.2014.10.010>.
- [33] A. Ishihara, D. Kawaraya, T. Sonthisawate, H. Nasu, T. Hashimoto, “Preparation and characterization of zeolite-containing silica-aluminas with three layered micro-meso-meso-

Chapter 4

structure and their reactivity for catalytic cracking of soybean oil using Curie point pyrolyzer”, *Fuel Process. Technol.*, 161 (2017) 8-16, <https://doi.org/10.1016/j.fuproc.2017.03.002>.

[34] T. Sonthisawate, T. Nakanishi, H. Nasu, T. Hashimoto, A. Ishihara, “Catalytic cracking reaction of vacuum gas oil and atmospheric residue by zeolite-containing microporous and mesoporous composites using Curie point pyrolyzer”, *Fuel Process. Technol.*, 142 (2016) 337-344, <https://doi.org/10.1016/j.fuproc.2015.10.016>.

[35] A. Ishihara, T. Tsukamoto, T. Hashimoto, H. Nasu, “Catalytic cracking of soybean oil by ZSM-5 zeolite-containing silicaaluminas with three layered micro-meso-meso-structure”, *Catalysis Today* 303 (2018) 123-129, <https://doi.org/10.1016/j.cattod.2017.09.033>.

[36] A. Ishihara, S. Matsuura, F. Hayashi, K. Suemitsu, T. Hashimoto, “Estimation of Catalytic Cracking of Vacuum Gas Oil by a Y Zeolite-Containing Two-Layered Catalyst and a Novel Three-Layered Hierarchical Catalyst Using a Curie Point Pyrolyzer Method”, *Energy Fuels*, 34 (2020) 7448-7454, <https://doi.org/10.1021/acs.energyfuels.0c00957>.

[37] A. Ishihara, “Preparation and reactivity of hierarchical catalysts in catalytic cracking” *Fuel Process. Technol.*, 194 (2019) 106116, <https://doi.org/10.1016/j.fuproc.2019.05.039>.

[38] P. R. Aravind, P. Mukundan, P. K. Pillai, K. G. K. Warriar, “Mesoporous silica–alumina aerogels with high thermal pore stability through hybrid sol–gel route followed by subcritical drying”, *Microporous Mesoporous Mater.*, 96 (2006) 14-20, <https://doi.org/10.1016/j.micromeso.2006.06.014>.

[39] A. Ishihara, K. Takai, T. Hashimoto, H. Nasu, “Effects of a Matrix on Formation of Aromatic Compounds by Dehydrocyclization of *n*-Pentane Using ZnZSM-5-Al₂O₃ Composite Catalysts”, *ACS Omega*, 5 (2020) 11160-11166, <https://doi.org/10.1021/acsomega.0c01147>.

[40] A. Ishihara, Y. Kodama, T. Hashimoto, “Effect of matrix on aromatics production by cracking and dehydrocyclization of *n*-pentane using Ga ion-exchanged ZSM-5-alumina composite catalysts”, *Fuel Process. Technol.*, 213 (2021) 106679, <https://doi.org/10.1016/j.fuproc.2020.106679>.

[41] E.V. Parkhomchuk, D.A. Sladkovskii, Y. Gunb, W. Wud, K.A. Sashkina, A.I. Lysikov, V.N. Parmon, “Catalytic cracking of *n*-hexane in the presence of zeolite ZSM-5 micro- and nanocrystals”, *Pet. Chem.*, 59, 3 (2019) 338-348, <https://doi.org/10.1134/S0965544119030113>.

Chapter 5

Estimation of catalytic cracking of vacuum gas oil by a Y zeolite-containing two-layered catalyst and a novel three-layered hierarchical catalyst using a Curie point pyrolyzer method

A Y zeolite-containing two-layered catalyst and a novel three-layered hierarchical catalyst were prepared using a template and the gel skeletal reinforcement (GSR) method. Initially, two-layered catalysts were prepared by the sol–gel method using malic acid as the template in the presence of HY zeolite (HYZ). The two-layered hierarchical catalyst, 2L(S-HYZ), consisted of 50 wt% the mesoporous part of silica (S) and 50 wt% the microporous part of HYZ. The three-layered hierarchical catalyst, 3L(GSR-S)2L(S-HYZ), was made by GSR silica (GSR-S) production in the presence of 2L(S-HYZ) where silica gel particles including 2L(S-HYZ) inside were reinforced by a reinforcing solution of hexamethyldisiloxane–acetic anhydride before aging and successive calcination and consisted of 50 wt% large-mesoporous GSR-S and 50 wt% the 2L(S-HYZ) hierarchical catalyst. It was confirmed by XRD and N₂ adsorption and desorption measurement that this catalyst possessed three characters of microporous zeolite crystals, small mesoporous silica, and large mesoporous silica. Catalytic cracking of vacuum gas oil over these hierarchical catalysts was performed using a Curie point pyrolyzer method. 3L(GSR-S)2L(S-HYZ)(Z25), which included 25 wt% HYZ, exhibited the highest activity. Further, it was proposed that the activity could be related to not only the amount of acid sites but also the size of mesoporous pore volume.

5.1 Introduction

Although the demand of gasoline is decreasing in Japan, it is still increasing in the world. Therefore, the technology for catalytic cracking of vacuum gas oil (VGO) and atmospheric residues (ARs) has become an essential process to use those heavier fractions in modern refinery [1-3]. VGO and ARs include very large molecules, which have to be cracked to smaller molecules

Chapter 5

like gasoline, and thus not only microporous zeolites but also mesoporous matrices have to be used as a catalyst [1-3]. Further, in order to increase the octane number, an important factor for a high quality of gasoline, the preferential formation of aromatic compounds, olefins, and branched hydrocarbons is very effective in this process [4]. Although olefins in gasoline produced in the process are lost by successive hydrodesulfurization (HDS), aromatics and branched hydrocarbons do not decrease and the octane number is maintained even after HDS. On the other hand, recent catalytic cracking is aimed to obtain light olefins of ethylene and propylene, raw materials for petrochemical products, as main products, which makes the process more important [5,6]. Zeolites and matrices are usually included in catalysts of catalytic cracking, and their types and ratios significantly have influence on conversion and product selectivity. Many catalysts for catalytic cracking have been developed; however, the improvement of zeolites is often aimed [7-29]. Although matrices have not been referred in many cases [1-4,30-40], it is known that there have been many positive effects with the use of matrices [41], for example, weakening zeolite acidity and activity, diffusing not only reactants but also products on the inside of catalysts, increasing the stability of catalysts, maintaining pore structure of zeolites, increasing heat transfer during catalysis and regeneration, etc. We have already reported the preparation and reactivity of many new types of matrices for catalytic cracking. Among them, the gel skeletal reinforcement (GSR) method was our original work and allowed the selective production of silica with very large mesopores [1,31,37-39,43-45]. We were able to use those materials as matrices, and their mixture with zeolite exhibited very high catalytic activity. Further, when the GSR method was applied during the preparation of ZSM-5 zeolite, the hierarchical microporous and mesoporous catalysts were successfully prepared and also exhibited very high activity and selectivity [31]. These series of studies clarified that zeolites mainly affected the selectivity of products while matrices largely affected the activity [1,2,42-46]. On the other hand, the Curie point pyrolyzer (CPP) method was found to be a very effective tool to estimate the catalytic cracking of VGO, ARs, and SBO [42-46]. The CPP method has some advantages of a very simple, small flow reactor with only very small weights of the reactant and catalyst, and the products formed in the CPP reactor are directly determined by gas chromatography.

In order to obtain higher activity of cracking catalysts, we prepared three-layered hierarchical catalysts [43,44] where GSR silica and two-layered catalysts were just mixed. The catalyst exhibited high activity; however, it was thought that the homogeneity in this catalyst would not be as high as that by the direct formation of GSR silica in the presence of a two-layered catalyst, which is presented here. In the present study, a novel three-layered catalyst was successfully prepared by the direct formation of GSR silica in the presence of a two-layered zeolite-containing mesoporous catalyst. The activity and selectivity for products of the novel hierarchical catalyst in catalytic cracking of VGO were estimated using the CPP method in comparison with those of

conventional catalysts including zeolite itself and a zeolite and kaolin mixed catalyst. The activity was quantitatively related with not only the amount of acid sites but also the size of the mesoporous pore volume for the first time.

5.2 Catalyst preparation

5.2.1 Preparation of the HY zeolite-containing two-layered catalyst

An HY zeolite-containing two-layered catalyst was prepared according to the procedure shown in Figure 5.1. The HY zeolite ($\text{SiO}_2/\text{Al}_2\text{O}_3 = 5.5$, reference catalyst supplied by Catalysis Society of Japan, JRC-HY5.5) was suspended in ethanol and stirred at 25 °C for 30 min. Tetraethyl orthosilicate (TEOS, Nakalai) was dropwise added into the suspension and stirred at 25 °C for 30 min. An aqueous solution of malic acid (MA, Nakalai), which was used as a carbon template and a catalyst for polymerization of TEOS [4], was dropwise added into the mixture and stirred at 25 °C for 30 min. After that, the mixture was stirred at 50 °C until gelation and then age-

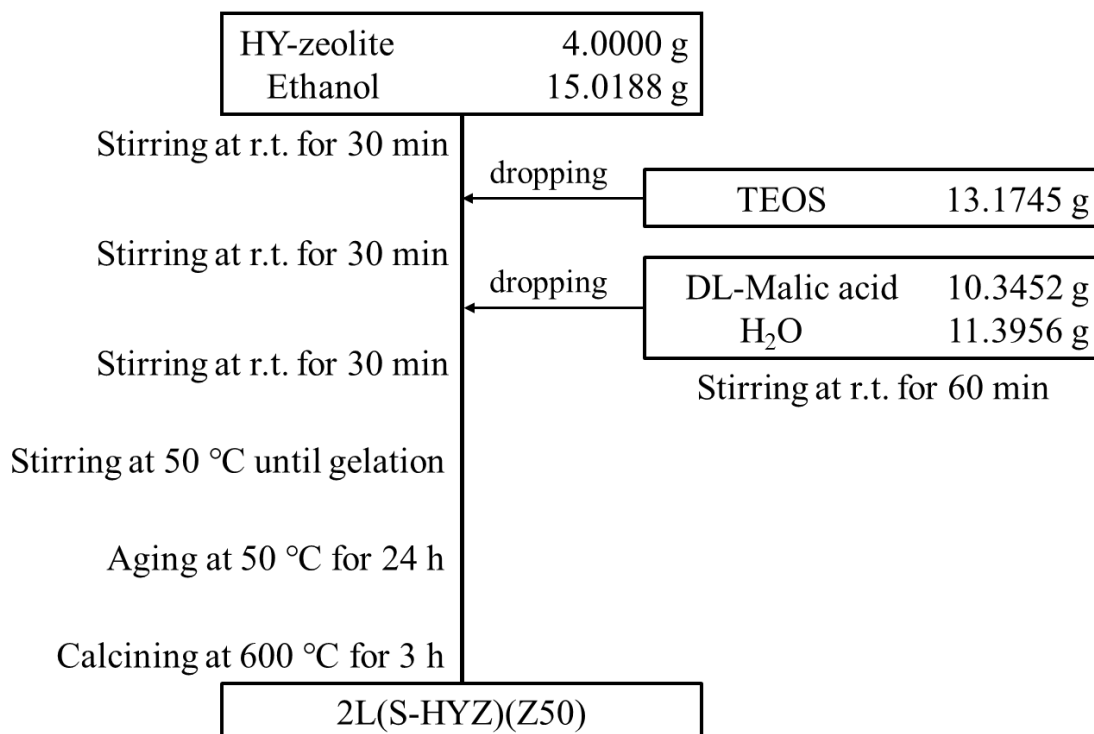


Figure 5.1 Flowchart for preparation of 2L(S-HYZ)(Z50).

d at 50 °C for 24 h. The resultant solid was calcined at 600 °C for 3 h. This two-layered catalyst was named 2L(S-HYZ)(Z50) where L represents layered, S is silica, HYZ is HY zeolite, and Z50 50 wt% zeolite included.

5.2.2 Preparation of the three-layered catalyst by co-gelation of GSR silica in the presence of the HY zeolite-containing two-layered catalyst

The three-layered catalyst was prepared by co-gelation of GSR silica in the presence of the HY-zeolite-containing two-layered catalyst (2L(S-HYZ)(Z50)) according to the procedure shown in Figure 5.2. 2L(S-HYZ)(Z50) was suspended in ethanol and was stirred at 25 °C for 30 min. TEOS was dropwise added, and the mixture was stirred at 25 °C for 30 min. An aqueous solution of HCl (0.5 wt%) was dropwise added and stirred at 25 °C for 30 min. An aqueous solution of N-

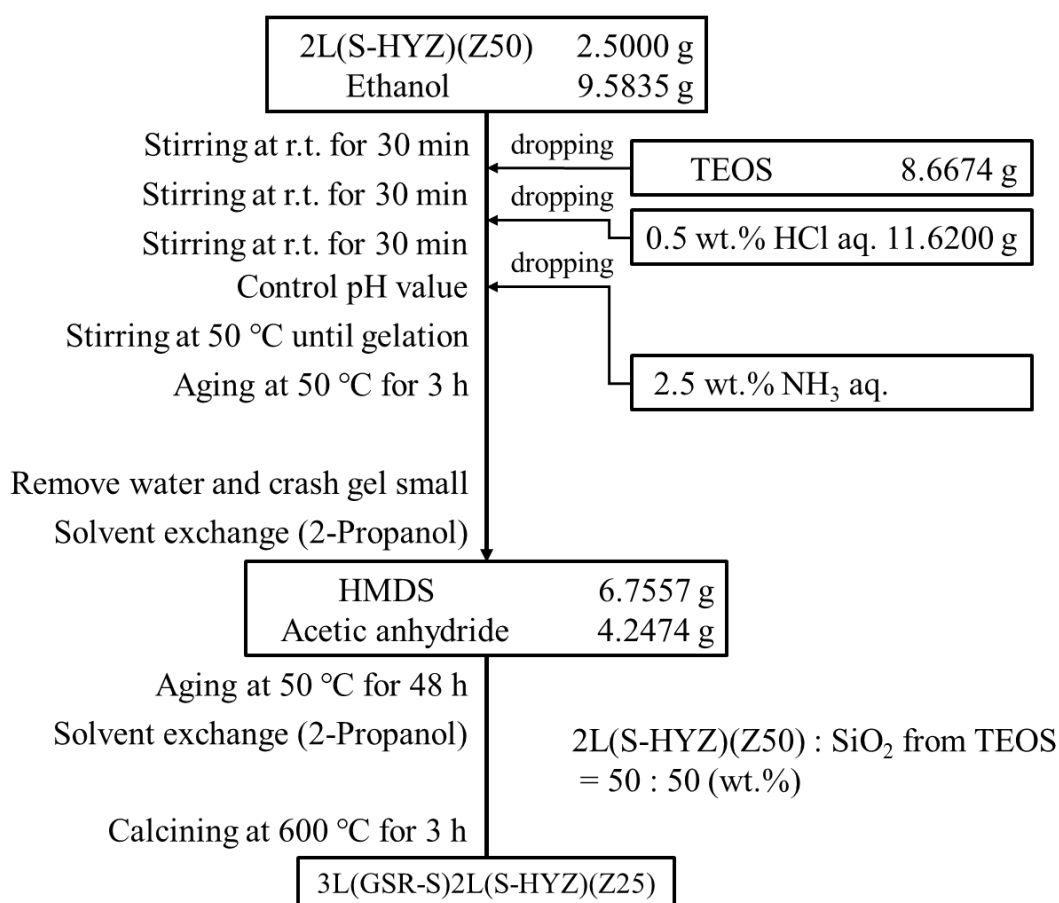


Figure 5.2 Flowchart for preparation of 3L(GSR-S)2L(S-HYZ)(Z25).

Chapter 5

H₃ (2.5 wt%) was dropwise added to control the pH to 5. After stirring at 50 °C until the occurrence of gelation, the mixture was aged at 50 °C for 3 h. The gel was transferred to water and aged at 50 °C for 18 h. After water was removed, the gel was crushed to 5 mm small particles, and solvent exchange was performed using 2-propanol at 50 °C for 5 min for five times. Into the resultant gel particles was added the hexamethyldisiloxane and acetic anhydride solution, and the mixture was aged at 50 °C for 48 h in the sealed PFA container. After that, the same solvent exchange by 2-propanol was performed at 50 °C for 5 min for five times. The resultant solid was dried in the airtight PFA container at 70 °C for 72 h and then calcined at 600 °C for 3 h to obtain a three-layered catalyst, which was named 3L(GSR-S)2L(S-HYZ)(Z25) where 3L means three-layered, GSR is gel skeletal reinforcement, and S is silica.

A mixed catalyst, Kaolin-HYZ(Z25), was prepared using a conventional kneading method (calcined at 600 °C for 3 h) from kaolin (Nakalai), alumina sol (Cataloid AP-1, Shokubai Kasei) as a binder, and the same HY zeolite. The contents of zeolite, kaolin, and the binder were 26, 58, and 16 wt%, respectively. In order to demonstrate that simple dispersion of HY zeolite with kaolin and binder does not increase the activity, this kaolin composite catalyst was prepared and tested. Further, this type of catalyst is used as a reference catalyst even in an actual cracking process [47] although the information of its industrial use is limited due to the range of secrets of a company.

5.3 Characterization of catalysts by NH₃ temperature-programmed desorption, N₂ adsorption and desorption, and XRD

NH₃ temperature-programmed desorption (TPD) was estimated by GC-TCD (Shimadzu GC-8A). Initially, NH₃ was adsorbed on a catalyst by the pulse method. TPD of adsorbed NH₃ was recorded by heating the catalyst from 100 to 600 °C at a heating rate of 10 °C/min.

N₂ adsorption and desorption data were measured using Belsorp (MicrotracBel, mini I), and results are shown in Table 5.1. A calcined catalyst (0.040 g) was degassed under 10⁻² kPa at 350 °C for 3 h by Belprep II (MicrotracBel). The BET surface area (SA) was calculated by the BET plot in the range of relative pressure from 0.05 to 0.3 and regarded as the total surface area of a catalyst. The total pore volume (TPV) was calculated from the amount of N₂ adsorption at a relative pressure of 0.99. An average pore diameter was calculated from these SA-BET and TPV values. The BJH method was adapted to estimate the surface area and pore volume of mesopores larger than 3.3 nm, and the measurement was performed in the range of relative pressures from 0.44 to 0.99. Therefore, SA-BJH and PV-BJH represent mesoporous SA and PV values, respectively. The

BJH pore diameter represents the pore diameter at the peak in the BJH pore size distribution. The micropore volume was defined as the difference between TPV and PV-BJH.

Rigaku Ultima IV was used to record X-ray diffraction (XRD). The conditions were as follows: slit: (SS) 1° (DS) 1° (RS) 0.3 mm, scan speed: 2°/min, $2\theta = 10\text{--}70^\circ$, scan mode: continuous, nickel-filtered Cu K α X-ray source radiation ($\lambda = 0.1541$ nm) operated at 40 kV and 20 mA, and time: 1 s.

5.4 Catalytic cracking by the CPP method

Catalytic cracking of vacuum gas oil (VGO: C 84.91%, H 12.13%, and sulfur content of 100 ppm; original VGO: V, Ni 0 ppm, S 2.85%, C 85.48%, H 11.6%, asphaltene 0.18%, IBP 281–FBP 570 °C; $d = 0.96$ g/mL at 15 °C), which was supplied by Nippon Ketjen, was performed using the CPP method [42,43] under conditions of 500 °C, 5 s, 1.0 mg of the catalyst, a 0.20 mg feed, and 0.60 MPa He. The reaction apparatus is shown in Figure 5.3. Amounts of 0.2 mg of VGO and 1.0 mg of a catalyst were put on a ferromagnetic pyrolysis foil (pyro-foil, F500, Japan Analytical Industry (JAI), Co. Ltd.) and wrapped. The pyro foil was set in the CPP (JAI, JCI-22) and preheated at 150 °C. A syringe was injected into a GC-FID, and VGO with the catalyst was reacted at 500 °C for 5 s. The products in this catalytic pyrolysis were directly analyzed by the GC-FID (Shimadzu GC-2010, injection temperature: 250 °C, carrier gas: He, pressure: 100.6 kPa, total flow rate: 170.9 mL/min, column flow rate: 0.83 mL/min, line speed: 16.8 cm/s, purge flow rate:

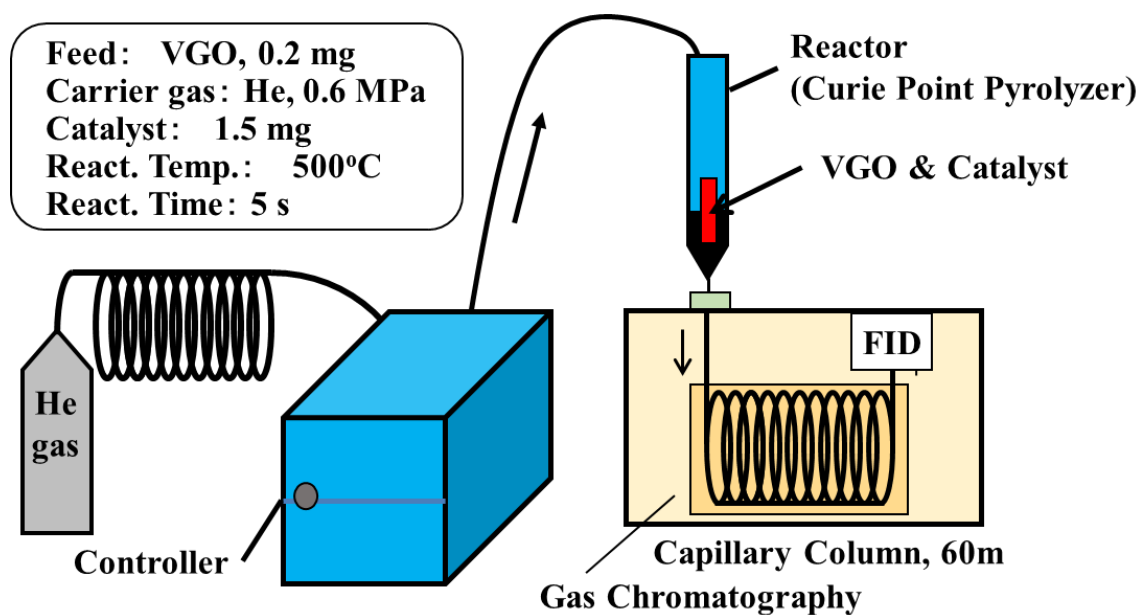


Figure 5.3 Reaction apparatus for catalytic cracking.

Chapter 5

4.0 mL/min, split ratio: 200.0, detector temperature: 320 °C, capillary column BP-1 (length of 60.0 m, inner diameter of 0.25 mm, and film thickness of liquid phase of 0.50 μm), initial column temperature: 0 °C for 16 min, heating rate: 2 °C/ min, and final column temperature: 228 °C). Products were identified in comparison with the holding time of each compound in the analysis of a standard gasoline supplied by the Japan Petroleum Institute under the same conditions. In order to determine the amount of products, 30 μL of a standard gas (methane: 1.01%, ethane: 1.02%, propane: 1.01%, iso-butane: 1.02%, and *n*-butane: 1.01%, GL Science) or 0.2 μL of 1 wt% toluene in *n*-dodecane was analyzed using auto-sampler (Shimadzu AOC-20i) by the same GC conditions. The ratio of the total peak areas of gases to the total amount of carbon in injected gases was almost the same as that of toluene. Conversion was defined by the percentage of the total amount of carbons in all products detected by GC (g) to the total amount of carbon in VGO used (g). In this experiment, only compounds with molecular weights lower than C15 were analyzed in detail, and other compounds were not determined for providing a simple catalyst-evaluating method. Although the coke formation of some catalysts was determined using thermogravimetric differential thermal analysis (TG-DTA), the experimental error was large due to the very small amount of the feed, and some explanations appear in a footnote of Table 5.2.

5.5 Results and discussion

5.5.1 Characterization of catalysts by XRD, N₂ adsorption and desorption, and NH₃ TPD

XRD patterns of the HY zeolite, mixed catalyst Kaolin-HYZ(Z25), two-layered hierarchical 2L(S-HYZ)(Z50), and three-layered hierarchical 3L(GSR-S)2L(S-HYZ)(Z25) catalysts are shown in Figure 5.4. These catalysts are further abbreviated to HY, Kaolin, 2L, and 3L. The intensity of XRD signals for the HY zeolite decreased with decreasing the content of zeolite as expected. Although malic acid is used in the preparation of the 2L catalyst, a sufficient amount of zeolite remained probably because TEOS added before addition of malic acid would have appropriately covered the surface of the zeolite [36]. It seems that, in the preparation of the 3L catalyst, TEOS initially added into the suspension of the 2L catalyst would also appropriately cover the surface of the 2L catalyst and inhibit the dissolution of the 2L catalyst by an acid, a base, and aging treatment. Kaolin signals were observed besides those of HY zeolite in the Kaolin catalyst.

Pore properties of catalysts obtained by N₂ adsorption and desorption measurement are shown in Table 5.1. The BET surface area (SA) and total pore volume (TPV) of the HY zeolite

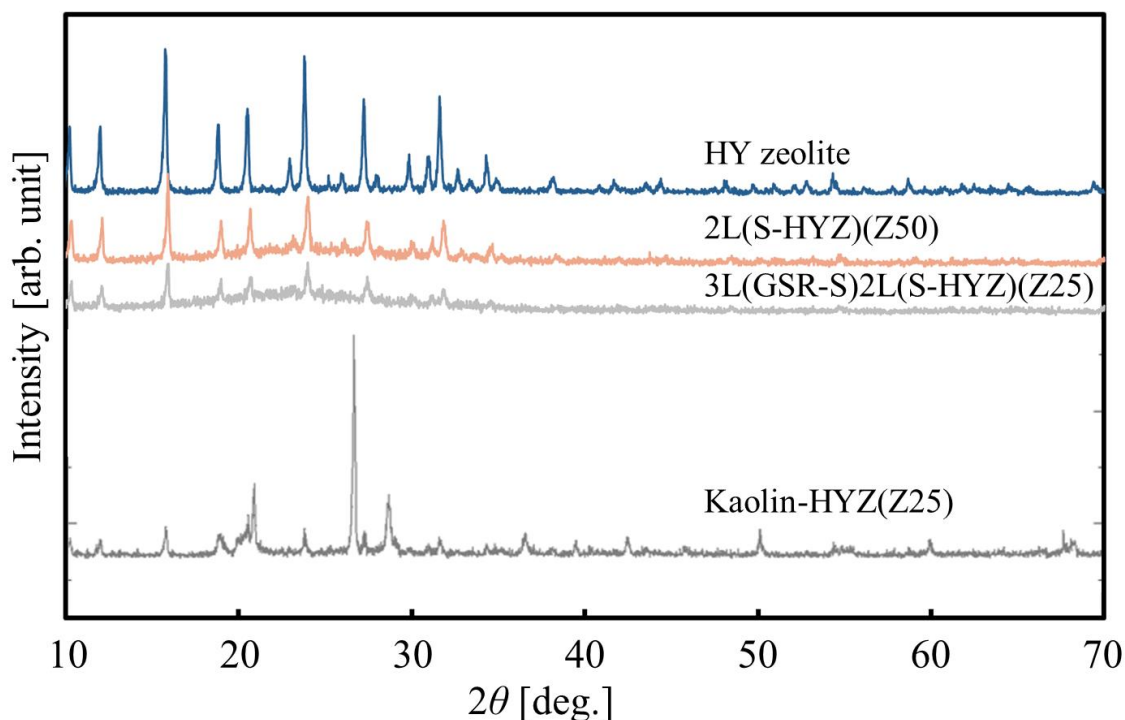


Figure 5.4 XRD patterns of HY zeolite, Kaolin-HYZ, and 2L and 3L catalysts.

include those for both micropores and mesopores of zeolite itself. On the other hand, the SA and PV of HY zeolite estimated from the BJH method are only regarded as those of mesopores of zeolite itself and were very small because the BJH method only estimates pore sizes larger than 3.3 nm and HY zeolite hardly has mesopores. Micropore volumes defined as the difference between TPV and BJH-PV were 0.25, 0.06, 0.17, and 0.07 cm³/g for HY, Kaolin, 2L, and 3L catalysts, respectively, and changed approximately depending on the content of Y zeolite, suggest-

Table 5.1 Pore properties of HY Zeolite, Kaolin-HYZ, and 2L and 3L catalysts obtained by N₂ adsorption measurement^a

Catalysts	NH ₃ -TPD (10 ⁻⁴ mol/g)	BET SA (m ² /g)	Microp. ^b PV (cm ³ /g)	Total PV (cm ³ /g)	Ave. PD (nm)	BJH SA (m ² /g)	BJH PV (cm ³ /g)	BJH PD (nm)
HY zeolite	7.8	725	0.25	0.41	2.3	36	0.16	3.3
Kaolin-HYZ(Z25)	2.3	225	0.06	0.22	4.0	55	0.16	3.8
2L(S-HYZ)(Z50)	2.9	839	0.17	0.93	4.4	518	0.75	4.8
3L(GSR-S)2L(S-HYZ)(Z25)	2.9	803	0.07	1.50	7.4	716	1.44	11

^a BET and BJH are measuring methods. SA: surface area; PV: pore volume; PD: pore diameter. The micropore volume was calculated.

^b Micropore volume was defined as the difference between total pore volume and BJH pore volume.

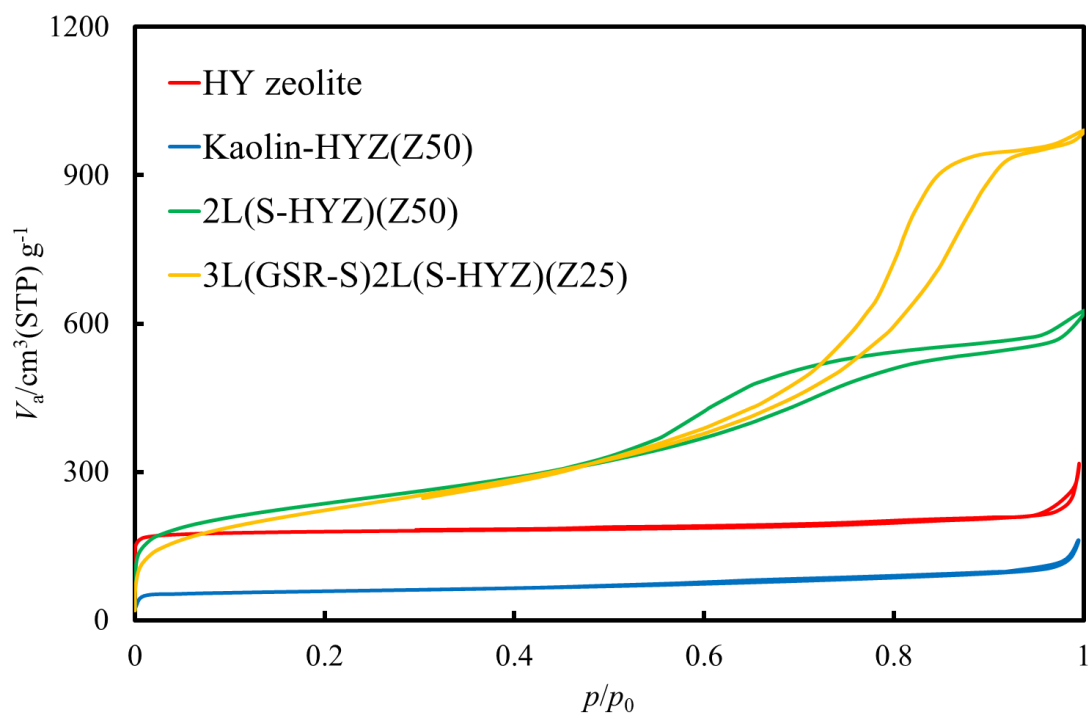


Figure 5.5 Nitrogen adsorption–desorption isotherms of HY zeolite, Kaolin-HYZ, and 2L and 3L catalysts.

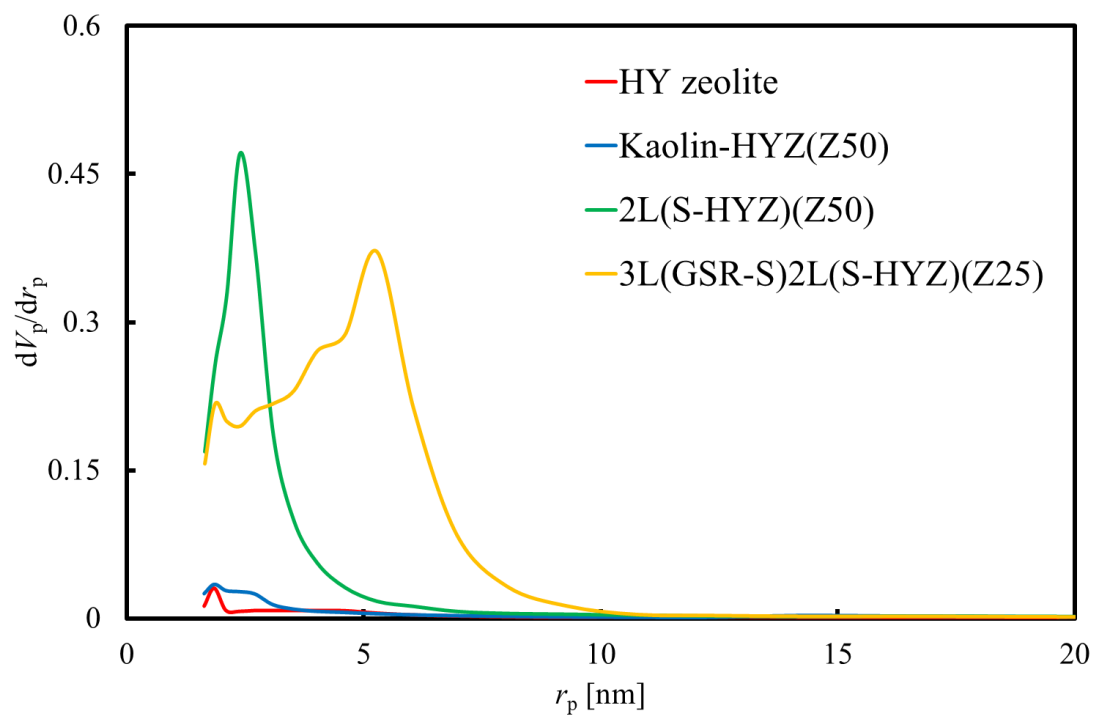


Figure 5.6 BJH pore size distribution of HY zeolite, Kaolin-HYZ, and 2L and 3L catalysts.

Chapter 5

ing that the required amount of zeolite in each catalyst would be included at the preparation. The Kaolin catalyst exhibited very small BET-SA, TPV, BJH-SA, and BJH-PV values because Kaolin hardly has pores. In contrast, 2L and 3L catalysts exhibited very high values of SA and PV in both BET and BJH methods. Although these values were not necessarily consistent each other, it is because the BET method and TPV includes those of not only mesopores but also micropores. BJH-SAs of 2L and 3L catalysts were 518 and 716 m²/g, and their BJH-PVs were 0.75 and 1.44 cm³/g, respectively, indicating that these catalysts would consist of both large amounts of mesopores around their external surface and micropores of HY zeolite in their insides forming the hierarchical structures. In previous work, micro-meso-meso three-layered catalysts made by simply mixing a 2L catalyst and GSR silica gel exhibited three-layered characters of zeolite and two sizes of mesopores [43,44]. In the present study, when GSR silica was prepared in the presence of the 2L catalyst, a micro-meso-meso three-layered catalyst, 3L(GSR-S)2L(S-HYZ)(Z25), was also successfully prepared. Nitrogen adsorption–desorption isotherms and BJH pore size distributions are shown in Figures 5.5 and 5.6. In Figure 5.5, HY zeolite showed the type-I isotherm, while 2L and 3L catalysts showed the type-IV hysteresis curves. The results suggested that the 2L catalyst would have a significant amount of mesopores and the 3L catalyst would have the larger amount and size of mesopores than those of the 2L catalyst. Figure 5.6 demonstrates that both 2L and 3L catalysts developed large mesopores and the 3L catalyst left characters of the 2L catalyst and had two types of mesopores besides micropores of zeolite. In contrast, the adsorption and desorption isotherms and pore size distribution of the Kaolin catalyst in Figures 5.5 and 5.6 show that pores other than those of zeolite did not develop although this catalyst left a character of HY zeolite to a smaller extent.

Results from NH₃-TPD are also summarized in Table 5.1. The amount of NH₃-TPD for HY zeolite was 7.8×10^{-4} mol/g. When the zeolite content of catalysts decreased in Kaolin, 2L, and 3L catalysts, their amounts of NH₃-TPD decreased. However, Kaolin and 3L catalysts exhibited amounts of NH₃-TPD larger than expected for the content of zeolite, while the 2L catalyst did not. A part of micropores in HY zeolite of the 2L catalyst may be covered by SiO₂ from TEOS during the preparation. Further, the GSR procedure with the 3L catalyst may have improved covering micropores by SiO₂ in the 2L catalyst. Another, aluminum components in HY zeolite of the 2L catalyst, which are not incorporated in the crystal structure of HY zeolite, may be dissolved in TEOS acid-catalyzed gelation in the preparation of the 3L catalyst. As the Kaolin catalyst included binder alumina, small amounts of acid sites may be formed.

5.5.2 Catalytic cracking of VGO over HY zeolite, kaolin, 2L, and 3L catalysts using the CPP method

Catalytic cracking of VGO over HY zeolite, Kaolin, 2L, and 3L catalysts was performed using the CPP method, and results are given in Figures 5.7 and 5.8 and Table 5.2. Figure 5.7 shows the carbon number distribution in catalytic cracking of VGO at 500 °C. Cracking by HY zeolite included over-cracking, and large amounts of lower-molecular hydrocarbons were produced. In contrast, when the concentration of zeolite was diluted in Kaolin, 2L, and 3L catalysts, larger amounts of higher-molecular hydrocarbons occurred and carbon number distributions got closer to each other. Figure 5.8 shows the distribution of paraffins, olefins, naphthenes, and aromatics (PONA) in catalytic cracking of VGO at 500 °C. Paraffins' selectivity of HY zeolite was very high due to their high ability for hydrogen transfer [1-4,36,42-46]. When the concentration of zeolite was diluted for Kaolin, 2L, and 3L catalysts, the selectivity for paraffins decreased and selectivities for olefins and aromatics increased due to their low ability for hydrogen transfer. Table 5.2 summarizes the reaction profiles including the selectivity for products and conversion and parameters in gasoline fractions. The conversion increased in the order Kaolin < Zeolite < 2L < 3L. The selectivity for gasoline fractions was almost the same at 70–71% for 2L, 3L, and Kaolin catalysts. The result was consistent with the reports in that the selectivity for products changed depending on only the type of zeolite and did not change if the activity changed by the amount and type of mesoporous materials [42-46]. Olefin/paraffin (O/P), branched/straight-chained products (*iso-/n-*), and multi-branched/single-branched product (m/s) ratios and the research octane number (RON) increased with the use of 2L and 3L catalysts. It is suggested that the dispersion of zeolite into the matrix part would decrease the ability of hydrogen

Table 5.2 Product Distribution and Catalytic Properties for HY Zeolite, Kaolin-HYZ, 2 L and 3 L Catalysts.

Catalysts	Selectivity for products (%)			Parameters in gasoline fraction				
	C2-C4	Gasoline (C5-C11)	C12-	Conv. ^a (%)	Olefin/Paraffin	<i>iso-/n-</i>	Multi-/Single-branch	RON
HY zeolite	36	62	2	24	0.12	7.3	0.12	87
Kaolin-HYZ(Z25)	26	71	2	21	0.38	5.3	0.31	89
2L(S-HYZ)(Z50)	27	70	3	32(50)	0.88	8.8	0.47	93
3L(GSR-S)2L(S-HYZ)(Z25)	27	71	2	46(70)	0.68	11	0.43	90

^a The value in a parenthesis represents total conversion which includes not only C2-C12-liquid fraction but also coke formation. The coke formation was estimated by weight loss at 400-600 °C in TG-DTA measurement of a used catalyst.

Chapter 5

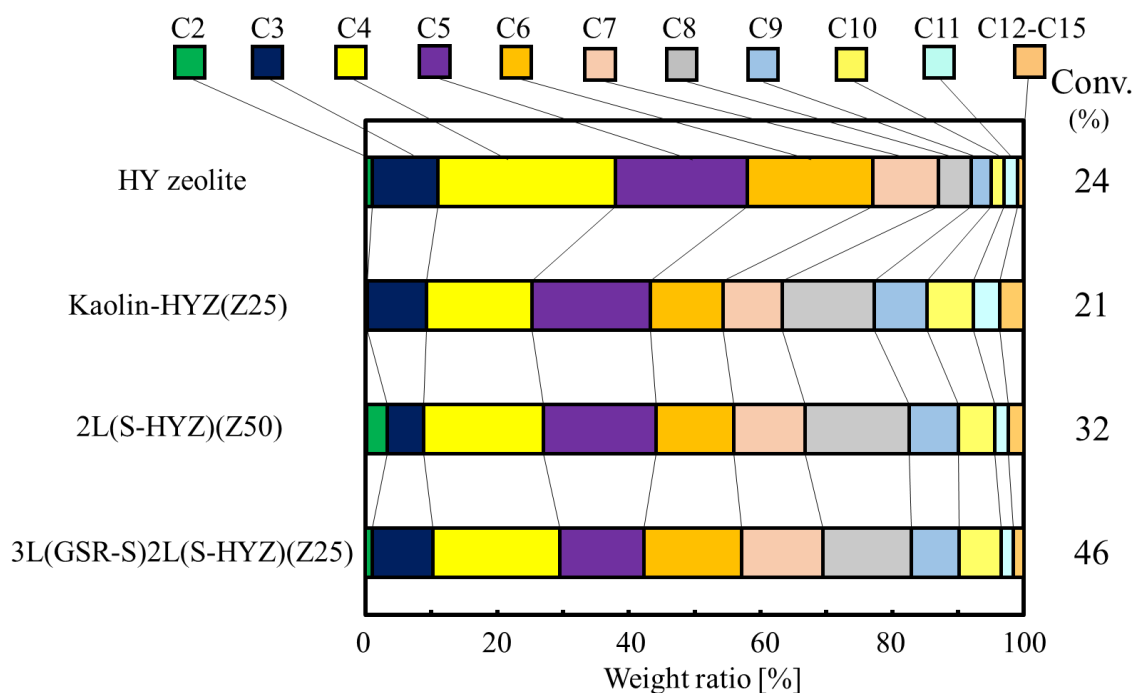


Figure 5.7 Distribution of carbon numbers of all products on catalytic cracking of VGO in 500 °C.

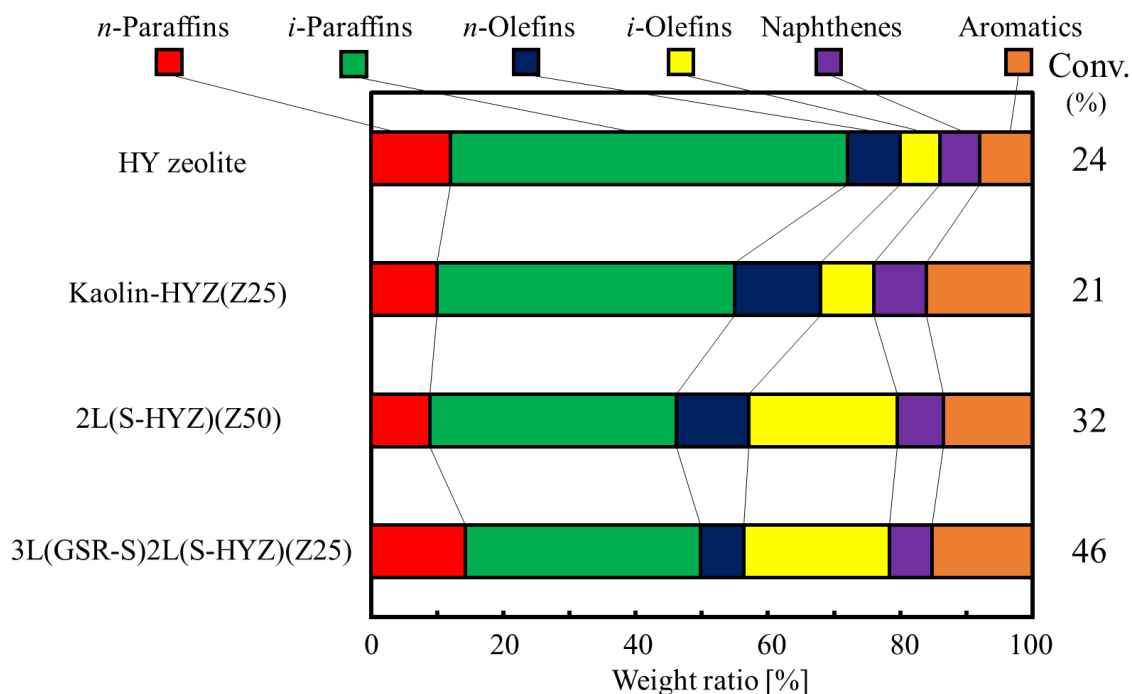


Figure 5.8 Selectivity for paraffins, olefins, naphthenes, and aromatics on catalytic cracking of VGO at 500 °C.

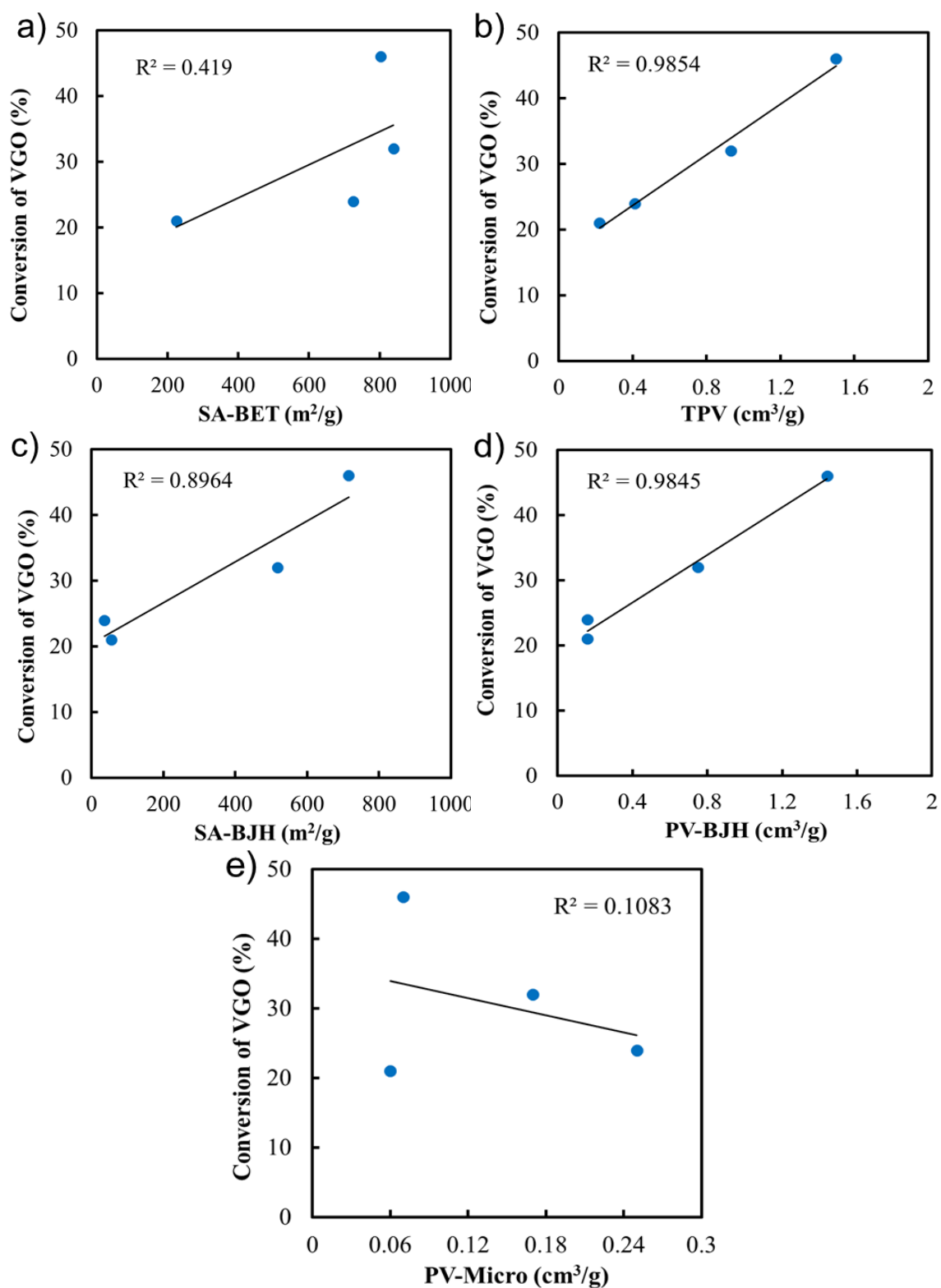


Figure 5.9 Relationship between conversion of VGO and a) surface area in BET method (SA-BET), b) total pore volume (TPV), c) surface area in BJH method (SA-BJH), d) pore volume in BJH method (PV-BJH) and e) micropore volume (PV-Micro).

Chapter 5

transfer by zeolite and increase O/P, *iso-/n-*, and m/s ratios and the selectivity for aromatics, which may lead to the increase in the RON value.

In order to investigate the relationship between the activity and the pore structure, the conversion of VGO was plotted against the surface area in the BET method (SA-BET), total pore volume (TPV), surface area in the BJH method (SA-BJH), pore volume in the BJH method (PV-BJH), and micropore volumes (PV-Micro) in Figure 5.9a–e. When the strength in the relationship between the activity and pore structure was estimated by the coefficient of determination (R^2) in the linear approximation, the value of R^2 between SA-BET and the conversion was much lower than in other relationships. The relationship between PV-Micro, which was estimated from the difference between TPV and PV-BJH, and the conversion of VGO was also very low as shown in Figure 5.9e. These results suggested that the effect of the size of micropores on the activity would be rather low. On the other hand, the relationship between TPV, SA-BJH, or PV-BJH and the conversion was very high, and R^2 values for TPV and PV-BJH exceeded 0.98, indicating that the size of mesopores would be closely related to the activity.

In order to investigate the relationship between the activity and the amount of acid sites and further the relationship between the activity and the product of the pore parameters of PV and SA and the amount of acid sites, the conversion of VGO was also plotted against NH_3 -TPD and the products of SA-BET and NH_3 -TPD, TPV and NH_3 -TPD, SA-BJH and NH_3 -TPD, PV-BJH and NH_3 -TPD, and PV-Micro and NH_3 -TPD in Figure 5.10. According to Figure 5.10a, values of NH_3 -TPD themselves were hardly related to the conversion of VGO. SA-BET was not related to the conversion originally, and therefore the product of SA-BET and NH_3 -TPD was not related to the conversion in Figure 5.10b either, suggesting that the relationship between the activity and the size of micropores would be rather low. Although TPV was closely related to the conversion originally (Figure 5.9b), the relationship between the product of TPV and NH_3 -TPD and the conversion decreased significantly (Figure 5.10c), suggesting that there would be a negative effect on the amount of acid sites and it may come from the fact that TPV includes not only the mesoporous volume but also the microporous volume. This was also confirmed by the fact that the relationship between the conversion of VGO and the product of PV-Micro and NH_3 -TPD was very low as seen in Figure 5.10e. In contrast, it was demonstrated that the relationships between the conversion and the products of SA-BJH and NH_3 -TPD (Figure 5.10d) and PV-BJH and NH_3 -TPD (Figure 5.10e) were very high, and further, the values of R^2 increased in comparison to the original R^2 between the conversion and the values of SA-BJH (Figure 5.9c) and PV-BJH (Figure 5.9d). As SA-BJH and PV-BJH are estimated for pore sizes of 3.3 nm and more than 3.3 nm, these results would be closely related to the presence of mesopores. Further, as the products of SA-BJH and NH_3 -TPD and PV-BJH and NH_3 -TPD are closely related to the conversion, it is suggested that the presence of acid sites distributed on mesopores would be very important for the activity.

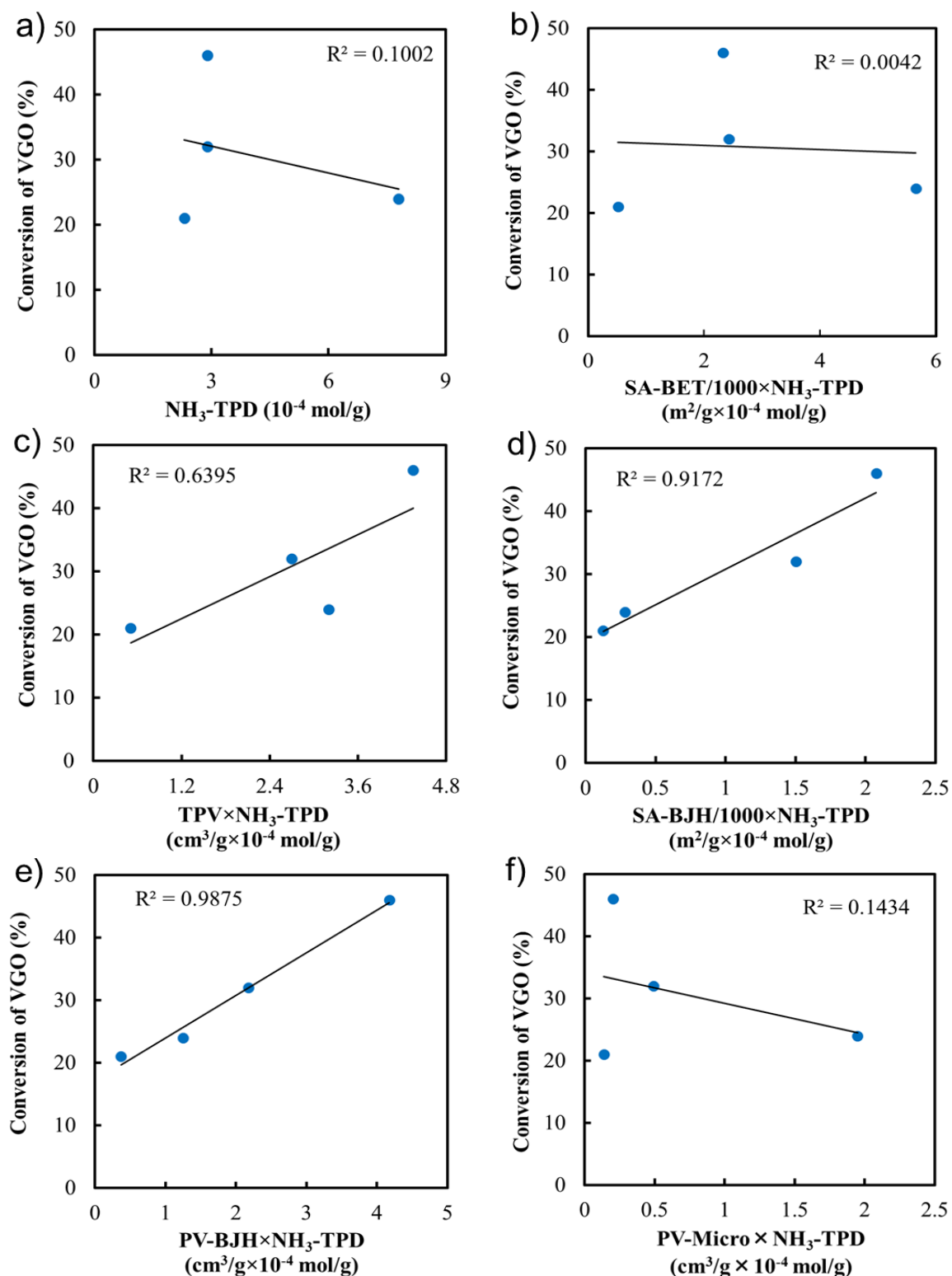


Figure 5.10 Relationship between conversion of VGO and a) $\text{NH}_3\text{-TPD}$, b) $\text{SA-BET} \times \text{NH}_3\text{-TPD}$, c) $\text{TPV} \times \text{NH}_3\text{-TPD}$, d) $\text{SA-BJH} \times \text{NH}_3\text{-TPD}$ and e) $\text{PV-BJH} \times \text{NH}_3\text{-TPD}$ f) $\text{PV-Micro} \times \text{NH}_3\text{-TPD}$. Abbreviation is same in Figure 5.9.

Chapter 5

In the previous paper [46], the authors performed VGO cracking using the CPP method, and the effects of the pore structure of matrices, SiO₂, Al₂O₃, TiO₂, and ZrO₂ and the acidity of catalysts on the activity and selectivity of zeolite-containing mixed catalysts prepared by the conventional kneading method were investigated. When the similar relationships using NH₃-TPD and N₂ adsorption and desorption were estimated, the coefficients of determination between the conversion of VGO and PV-BJH and between the conversion and the product of PV-BJH and NH₃-TPD were approximately 0.6 and 0.7, respectively, which were relatively higher values in that study. However, these values were much lower than those of the present study probably because the types of the matrix oxide largely changed and the subtle properties of the interfaces between the matrix oxide and zeolite, which often change the acid nature of catalysts, may have been different. In the present study, the acid sites were supplied only by HY zeolite and the matrix was composed of SiO₂, and therefore it seems that the mesopore size of catalysts would have had a relationship with the activity precisely.

In the processing of hydrocarbons, the importance of mesoporosity was recognized [12-15,18,19,21,48], and specifically, high mesoporosity is intrinsic for the processing of large molecules such as polyolefins [20,23,34,49], biomass, and VGO [22,24]. It was reported that hierarchical ZSM-5 prepared by using organosilanes as a mesopore-directing agent and desilication treatment with alkali exhibited the higher yield of C₂–C₅ hydrocarbons and the lower deactivation rate due to their secondary porosity [20] in catalytic cracking of low-density polyethylene (LDPE). LDPE was also rapidly cracked in the presence of hierarchical ZSM-5 in the experiment using a TG apparatus [23]. In general, LDPE has a large molecular size and cannot approach the acid sites on the inside of micropores of zeolite. Therefore, the catalytic cracking of LDPE is expected to occur on the acid sites of the external surface of zeolite, and the higher catalytic performance of nanosized and hierarchical zeolite as well as mesoporous materials with acid sites was ascribed to its larger external surface areas, the presence of developed mesopores, and acid sites dispersed on their surface compared with a commercial micro-sized zeolite [34,48]. Hierarchical ZSM-5 treated with alkali was also applied for catalytic cracking of lignin to aromatics, and moderately mesoporous ZSM-5 exhibited the higher yield [22]. When a hierarchical zeolite with a macro-meso-microporous network was prepared by growing a ZSM-5 shell on a Y zeolite surface, the catalysts exhibited an increase in activity, the yield of gasoline and isoparaffins and olefins in gasoline, and the decrease of LPG and aromatics in catalytic cracking of VGO probably because of the presence of a hierarchical structure [24].

As shown above, recent studies reported ZSM-5 zeolites since ZSM-5 is easy to prepare using a template and has high activity in cracking. We have already confirmed that ZSM-5 exhibited the significantly high activity in catalytic cracking of linear hydrocarbons, for example, *n*-dodecane, compared to Y and β zeolites probably because terminal ends of linear hydrocarbons

Chapter 5

would be easier to be adsorbed in the ZSM-5 pore mouth [1,36-40]. However, when heavier fractions such as fats, VGO, and ARs were used in our CPP method, ZSM-5-containing hierarchical catalysts exhibited similar activity to that of Y and β zeolite-containing hierarchical catalysts [2,42-46]. Further, when the yield of gasoline fractions was compared at the same conversion, it decreased in the order $Y > \beta > ZSM-5$, which is consistent with the order of their sizes of micropores. These results suggested that, in the treatment of the large molecules, the diffusion rate to approach the highly active acid sites of zeolites would have the intrinsic effect on the total activity. In this study, it seems that our prepared three-layered catalyst would have the ideal structure, which accelerates not only adsorption of heavy large molecules but also elimination of reactive products after cracking of larger molecules as shown in the graphical abstract.

5.6 Conclusions

In the present study, a novel hierarchical three-layered catalyst (3L), which has large mesoporous GSR silica on the outer side and small mesoporous silica on the inside around zeolite crystals in the core, was successfully prepared by using the gel skeletal reinforcement method in the presence of a two-layered zeolite-containing catalyst (2L). The BET surface area, BJH pore volume, and BJH pore diameter of the 3L catalyst were 716 m²/g, 1.44 cm³/g, and 10.6 nm, respectively. Catalytic cracking of VGO catalyzed by the hierarchical catalyst was performed using the CPP method. 3L, 2L, and Kaolin catalysts exhibited a selectivity of gasoline of more than 70%, while that of HY zeolite was only 62%, indicating that over-cracking of VGO occurred with the use of HY zeolite. Parameters in the gasoline fraction, O/P, *iso-/n-*, and m/s ratios, and RON values significantly increased in the cases of 2L and 3L hierarchical catalysts compared to those of HY zeolite and Kaolin catalysts. The conversion of VGO using the CPP method decreased in the order 3L (46%) > 2L (32%) > HY zeolite (24%) > Kaolin-HYZ(Z25) (21%). Although 3L and 2L hierarchical catalysts had smaller zeolite content, the activity increased probably because the hierarchical catalysts had very large mesopores. The clear linear relationship between the conversion of VGO and the product of PV-BJH and NH₃-TPD was observed, and the coefficient of determination (R^2) reached 0.99 for the first time, suggesting that the mesopore volume and the acid site of zeolite dispersed on mesopores would be closely related to the conversion of VGO.

Acknowledgements

Authors thanks Ms. Shiho Aoki, Mr. Kazuya Mori, and Dr. Hiroyuki Nasu for their helpful work.

References

- [1] A. Ishihara, "Preparation and reactivity of hierarchical catalysts in catalytic cracking", *Fuel Process. Technol.*, 194 (2019) 106116, <https://doi.org/10.1016/j.fuproc.2019.05.039>
- [2] A. Ishihara, D. Kawaraya, T. Sonthisawate, K. Kimura, T. Hashimoto, H. Nasu, "Catalytic cracking of soybean oil by hierarchical zeolite containing mesoporous silica-aluminas using a Curie point pyrolyzer" *J. Mol. Catal. A: Chem.*, 396 (2015) 310-318, <https://doi.org/10.1016/j.molcata.2014.10.010>
- [3] A. Ishihara, N. Fukui, H. Nasu, T. Hashimoto, "Hydrocracking of soybean oil using zeolite-alumina composite supported NiMo catalysts", *Fuel*, 134 (2014) 611-617, <https://doi.org/10.1016/j.fuel.2014.06.004>
- [4] A. Ishihara, H. Negura, T. Hashimoto, H. Nasu, "Catalytic properties of amorphous silica-alumina prepared using malic acid as a matrix in catalytic cracking of n-dodecane", *Appl. Catal. A: Gen.*, 388 (2010) 68-76, <https://doi.org/10.1016/j.apcata.2010.08.027>
- [5] J. Li, H. Ma, Q. Sun, W. Ying, D. Fang, "Effect of iron and phosphorus on HZSM-5 in catalytic cracking of 1-butene", *Fuel Process. Technol.*, 134 (2015) 32-38, <https://doi.org/10.1016/j.fuproc.2014.11.026>
- [6] J. Lee, U. G. Hong, S. Hwang, M. H. Youn, I. K. Song, "Catalytic cracking of C₅ raffinate to light olefins over lanthanum-containing phosphorous-modified porous ZSM-5: Effect of lanthanum content", *Fuel Process. Technol.*, 109 (2013) 189-195, <https://doi.org/10.1016/j.fuproc.2012.10.017>
- [7] X. Su, Y. Fang, X. Bai, W. Wu, "Synergic Effect of GaO⁺/Brønsted Acid in Hierarchical Ga/Al-ZSM-5 Bifunctional Catalysts for 1-Hexene Aromatization", *Ind. Eng. Chem. Res.*, 58 (2019) 20543-20552, <https://doi.org/10.1021/acs.iecr.9b03791>
- [8] W. Li, F. Li, H. Wang, M. Liao, P. Li, J. Zheng, C. Tu, R. Li, "Hierarchical mesoporous ZSM-5 supported nickel catalyst for the catalytic hydrodeoxygenation of anisole to cyclohexane" *Mol. Catal.*, 480 (2020) 110642, <https://doi.org/10.1016/j.mcat.2019.110642>
- [9] T. Zhao, Y. Wang, C. Sun, A. Zhao, C. Wang, X. Zhang, J. Zhao, Z. Wang, J. Lu, S. Wu, W. Liu, "Direct synthesis of hierarchical binder-free ZSM-5 and catalytic properties for MTP", *Microporous Mesoporous Mater.*, 292 (2020) 109731, <https://doi.org/10.1016/j.micromeso.2019.109731>
- [10] H. Issa, N. Chaouati, J. Toufaily, T. Hamieh, A. Sachse, L. Pinard, "Toolbox of Post-Synthetic Mordenite Modification Strategies: Impact on Textural, Acidic and Catalytic Properties", *ChemCatChem*, 11 (2019) 4581-4592, <https://doi.org/10.1002/cctc.201900927>
- [11] Y. Tian, Y. Che, M. Chen, W. Feng, J. Zhang, Y. Qiao, "Catalytic Upgrading of Vacuum Residue-Derived Cracking Gas-Oil for Maximum Light Olefin Production in a Combination of a

Chapter 5

- Fluidized Bed and Fixed Bed Reactor”, *Energy Fuels*, 33 (2019) 7297-7304, <https://doi.org/10.1021/acs.energyfuels.9b01949>
- [12] C. Wen, X. Wang, J. Xu, Y. Fan, “Hierarchical SAPO-11 molecular sieve-based catalysts for enhancing the double-branched hydroisomerization of alkanes”, *Fuel*, 255 (2019) 115821, <https://doi.org/10.1016/j.fuel.2019.115821>
- [13] A. Bolshakov, N. Kosinov, D. E. Romero Hidalgo, B. Mezari, A. J. F. van Hoof, E. J. M. Hensen, “Mild dealumination of template-stabilized zeolites by NH₄F”, *Catal. Sci. Technol.*, 9 (2019) 4239-4247, <https://doi.org/10.1039/c9cy00593e>
- [14] T. Imyen, W. Wannapakdee, J. Limtrakul, C. Wattanakit, “Role of hierarchical micro-mesoporous structure of ZSM-5 derived from an embedded nanocarbon cluster synthesis approach in isomerization of alkenes, catalytic cracking and hydrocracking of alkanes”, *Fuel*, 254 (2019) 115593, <https://doi.org/10.1016/j.fuel.2019.06.001>
- [15] E. V. Parkhomchuk, D. A. Sladkovskii, Y. Gun, W. Wu, K.A. Sashkina, A.I. Lysikov, V. N. Parmon, “Catalytic Cracking of n-Hexane in the Presence of Zeolite ZSM-5 Micro- and Nanocrystals”, *Pet. Chem.*, 59 (2019) 338-348, <https://doi.org/10.1134/S0965544119030113>
- [16] K. M. Kwok, S. W. D. Ong, L. Chen, H. C. Zeng, “Transformation of Stöber Silica Spheres to Hollow Hierarchical Single-Crystal ZSM-5 Zeolites with Encapsulated Metal Nanocatalysts for Selective Catalysis”, *ACS Appl. Mater. Interfaces*, 11 (2019) 14774-14785, <https://doi.org/10.1021/acsami.9b00630>
- [17] W. Wannapakdee, T. Yutthalekha, P. Dugkhuntod, K. Rodponthukwaji, A. Thivasasith, S. Nokbin, T. Witoon, S. Pengpanich, C. Wattanakit, “Dehydrogenation of Propane to Propylene Using Promoter-Free Hierarchical Pt/Silicalite-1 Nanosheets”, *Catalysts*, 9 (2019) 174-393, <https://doi.org/10.3390/catal9020174>
- [18] Z. Diao, L. Cheng, X. Hou, D. Rong, Y. Lu, W. Yue, D. Sun, “Fabrication of the Hierarchical HZSM-5 Membrane with Tunable Mesoporosity for Catalytic Cracking of n-Dodecane”, *Catalysts*, 9 (2019) 155, <https://doi.org/10.3390/catal9020155>
- [19] Y. Tian, B. Zhang, H. Liang, X. Hou, L. Wang, X. Zhang, G. Liu, “Synthesis and performance of pillared HZSM-5 nanosheet zeolites for n-decane catalytic cracking to produce light olefins”, *Appl. Catal. A: Gen.*, 572 (2019) 24-33, <https://doi.org/10.1016/j.apcata.2018.12.029>
- [20] K. A. Tarach, K. Pyra, S. Siles, I. Melián-Cabrera, K. Góra-Marek, “Operando Study Reveals the Superior Cracking Activity and Stability of Hierarchical ZSM-5 Catalyst for the Cracking of Low-Density Polyethylene”, *ChemSusChem*, 12 (2019) 633-638, <https://doi.org/10.1002/cssc.201802190>
- [21] P. Maki-Arvela, T. A. Kakakhel, M. Azkaar, S. Engblom, D. Y. Murzin, “Catalytic Hydroisomerization of Long-Chain Hydrocarbons for the Production of Fuels”, *Catalysts*, 8 (2018) 534-534, <https://doi.org/10.3390/catal8110534>

Chapter 5

- [22] S. Tang, C. Zhang, X. Xue, Z. Pan, D. Wang, R. J. Zhang, “Catalytic pyrolysis of lignin over hierarchical HZSM-5 zeolites prepared by post-treatment with alkaline solutions”, *J. Anal. Appl. Pyrolysis*, 137 (2019) 86-95, <https://doi.org/10.1016/j.jaap.2018.11.013>
- [23] G. Song, W. Chen, P. Dang, S. Yang, Y. Zhang, Y. Wang, R. Xiao, R. Ma, F. Li, “Fabrication, Characterization and Cytotoxicity of Spherical-Shaped Conjugated Gold-Cockle Shell Derived Calcium Carbonate Nanoparticles for Biomedical Applications”, *Nanoscale Res. Lett.*, 13 (2018) 1-13, <https://doi.org/10.1186/s11671-017-2411-3>
- [24] M. Pan, J. Zheng, Y. Liu, W. Ning, H. Tian, R. Li, “Construction and practical application of a novel zeolite catalyst for hierarchically cracking of heavy oil”, *J. Catal.*, 369 (2019) 72-85, <https://doi.org/10.1016/j.jcat.2018.10.032>
- [25] X. Dong, S. Shaikh, J. R. Vittenet, J. Wang, Z. Liu, K. D. Bhatte, O. Ali, W. Xu, I. Osorio, Y. Saih, J. M. Basset, S.A. Ali, Y. Han, “Fine Tuning the Diffusion Length in Hierarchical ZSM-5 To Maximize the Yield of Propylene in Catalytic Cracking of Hydrocarbons”, *ACS Sustainable Chem. Eng.*, 6 (2018) 15832-15840, <https://doi.org/10.1021/acssuschemeng.8b04441>
- [26] Z. Lian, C. Yang, L. Shi, X. Meng, N. Liu, Y. Yang, X. Wang, “Non-hydrocracking of diesel over hierarchical hzsm-5 zeolite to produce gasoline”, *Appl. Organomet. Chem.*, 32 (2018) e4587, <https://doi.org/10.1002/aoc.4587>
- [27] Z. Peng, L.-H. Chen, M.-H. Sun, H. Zhao, Z. Wang, Y. Li, L.-Y. Li, J. Zhou, Z.-C. Liu, B.-L. Su, “A hierarchical zeolitic Murray material with a mass transfer advantage promotes catalytic efficiency improvement”, *Inorg. Chem. Front.*, 5 (2018) 2829-2835, <https://doi.org/10.1039/C8QI00761>
- [28] M. Raad, S. Hamieh, J. Toufaily, T. Hamieh, L. J. Pinard, “Propane aromatization on hierarchical Ga/HZSM-5 catalysts”, *J. Catal.* 366 (2018) 223-236, <https://doi.org/10.1016/j.jcat.2018.07.035>
- [29] Z. Qin, B. Shen, Z. Yu, F. Deng, L. Zhao, S. Zhou, D. Yuan, X. Gao, B. Wang, H. Zhao, H. J. Liu, “A defect-based strategy for the preparation of mesoporous zeolite Y for high-performance catalytic cracking”, *J. Catal.*, 298 (2013) 102-111, <https://doi.org/10.1016/j.jcat.2012.11.023>
- [30] P. Lovás, P. Hudec, M. Hadvinová, A. Ház, “Conversion of rapeseed oil via catalytic cracking: Effect of the ZSM-5 catalyst on the deoxygenation process”, *Fuel Process. Technol.*, 134 (2015) 223-230, <https://doi.org/10.1016/j.fuproc.2015.01.038>
- [31] A. Ishihara, K. Mori, K. Mori, T. Hashimoto, H. Nasu, “Preparation of hierarchical catalysts with the simultaneous generation of microporous zeolite using a template and large mesoporous silica by gel skeletal reinforcement and their reactivity in the catalytic cracking of *n*-dodecane”, *Catal. Sci. Technol.*, 9 (2019) 3614-3618, <https://doi.org/10.1039/C9CY00693A>
- [32] Y. Shirasaki, H. Nasu, T. Hashimoto, A. Ishihara, “Effects of types of zeolite and oxide and preparation methods on dehydrocyclization-cracking of soybean oil using hierarchical zeolite-

Chapter 5

- oxide composite-supported Pt/NiMo sulfided catalysts”, *Fuel Process. Technol.*, 194 (2019) 106109, <https://doi.org/10.1016/j.fuproc.2019.05.032>
- [33] Z. Zhang, Q. Wang, X. Zhang, “Hydroconversion of Waste Cooking Oil into Bio-Jet Fuel over NiMo/SBUY-MCM-41”, *Catalysts*, 9 (2019) 466, <https://doi.org/10.3390/catal9050466>
- [34] C. Shang, Z. Wu, W. D. Wu, X. D. Chen, “Chemical Crosslinking Assembly of ZSM-5 Nanozeolites into Uniform and Hierarchically Porous Microparticles for High-Performance Acid Catalysis”, *ACS Appl. Mater. Interfaces*, 11 (2019) 16693-16703, <https://doi.org/10.1021/acsami.9b01681>
- [35] Y. Lv, X. Wang, D. Gao, X. Ma, S. Li, Y. Wang, G. Song, A. Duan, G. Chen, “Hierarchically Porous ZSM-5/SBA-15 Zeolite: Tuning Pore Structure and Acidity for Enhanced Hydro-Upgrading of FCC Gasoline”, *Ind. Eng. Chem. Res.*, 57 (2018) 14031-14043, <https://doi.org/10.1021/acs.iecr.8b02952>
- [36] A. Ishihara, K. Inui, T. Hashimoto, H. Nasu, “Preparation of hierarchical β and Y zeolite-containing mesoporous silica–aluminas and their properties for catalytic cracking of *n*-dodecane”, *J. Catal.*, 295 (2012) 81-90, <https://doi.org/10.1016/j.jcat.2012.07.027>
- [37] A. Ishihara, K. Nakajima, M. Hirado, T. Hashimoto, H. Nasu, “Novel Method for Generating Large Mesopores in an Amorphous Silica–Alumina by Controlling the Pore Size with the Gel Skeletal Reinforcement and Its Catalytic Cracking Properties as a Catalyst Matrix”, *Chem. Lett.*, 40 (2011) 558-560, <https://doi.org/10.1246/cl.2011.558>
- [38] A. Ishihara, T. Hashimoto, H. Nasu, “Large Mesopore Generation in an Amorphous Silica–Alumina by Controlling the Pore Size with the Gel Skeletal Reinforcement and Its Application to Catalytic Cracking”, *Catalysts*, 2 (2012) 368-385, <https://doi.org/10.3390/catal2030368>
- [39] A. Ishihara, H. Oono, T. Hashimoto, H. Nasu, “Preparation of SiO₂ and SiO₂–Al₂O₃ catalysts by gel skeletal reinforcement using hexamethyldisiloxane (HMDS) and acetic anhydride and aluminum tri-sec-butoxide (ASB) systems and elucidation of their catalytic cracking properties as matrices”, *Microporous Mesoporous Mater.*, 233 (2016) 163-170, <https://doi.org/10.1016/j.micromeso.2016.01.025>
- [40] A. Ishihara, T. Wakamatsu, H. Nasu, T. Hashimoto, “Preparation of amorphous silica-alumina using polyethylene glycol and its role for matrix in catalytic cracking of *n*-dodecane”, *Appl. Catal. A: Gen.*, 478 (2014) 58-65, <https://doi.org/10.1016/j.apcata.2014.03.016>
- [41] A. G. Oblad, *Oil Gas J.*, 27 (1972) 84
- [42] A. Ishihara, K. Kimura, A. Owaki, K. Inui, T. Hashimoto, H. Nasu, “Catalytic cracking of VGO by hierarchical ZSM-5 zeolite containing mesoporous silica–aluminas using a Curie point pyrolyzer”, *Catal. Commun.*, 28 (2012) 163-167, <https://doi.org/10.1016/j.catcom.2012.08.023>
- [43] A. Ishihara, D. Kawaraya, T. Sonthisawate, H. Nasu, T. Hashimoto, “Preparation and characterization of zeolite-containing silica-aluminas with three layered micro-meso-meso-

Chapter 5

- structure and their reactivity for catalytic cracking of soybean oil using Curie point pyrolyzer”, *Fuel Process. Technol.*, 161 (2017) 8-16, <https://doi.org/10.1016/j.fuproc.2017.03.002>
- [44] A. Ishihara, T. Tsukamoto, T. Hashimoto, H. Nasu, “Catalytic cracking of soybean oil by ZSM-5 zeolite-containing silica-aluminas with three layered micro-meso-meso-structure”, *Catal. Today*, 303 (2018) 123-129, <https://doi.org/10.1016/j.cattod.2017.09.033>
- [45] T. Sonthisawate, T. Nakanishi, H. Nasu, T. Hashimoto, A. Ishihara, “Catalytic cracking reaction of vacuum gas oil and atmospheric residue by zeolite-containing microporous and mesoporous composites using Curie point pyrolyzer”, *Fuel Process. Technol.*, 142 (2016) 337-344, <https://doi.org/10.1016/j.fuproc.2015.10.016>
- [46] A. Ishihara, K. Tatebe, T. Hashimoto, H. Nasu, “Preparation of Silica, Alumina, Titania, and Zirconia with Different Pore Sizes Using Sol–Gel Method and Their Properties as Matrices in Catalytic Cracking”, *Ind. Eng. Chem. Res.*, 57 (2018) 14394-14405, <https://doi.org/10.1021/acs.iecr.8b03019>
- [47] B. C. Gates, J. R. Katzer, G. C. A. Schuit, “Chemistry of Catalytic Processes”, *McGraw-Hill*, Chapter 1 Cracking (1979) 1-111, <https://doi.org/10.1002/aic.690250427>
- [48] H. Konno, R. Ohnaka, J. Nishimura, T. Tago, Y. Nakasaka, T. Masuda, “Kinetics of the catalytic cracking of naphtha over ZSM-5 zeolite: effect of reduced crystal size on the reaction of naphthenes”, *Catal. Sci. Technol.*, 4 (2014) 4265-4273, <https://doi.org/10.1039/C4CY00733F>
- [49] D. P. Serrano, J. Aguado, J. M. Escola, “Developing Advanced Catalysts for the Conversion of Polyolefinic Waste Plastics into Fuels and Chemicals”, *ACS Catal.*, 2 (2012) 1924-1941, <https://doi.org/10.1021/cs3003403>

Chapter 5

Chapter 6

Conclusion

The use of gel skeletal reinforcement (GSR) in the preparation of alumina and titania matrices by the sol-gel method enabled the preparation of matrices with new acid sites and improved stability of the crystalline phase. Conventionally, catalysts using matrix with GSR were prepared by physically mixing the calcined matrix with zeolite and calcining it again, but by adding zeolite beforehand during the preparation of the gel, zeolite-containing hierarchical two-layered (ZC2L) catalysts with more uniformity and larger mesopore size could be prepared. In addition, it was succeeded in preparing three-layered catalysts by applying GSR to two-layered catalysts using malic acid as a template. All of the catalysts had large mesopores after preparation while maintaining the unique structure of zeolite. The mesopore characteristics could be changed by varying the amount of the reinforcing agents used to GSR. As a result, the maximum pore volume and pore diameter of the ZC2L catalysts reached about 5 cm³/g and 50 nm, respectively.

Catalytic cracking of *n*-dodecane, vacuum gas oil (VGO) or low-density polyethylene (LDPE) was performed on the prepared zeolite-containing hierarchical catalysts using a fixed bed reactor or a Curie point pyrolyzer to evaluate the effect of the zeolite used, hierarchical structure and acidity.

Compared to zeolite single, the prepared zeolite-containing hierarchical catalysts showed improved conversion and selectivity of the obtained products, especially the olefin/paraffin ratio (O/P), indicating that the presence of mesopores in the catalysts had a significant effect on catalytic cracking. Although the zeolite-containing hierarchical catalyst has mesopores and therefore less zeolite than zeolite single, the presence of mesopores and dilution of zeolite may have facilitated diffusion in the catalyst, resulting in improved conversion. Also, the suppression of the hydrogen transfer reaction in the zeolite may have inhibited the formation of paraffins and increased the amount of olefins produced. When compared among the different zeolites, ZSM-5, β and Y zeolites, the product selectivity tended to be dependent on the micropore size of the zeolite. XRD measurements confirmed that the zeolite-containing hierarchical catalyst maintained the structure of zeolite, but the product selectivity of the zeolite-containing hierarchical catalyst was enhanced compared to zeolite single, confirming that the structure of zeolite was utilized more effectively in catalytic cracking by using the hierarchical catalyst. ZSM-5 zeolite-containing catalysts increased the selectivity for aromatic compounds, which is characteristic of ZSM-5

Chapter 6

zeolite. β and Y zeolite-containing catalysts also increased the O/P due to reduced hydrogen transfer reactions, but the iso-/n-hydrocarbon and multi-/single-branched hydrocarbon ratios were equal to or higher than those of the respective zeolites single. As described above, the prepared zeolite-containing hierarchical catalysts exhibit product selectivity, which is characteristic of zeolites, suggesting that the catalysts can improve the conversion while taking advantage of the characteristics of the zeolites used. In the catalytic cracking of bulky molecules such as LDPE and VGO, the zeolite-containing hierarchical catalysts showed high conversions and O/P, as in the catalytic cracking of *n*-dodecane, demonstrating their effectiveness.

List of Publications

- Chapter 2** Preparation of β -zeolite mixed catalysts using alumina and titania matrices modified by silication of gel skeletal reinforcement and their reactivity for catalytic cracking of *n*-dodecane
Applied Catalysis A, General 610 (2021) 117959
DOI: <https://doi.org/10.1016/j.apcata.2020.117959>
- Chapter 3** Preparation of novel zeolite-containing hierarchical two-layered catalysts with large mesopores by gel skeletal reinforcement and their reactivities in catalytic cracking of *n*-dodecane
Journal of Porous Materials, 28 (2021) 1935-1944
DOI: <https://doi.org/10.1007/s10934-021-01133-w>
- Chapter 4** Catalytic cracking of low-density polyethylene over zeolite-containing hierarchical two-layered catalyst with different mesopore size using Curie point pyrolyzer
Fuel Processing Technology, 227 (2022) 107106
DOI: <https://doi.org/10.1016/j.fuproc.2021.107106>
- Chapter 5** Estimation of catalytic cracking of vacuum gas oil by a Y zeolite-containing two-layered catalyst and a novel three-layered hierarchical catalyst using a Curie point pyrolyzer method
Energy Fuels, 34 (2020) 7448–7454
DOI: <https://doi.org/10.1021/acs.energyfuels.0c00957>

Acknowledgements

The studies presented in this thesis are the summaries of the author's work carried out at the Inorganic Materials Chemistry Laboratory, Graduate School of Engineering, Mie University.

The author would like to express his sincerest gratitude to Professor Dr. Atsushi Ishihara for providing a chance to study at this Laboratory, and for his suggestions, discussions, and encouragement.

Heartfelt thanks go to Associate Professor Dr. Tadanori Hashimoto who has given the author so much discussion and suggestion during the course of study. Thanks, are also due to Dr. Hiroyuki Nasu for their helpful discussions, advises, and encouragement.

It is his great pleasure to thank Mr. Hiroaki Oono, Mr. Koki Mori, Mr. Kazuya Mori, Mr. Fumiya Hayashi, Mr. Koki Suemitsu, Ms. Haruna Oshimura and Mr. Koudai Mizuno for their valuable collaboration to this work, and all the members of Inorganic Materials Chemistry Laboratory.

In addition, I would like to express my gratitude to the Director of Mie Prefecture Industrial research institute (MIRI) for his approval to dispatch me to the graduate school and to some staff members of the MIRI for their special consideration regarding my research at the graduate school.

Finally, the author would like to give his greatest thank to his parents and brother for continuous encouragement throughout the present study.